NREL/TP-411-8111 • UC Category: 1250 • DE95009243

Research on Silicon-Carbon Alloys and Interfaces

Final Subcontract Report
15 February 1991 – 31 July 1994

J. R. Abelson
University of Illinois
Urbana, Illinois

NREL technical monitor: W. Luft

National Renewable Energy Laboratory
1617 Cole Boulevard
Golden, Colorado 80401-3393
A national laboratory of the U.S. Department of Energy
Managed by Midwest Research Institute
for the U.S. Department of Energy
under contract No. DE-AC36-83CH10093

Prepared under Subcontract No. XG-1-10063-6

July 1995

NOTICE

Available to DOE and DOE contractors from:
Office of Scientific and Technical Information (OSTI)
P.O. Box 62
Oak Ridge, TN 37831
Prices available by calling (615) 576-8401

Available to the public from:
National Technical Information Service (NTIS)
U.S. Department of Commerce
5285 Port Royal Road
Springfield, VA 22161
(703) 487-4650

Printed on paper containing at least 50% wastepaper and 10% postconsumer waste

Preface

This report presents highlights of research performed from February 15, 1991 to July 31, 1994 under a cost-reimbursable, phased 3-year subcontract from the National Renewable Energy Laboratory (a national laboratory of the U. S. Department of Energy operated by Midwest Research Institute) to the University of Illinois (subcontract number XG-1-10063-6 to the prime contract DE-AC02-83CH10093). The research was carried out under the direction of John R. Abelson, Associate Professor of Materials Science and Engineering and of the Coordinated Science Laboratory, and Dr. Nagi Maley of the Coordinated Science Laboratory (now at the Solarex Thin Film Division). Materials preparation and characterization, including in-situ spectroscopic ellipsometry, were carried out in the Thin Film Physics group of the Coordinated Science Laboratory. Ex-situ XPS, Auger, and SNMS analyses were carried out in the Center for Microanalysis of Materials, University of Illinois, which is supported by the U.S. Department of Energy under contract #DEFG02-91-ER45439. The small angle X-ray scattering measurements and analyses were performed by Professor Don Williamson of the Colorado School of Mines.

Graduate research assistant S.-Y. Yang performed the film growth and adhesion studies in all three phases of this work; he is now a staff member at Applied Materials in Santa Clara, California. Graduate research assistant Y. Yang performed the analyses of TCO reduction during the second phase of this work, and discovered the new phenomenon of sub-surface a-Si:H to μc-Si:H transformation during the third phase of this work; he is currently completing his Ph.D. at the University of Illinois. Graduate research assistant Y.-H. Liang performed the growth of p^+ a-Si,C:H films during the third phase of this work; he is currently completing his Ph.D. at the University of Illinois and will join Intel in Portland, Oregon, as a staff member. The contract monitor in the first phase of this work was Brian Stafford, in the second phase was Tom McMahon, and in the third phase was Werner Luft. Helpful comments on the content and presentation of this report were provided by Werner Luft. The author is grateful to Dr. Nagi Maley of the Solarex Thin Film Division for providing TCO-coated substrates, and for numerous illuminating technical discussions.

Individual Objective

The objective of this program is to understand and improve the optical and electronic properties of the TCO/p/i interface through (i) the use of a novel deposition technique (reactive magnetron sputtering), (ii) in-situ analyses of the film growth and properties, and (iii) ex-situ measurements of interface structure, composition, and performance. The relationship derived between the mechanisms of growth and the "top junction" properties is expected to be particularly important for technological progress.

Wide Bandgap Team Goal

Demonstrate, characterize, understand, and improve the optical and electronic properties of the TCO/p/i interface for use in achieving 15% efficient stabilized photovoltaic modules. (Wide bandgap materials are defined as those with a bandgap over 1.9 eV.)

Executive Summary

The motivation of this project is the development of improved thin films and interfaces for the "top junction" in hydrogenated amorphous silicon (a-Si:H) based p-i-n solar cells. We have used dc reactive magnetron sputtering (RMS) to deposit undoped and p-type wide bandgap hydrogenated amorphous silicon-carbon alloy (a-Si,C:H) and micro-crystalline (μc-Si:H) thin films. We have also used *in situ* probes to understand the atomic-level mechanisms of film and interface formation; the techniques are modulated mass spectroscopy to measure the identity and energy distribution of the growth flux, spectroscopic ellipsometry to determine the microstructure of the films and interfaces, and infrared reflectance spectroscopy to observe the composition and bonding in real time.

The RMS growth technique has three advantages over plasma-assisted chemical vapor deposition: (i) RMS provides explicit control of the hydrogen flux during deposition, and the bonded hydrogen content, via the injection of H_2 during sputtering. We have used the independent control of hydrogen to tailor the a-Si:H bandgap from 1.6-1.9 eV at constant substrate temperature, and to suppress chemical reduction at the interface with tin oxide coated substrates. (ii) The RMS growth fluxes are energetic, due to sputtering and particle reflection processes at the Si target. We find that the translational energy of hydrogen atoms promotes the nucleation of μc-Si:H, and the energy of sputtered Si and C atoms produces dense a-Si,C:H with excellent electronic properties. (iii) No toxic or pyrophoric hydride gases are used during RMS, which offers significant safety advantages and cost reduction for solar cell production. The quality of the films and interfaces results reported here strongly support the feasibility of this approach.

The key results of this work are the following.

Growth and Properties of Wide Bandgap a-Si,C:H

We deposit a- $Si_{1-x}C_x$:H films by sputtering a silicon target in Ar + H_2 + CH_4. Films with optical bandgaps of 1.8 - 2.0 eV and $x \leq 0.2$ have a compact microstructure: no CH_x groups are detected by infrared absorption, and the microvoid volume is ≤ 2.5 % as determined by small angle X-ray scattering. The electronic properties are also excellent: for a Tauc bandgap E_g = 1.90 eV, the sub-bandgap absorption is 0.4 at 1.2 eV, the Urbach energy is 55 meV, the ambipolar diffusion length is 1000 Å, the air-mass-1 photoconductivity is 10^{-6} /Ω-cm and the dark conductivity is 10^{-11} /Ω-cm. We also discuss which combination of growth parameters leads to the best film properties, provide evidence for the mechanisms of carbon and hydrogen incorporation, and resolve several long standing debates in the literature concerning the roles of carbon and substrate temperature on the electronic properties.

p-type Doping of a-Si,C:H

We deposit p^+ a-Si,C:H films using a silicon target sintered with 1 atomic % boron. For a Tauc bandgap of 1.85 eV, the dark conductivity is $8x10^{-6}$ /Ω-cm, the thermal activation energy is 0.28 eV, and the photoconductivity mobility-lifetime product is $3x10^{-8}$ cm^2/V. These results are slightly better than for p^+ a-Si,C:H films grown by plasma-assisted chemical vapor deposition. We discuss the film microstructure, as reflected in infra-red absorption and hydrogen thermal evolution spectra, as a function of the absolute composition.

Chemical Reduction of Transparent Conductive Oxide Substrates

Very thin layers of hydrogenated or unhydrogenated amorphous silicon are deposited on tin oxide (SnO_2) or zinc oxide (ZnO) using different substrate temperatures and H_2 partial pressures. The deposition processes are monitored by spectroscopic ellipsometry and X-ray photoelectron spectroscopy. We determine that *either* H or Si in the deposition flux leads to SnO_2 reduction in the early stages of film growth. However, the contribution of Si to the oxide reduction is secondary to that of H atoms. No reduction of ZnO is found, even under high hydrogen fluxes.

Sub-surface Transformation of a-Si:H to μc-Si:H

We use spectroscopic ellipsometry to monitor the nucleation and growth of μc-Si:H on a-Si:H. This interface is important for multi-junction devices which incorporate microcrystalline doped layers. We increase the hydrogen pressure to promote μc-Si:H formation and observe several effects: initially, H penetrates 45 Å into the a-Si:H substrate and increases its hydrogen content; then 55 Å of hydrogen-rich a-Si:H deposits; finally, μc-Si:H nucleates on top of this 100 Å thick, high H-content a-Si:H interface layer. As μc-Si:H grows, the thickness of the amorphous interface layer *decreases* by 40Å. These results demonstrate that a-Si:H can be transformed into μc-Si:H in a sub-surface region under appropriate conditions. The technological implication is that the phase boundary can be made relatively sharp.

Improved Film Adhesion by UV-ozone Substrate Cleaning

Substrate cleaning and ion bombardment play important roles in the adhesion, morphology and structure of hydrogenated amorphous silicon and silicon-carbon alloys. We examine differences in film adhesion as a function of substrate cleaning method and ion bombardment energy during growth. The UV-ozone cleaning technique, as used industrially for various oxide substrates, is found to increase film adhesion. Lowering the ion bombardment energy by electrically floating the substrate also improves adhesion, presumably through a reduction in the stress of the film.

Table of Contents

List of Tables

List of Figures

Introduction

The performance of amorphous silicon based p-i-n solar cells is limited by optical absorption, small built-in potential, and free carrier recombination at the TCO/p/i "top junction." The goal is to achieve large open circuit voltages (V_{oc} > 0.9 V), and to maintain or improve fill factors and short circuit current densities. The spectral response for surface-absorbed (blue) light provides a sensitive check for the quality of the TCO/p/i layers and interfaces. Metastable defect formation (the Staebler-Wronski effect) also degrades solar cell performance, and must be reduced through new approaches to layer deposition which improve the materials and interfaces.

The relationship between the growth process, film microstructure, and the properties of the top junction is poorly understood. Key issues include: the density of electronic states at the interface and near surface; dopant incorporation efficiency in the p-layer and diffusion into the i-layer; chemical reduction of the TCO and contamination of the p- or i-layers; conformal coverage of highly textured TCO by the thin p-layer; incorporation and diffusion of hydrogen; the role of H and network structure in metastable defect formation; and thickness dependence of the p- and i-layer electronic properties.

This project utilizes reactive magnetron sputtering (RMS) to deposit a-Si:H, μc-Si:H and a-SiC:H layers because this technique provides independent control of H incorporation, and considerable control over film microstructure. In situ analyses of the growth process are used to analyze the microstructure, H bonding, doping, and electronic defects of the films and interfaces. The principle techniques are modulated mass spectroscopy to measure the identity and energy distribution of the growth flux, spectroscopic ellipsometry to determine the microstructure of the films and interfaces, and IR reflectance spectroscopy to observe the composition and bonding in real time.

The RMS growth technique has three advantages over plasma-assisted chemical vapor deposition: (i) RMS provides explicit control of the hydrogen flux during deposition, and the bonded hydrogen content, via the injection of H_2 during sputtering. We have used the independent control of hydrogen to tailor the a-Si:H bandgap from 1.6-1.9 eV at constant substrate temperature, and to suppress chemical reduction at the interface with tin oxide coated substrates. (ii) The RMS growth fluxes are energetic, due to sputtering and particle reflection processes at the Si target. We find that the translational energy of hydrogen atoms promotes the nucleation of μc-Si:H, and the energy of sputtered Si and C atoms produces dense a-Si,C:H with excellent electronic properties. (iii) No toxic or pyrophoric hydride gases are used during RMS, which offers significant safety advantages and cost reduction for solar cell production. We have produced excellent p^+ and n^+ doped films simply by using sputtering targets containing ~ 1 atomic % boron or phosphorous, respectively. The excellent quality of the films and interfaces results reported here strongly support the feasibility of RMS for industrial production of solar cells.

This report is divided into five sections which focus on different aspects of the top junction problem. As of this writing, pin solar cells are being fabricated using the RMS process. The performance of these devices will provide a crucial test of the material and interface quality.

Growth and Properties of Wide Bandgap a-Si, C:H

Introduction

Hydrogenated amorphous silicon–carbon alloy films (a-$Si_{1-x}C_x$:H) can be deposited with an optical bandgap of 1.8 – 2.5 eV, which is attractive for use in thin film transistors, photoreceptors, X-ray and color sensors, and photovoltaic (solar) cells (Kruangam 1991). Advanced solar cell designs feature an integrated stack of three p-i-n junctions with different optical absorption thresholds, in order to achieve the best match with the power spectrum of sunlight. Wide bandgap (~ 1.9 eV) a-$Si_{1-x}C_x$ H is the leading candidate for the front junction light absorber (Li, Fielselmann, and Catalano 1991 and Li and Fieselmann 1991). However, the presence of carbon has been found to deteriorate the electronic transport properties with respect to hydrogenated amorphous silicon (a-Si:H). Thus, there is a scientific interest in understanding the a-$Si_{1-x}C_x$ H deposition process, and a technological interest in producing better quality films.

Various deposition techniques have been used to deposit a-$Si_{1-x}C_x$:H (Schlichting, et al., 1994, Bullot and Schmidt 1987, and Li, 1993). Plasma-assisted chemical vapor deposition (PACVD) and reactive sputter deposition (SP) have been the most investigated techniques. Historically, sputtering has not appeared to be capable of preparing a-$Si_{1-x}C_x$:H films with high electronic quality (Bullot and Schmidt 1987, and Morimoto ,et al., 1982). This conclusion was based on a comparison between a-$Si_{1-x}C_x$:H films grown by rf plasma-assisted chemical vapor deposition and by rf diode reactive sputtering. However, the latter also produced much poorer a-Si:H films than PACVD a-Si:H films.

Recently, our group used dc reactive magnetron sputtering (RMS) to deposit a-Si:H of electronic quality equivalent to state-of-the-art PACVD films (Pinarbasi, et al., 1989a and Pinarbasi, Kushner, and Abelson 1990). This advance is largely attributed to the low working gas pressure and plasma confinement in magnetron sputtering compared with diode sputtering. In RMS, a silicon target is sputtered in mixture of argon and hydrogen at a total pressure of ~ 3 mTorr. Sputtered atoms reach the growing surface with moderate (~ 10 eV) translational energy and little angular divergence, both of which favor the deposition of smooth and dense films (Thornton 1986). RMS has a high growth rate, is easy to scale for large area deposition, and the hydrogen incorporation is easily controlled via the hydrogen pressure in the discharge. In this work, we produce high quality a-$Si_{1-x}C_x$:H alloys by adding methane to the plasma discharge.

Previous studies have examined the effects of substrate temperature during growth (T_s), composition, and microstructure on the optical and electronic properties of a-$Si_{1-x}C_x$:H. But these works involved coupled variations in two or more parameters, as described below. The present work resolves these ambiguities through a series of careful single–parameter experiments.

Chaudhuri (Chaudhuri, et al., 1984) and Ray (Ray 1989) studied the effects of substrate temperature on the properties of a-$Si_{1-x}C_x$:H grown by PACVD with the other growth parameters held constant. However, both the composition and optical bandgap of their films changed with temperature. A comparison of electronic properties between films with different bandgaps is meaningless from the point of view of solar cell making, where E_g is a design constant. Li (Li, Catalano, and Fielselmann 1992) compared films grown at different T_s but with the same E_g. They found that a-$Si_{1-x}C_x$:H films grown at higher T_s (250–310 °C) were inferior to those grown at lower T_s (170–230 °C). However, the carbon concentration was higher in their films grown at higher T_s. Therefore, no study has yet examined the true growth temperature effects, i.e., at fixed composition.

The increase of optical bandgap has been studied for both SP and PACVD a-$Si_{1-x}C_x$:H films (Bullot and Schmidt 1987, Watanabe, et al., 1982, Enomoto, et al., 1982, Saito, Tanaka, and Nakaaki, 1985, Saito, et al., 1985, Petrich, Gleason, and Reimer 1987, and Banerjee 1989). Based on the fact that crystalline SiC has wide bandgap, 2.39–3.76 eV depending on polytype, it has been believed that the addition of carbon to a-Si:H is responsible for the bandgap increase (Schlichting, et al., 1984 and Banerjee 1989). A linear relation between bandgap and carbon content x has been reported in PACVD a-$Si_{1-x}C_x$:H with x up to 0.6 (Watanabe, et al., 1982 and Enomoto, et al., 1982). However, significantly different dependencies of the bandgap on the carbon incorporation have been reported in the literature (Saito, Tanaka, and Nakaai 1985, Saito et al., 1985, and Shimada, Katayama, and Komatsubara 1979), as shown in Figure 1-1. On the other hand, H incorporation in a-Si:H causes a large increase in bandgap. Therefore, it is not clear what the relative contributions of H and C are to the bandgap increase in a-$Si_{1-x}C_x$:H (Li 1993, and Patrich, Gleason, and Reimer 1987).

It has been reported that the addition of carbon in PACVD films leads to an increase in the density of mid-gap defect states (DOS) and Urbach energy (E_U) (Madan and Shaw 1988 and Schmidt, et al., 1985). In those studies, the H content increased concomitantly with the C content. A large increase in the H content of PACVD a-Si:H also leads to an increase of DOS and E_U (Yoon, et al., 1991). Therefore, the effects of C incorporation in a-$Si_{1-x}C_x$:H have not yet been isolated from those of H.

The microstructure of a-$Si_{1-x}C_x$:H has an influence on the electronic transport properties. The microstructure of an amorphous film refers to the structure on a scale of 10 nm down to the atomic level. It includes aspects such as strain in the tetrahedral network, internal surfaces associated with microvoids, density fluctuations, hydrogen bonding configurations, and the spatial distribution of C and H (Luft and Tsuo, 1993).

Several studies have correlated the hydrogen bonding with the electronic properties of a-Si:H and a-$Si_{1-x}C_x$:H films (Luft and Tsuo 1993, Beyer 1985, Baum, et al., 1986, Mahan, et al., 1987, Mahan, Raboisson, and Tsu 1987, Bhattacharya and Mahan 1988, Baker, Spear, and Gibson 1990, and Lu and Petrich 1992). Hydrogen bonding has been studied by infra-red absorption (IR) (Mahan, et al., 1987 Mahan, Raboisson, and Tsu 1987), thermal evolution (TE) (Beyer 1985 and Baker, Spear, and Gibson 1990) and nuclear magnetic resonance (Petrich, Gleason, and Reimer 1987 and Baum, et al., 1986). IR spectra reveal the density of SiH_m, CH_m and SiC groups via the absorption intensity for each vibrational mode, and provide information on bonding configuration and local environment via shifts in peak position and width (Rubel, et al., 1987 and Wieder, Cardona, and Guarnieri 1979). The SiH_m rocking and wagging mode absorptions are located around 640 cm^{-1} (Zanzucchi 1984). SiH_m and CH_m stretching modes are at 2000–2100 cm^{-1} and 2800–3000 cm^{-1}, respectively (Rubel, et al., 1987 and Wieder, Cardona, and Guarnieri 1979). The SiH stretching mode centered at 2000 cm^{-1} is associated with isolated SiH bonds, and the one at 2100 cm^{-1} with SiH_2 and/or clustered SiH bonds on the internal surfaces of microvoids (Shanks, et al., 1980 and Reimer, Vaughan, and Knights 1981). Due to the strength of the SiH_m stretching modes, considerable effort has been placed on extracting microstructural information from them.

Microvoids in a-Si:H and a-$Si_{1-x}C_x$:H have been studied by small angle X-ray scattering (SAXS), which measures fluctuations in the electron density on a size scale from 1 to 100 nm. In PACVD films, the microvoid volume fraction increases with [H] in a-Si:H, and with x in a-$Si_{1-x}C_x$:H films (Mahan, et al., 1989a, Mahan, et al., 1989b, and Williamson, et al., 1989). However, the x and [H] are coupled in these a-$Si_{1-x}C_x$:H films. Below, we will examine the effects of C incorporation on the microvoid formation, the differences in the microvoid content and size distribution between RMS and PACVD a-$Si_{1-x}C_x$:H films.

Experimental

We deposit a-$Si_{1-x}C_x$:H alloys by dc reactive magnetron sputtering of a 5x12" Si target in Ar, CH_4 and H_2. The system is a load-locked UHV chamber which produces excellent a-Si:H films, and is essentially identical to the one previously described (Pinarbasi, et al., 1987). The films are deposited 1 – 2 μm thick at a rate of 1–10 Å/sec, with a substrate temperature of 150–310°C, argon partial pressure of 1.7 mTorr, methane partial pressure of 0–0.15 mTorr, and hydrogen partial pressure of 0–6 mTorr. The experiments are centered around conditions which produce films with an optical bandgap of ~ 1.9 eV, since this is of greatest interest for multi-junction solar cells.

Films are simultaneously deposited on Corning 7059 glass substrates for optical and electrical measurements, and on c-Si for compositional and infra-red absorption measurements. We use the Tauc definition for the optical bandgap E_g; we also report E_{04} and E_{203}, defined as the photon energies at which the optical absorption reaches $1x10^4$ and $2x10^3$ cm^{-1}, respectively, in the Tables. The density

of states (DOS) and Urbach energy (E_U) are determined from the absorption coefficient measured by subgap photocurrent. To determine the DOS, we integrate the subgap absorption and multiply by the proportionality constant A = 1.9×10^{16} cm^{-2} used for a-Si:H. The mobility lifetime ($\mu\tau$) product of the majority carrier electrons is computed from the photocurrent measured with a filtered red light (620-680 nm) of 100mW/cm^2. The ambipolar diffusion length (L_h) is measured by the steady state photocarrier grating method (SSPG). The dark conductivity σ_d is measured from 50–150 °C and the conductivity activation energy is determined from the low temperature portion of the Arrhenius plot. We interpret the value of the activation energy as the position of the dark Fermi energy with respect to the conduction band edge.

Carbon/silicon ratios are measured by X-ray photoelectron spectroscopy (XPS); to obtain reliable data, the surface oxide layer is removed by HF etching and mild sputter etching using 1 keV Ar^+ ions. For selected films, sputtered neutral mass spectroscopy and electron probe microanalysis were also employed to determine the C/Si ratio and the results were consistent with the XPS results.

The hydrogen bonding modes are determined by infra-red absorption. A FTIR spectrometer is used to measure the infra-red transmittance, which is converted to the absorption coefficients using the method developed by Maley (Maley and Szafranek 1990). Infra-red absorption can not be used to determine H content in a-$Si_{1-x}C_x$:H films since the oscillator strengths of both SiH_x and CH_x stretching modes depend on carbon concentration (Wieder, Cardona, and Guarnieri 1979). We determine the H content of a-$Si_{1-x}C_x$ H films from thermal evolution measurements (Maley, et al., 1989). Samples of known volume are heated in a quartz tube at a constant rate of 15 °C/min, and the pressure rise in a closed cell of known volume is measured. For simplicity in calculating the hydrogen content [H]($=N_H/(N_H + N_{Si} + N_C)$, the atomic number density of a-$Si_{1-x}C_x$:H is assumed to be the same as crystalline Si ($N_{Si} = 5.0 \times 10^{22}$ /cm^3). The actual atomic density is typically higher than this and varies with both hydrogen and carbon contents, i.e., the assumption overestimates the hydrogen content. For example, with $x = 0.20$ and [H] = 23 at. %, the atomic density ($N_H + N_{Si} + N_C$) is 9.0×10^{22} cm^{-3}. When accurate results are needed, the atomic density has been calculated using the mass density determined by floatation (with an accuracy of 0.01 g/cm^3) and the known silicon and carbon contents.

Films are deposited on low-impurity content aluminum foil for SAXS measurements. The SAXS intensity, corrected for background and normalized, provides information about the size distribution of density fluctuations in the sample through the Guinier plot, i.e. I(h) versus h^2, where the scattering vector $h = 4\pi \sin\theta / \lambda$. The integrated SAXS intensity ($Q = \int I(h)*h\ dh$) reflects the electron density contrast, and thus the microvoid volume fraction (V_f). Any preferred orientation of the microvoids can be inferred from tilting measurements with the sample oriented at 0° (Q_0) (with x-ray beam perpendicular to the film surface) and 45° (Q_{45}) (Williamson, et al., 1989). The SAXS measurements and analysis of V_f and void size distribution are provided by Department of Physics, Colorado School of Mines.

Results and Discussion

Effects of Growth Parameters

There are four explicit growth parameters in dc magnetron sputtering: the discharge current (I_C), substrate temperature (T_S), methane and hydrogen partial pressures (P_{CH4} and P_{H2}). In order to optimize film properties, we first investigated how each parameter affects film composition and film properties.

Discharge Current. A series of a-$Si_{1-x}C_x$:H films were grown with discharge currents I_C = 0.2–1.6 amperes at fixed T_S = 275°C, P_{CH4} = 0.10 mTorr, and P_{H2} = 0.8 mTorr. With increasing current, the deposition rate increases from 47–590 Å/min, and the carbon and hydrogen contents decrease, as shown in Figure 1-2. These data indicate changes in the sputtering process at the target surface. The increase in growth rate is 1.6 times faster that the cathode current; this is due to a change in cathode-anode voltage, which varies only from 350 - 510 V. The sputtering yield is increased 1.5 times from 3.4 to 5.0 correspondingly for Ar^+ of 350 eV to 510 eV (Anderson and Bay 1981). Mass spectrometric measurements in our group indicate that the total decomposition of methane increases sub-linearly with current, and that a considerable quantity of carbon is re-sputtered from the Si target (Fitzner and Abelson 1994). We interpret that the steady-state carbon coverage of the target decreases with increasing current. Since the sputter yield for Si is larger than for C (Anderson and Bay 1981), both the growth rate and Si content increase superlinearly.

The optical bandgap E_g and Urbach slope E_u decrease with increasing discharge current, as shown in Figure 1-3. The photoconductivity $\mu\tau$ product increases and the DOS decreases with I_C, as shown in Figure 1-4. Since the film composition is changing, these differences cannot be attributed to growth rate *per se*. Note that the composition and properties of hydrogenated amorphous silicon films grown in the same system exhibit nearly no dependence on growth rate from ~ 30 - 130 Å/min (Pinarbasi, et al., 1989b).

Methane Partial Pressure. A series of films were grown with methane partial pressures P_{CH4} = 0–0.15 mTorr at fixed T_S = 275 °C, P_{H2} = 0.80 mTorr, and I_C = 0.80 Amp. The carbon content increases linearly with methane partial pressure, and the hydrogen content increases and then saturates, as shown in Figure 1-5. E_g and E_U increase, as shown in Figure 1-6. The DOS increases and the $\mu\tau$ product decreases, as shown in Figure 1-7. The film properties clearly worsen with bandgap; later, we will distinguish the relative importance of H and C in these changes.

Hydrogen Partial Pressure. We prepared a-$Si_{1-x}C_x$:H films with P_{H2} = 0–6.0 mTorr at fixed T_S = 275°C, P_{CH4} = 0.10 mTorr, and I_C = 0.80 amp. As shown in Figure 1-8, the carbon content is almost constant at $x = 0.17 \pm 0.02$; the hydrogen content increases with P_{H2} from 0–1.2 mTorr, and then remains constant. As shown in Figure 1-9, the bandgap increase has the same dependence as the

hydrogen content, and the decrease in Urbach slope occurs even more rapidly, i.e., from 0–0.5 mTorr. Figure 1-10 shows similar effects in the $\mu\tau$ product and DOS, which improve dramatically from 0–0.4 mTorr and remain constant. At very high P_{H2} = 6 mTorr, both the $\mu\tau$ product and DOS degrade measurably. The normalized photosensitivity ($\mu\tau/\sigma_D$) is improved about five orders of magnitude with the introduction of H_2 partial pressure, as shown in Figure 1-11.

Growth Temperature (T_S). More hydrogen is incorporated into a-Si:H and a-$Si_{1-x}C_x$:H films at low substrate temperature, with all other growth parameters held fixed (Morimoto, et al., 1982). Our objective is to understand the effects of growth temperature alone. We grew films at 5 different substrate temperatures from 150–310 °C, and tailored the hydrogen partial pressure at each substrate temperature to achieve E_g = 1.90 eV. I_C = 0.30 amp and P_{CH4} = 0.06 mTorr were held constant. The required hydrogen partial pressures, the measured film compositions, and selected properties are shown in Table 1-1.

Table 1-1 Comparison of the Effect of Substrate Temperature on the Electronic Properties of RMS a-$Si_{1-x}C_x$:H Films of Same Composition.

	T_S (°C)	P_{H2} (mTorr)	x (at.%)	$E_{e.Tauc}$ (eV)	σ_{ph} (1/Wcm)	σ_D (1/Wcm)	$A_{1.2}$ (cm^{-1})
A	150	0.28	0.19	1.91	$1.5x10^{-7}$	$7.2x10^{-11}$	3.40
B	190	0.40	0.14	1.90	$4.3x10^{-7}$	$1.1x10^{-11}$	0.74
C	230	0.53	0.18	1.91	$6.2x10^{-7}$	$1.5x10^{-12}$	0.72
D	270	0.80	0.17	1.89	$1.3x10^{-6}$	$6.9x10^{-12}$	0.40
E	310	2.20	0.19	1.90	$1.0x10^{-6}$	$2.7x10^{-12}$	0.35

The hydrogen and carbon contents are nearly constant at C_H = 25 ± 3 at.% and x = 0.17 ± 0.02, respectively. As shown in Figs. 12a-c, $\mu\tau$ increases, E_U and DOS decrease as T_S increases. For T_S above 310°C, an optical gap of 1.90 eV can not be achieved even for high H_2 pressures. The results suggest that the best quality films are grown in the temperature range from 230–310 °C. This is opposite to the trends observed in PACVD films by Li et al., who find the best properties at 170 - 230°C (Li, Catalano, and Fieselmann 1992). We interpret the difference as due to compositional effects: their films have increasing carbon content with temperature at constant bandgap.

Figure 1-13a-b show the growth temperature dependence of the Fermi level and the normalized photosensitivity, from which we can see that the Fermi level is pulled back towards midgap and much higher normalized photosensitivity is also obtained at higher substrate temperatures.

Dependence of Bandgap on Film Composition

One of the important effects of carbon incorporation is to increase the hydrogen content. For reference, we deposited a-Si:H films with P_{H2} = 0–4 mTorr at a substrate temperature of 230 °C. As shown in Figure 1-14, the hydrogen content increases with P_{H2} up to 1.6 mTorr and then levels off at ~ 16 at. %. When P_{CH4} = 0.10 mTorr is added, the hydrogen content increases to 25 at. %. That is, carbon raises the temperature-dependent solubility limit for H incorporation.

To investigate the relationship between composition and bandgap, we determined the hydrogen and carbon contents of three RMS and two PACVD (provided by Solarex Thin Film Division) a-$Si_{1-x}C_x$:H samples, including the correction for atomic density. Figure 1-15 shows the bandgap as a function of hydrogen content, including the a-Si:H samples of Figure 1-14. All films fall on the same straight line, whereas the carbon contents of the a-$Si_{1-x}C_x$:H samples do not correlate well with bandgap. The linear relation obtained by least squares fitting is E_g (eV) = 1.33 + 0.026 [H] (at.%).

It has been reported that E_g = 1.48 + 0.019 [H] for SP and PACVD a-Si:H films with 2 ≤ [H] ≤ 17 at.% grown at T_S = 300°C and that E_g = 1.5 + 0.015 [H] for PACVD films with 10 ≤ [H] ≤ 30 at.% (Ley 1984). A similar linear relation has been reported for rf sputtered a-$Si_{1-x}C_x$:H films with hydrogen contents C_H = 26–40 at. % (Guivarc'h, et al., 1980). In the latter study, all films had a carbon content $x \sim 0.5$ and it was determined that E_g (eV) = 1.32 + 0.031 [H] (at.%). In comparison with our result, the slope is slightly different but the intercept at zero hydrogen content is same. However, the difference is that our study shows that the same linear relation still holds for various carbon contents of $x < 0.30$ and is nearly independent of carbon content. Thus, the increase of optical bandgap in a-$Si_{1-x}C_x$:H *appears* to be due to the carbon-induced increase of hydrogen content for a given growth temperature. Of course, carbon bonding must modify the band structure, so the *actual* reasons for the observed trend remain to be elucidated by a clever theorist.

Effect of Incorporated Carbon on Electronic Properties

In the previous sections, an increase in C and H contents was associated with a degradation in the electronic properties of RMS a-$Si_{1-x}C_x$:H; the same conclusion has been reported in previous studies (Madan and Shaw 1988 and Schmidt, et al., 1985). Here, we rigorously isolate the C effect by comparing samples with the same H concentrations. Figure 1-16 shows the measured DOS and E_U for two pairs of samples grown at T_S = 275 °C. The first pair has [H] = 13 at.% and [C] of 0 and 8 at.%; the second pair has [H] = 25 at.% and [C] of 16 and 22 at.%. The DOS and E_U increase with C addition in both cases, proving that the trend is general. This explains why (Li, Catalano, and

Fieselmann 1992). observed a degradation in the properties of PACVD a-$Si_{1-x}C_x$:H grown at higher temperature -- the samples possessed higher C contents.

Relation Between Microstructure and Electronic Properties

Hydrogen Bonding. Carbon polyhydride bonding (CH_2, CH_3) has been believed to cause a low density network structure and a higher degree of disorder, and has been correlated with inferior electronic properties in PACVD a-$Si_{1-x}C_x$:H (Matsuda, et al., 1986). Our RMS a-$Si_{1-x}C_x$:H films with $E_g \leq 2.0$ eV have nearly undetectable CH_2 and CH_3 in the IR stretching mode region, as shown in Figure 1-17.

The Si-H stretching mode absorptions have also been used as a measure of the H-related network structure. Mahan et al., defined a "microstructure fraction" R as the ratio of the IR absorption intensity at 2100 cm^{-1} (Si H_2 and clustered SiH) to the sum of the intensities at 2100 and 2000 cm^{-1} (isolated SiH) (Mahan, et al., 1987). For PACVD a-Si:H and a-$Si_{1-x}C_x$:H films, they found that the photoconductive $\mu\tau$ product falls monotonically with increasing R. They concluded that the electronic properties are correlated with this measure of microstructure, and conversely, that R can be used as a metric of the electronic quality. Note that this correlation involves implicit variables: R was changed by varying the substrate temperature and rf powers (Mahan, et al., 1987 and Bhattacharya and Mahan 1988), which varies both the H and C contents and the bandgap, and ion bombardment.

Figure 1-18 shows the relation between the $\mu\tau$ product and the microstructure fraction R in RMS a-Si:H and a a-$Si_{1-x}C_x$:H films grown at the same substrate temperature, as well as the data from Mahan (Mahan, et al., 1987). Both RMS a-Si:H and RMS a-$Si_{1-x}C_x$:H show a maximum in the variation of $\mu\tau$ product versus R. Our data agree with Mahan's monotonic decreasing correlation only at high R values. We also investigated the relations between DOS, E_U and R for RMS a-Si:H, which are shown in Figure 1-19. At low R values (< 0.3), both DOS and E_U are improved as R is increased. Our results suggest that at low R region, the electronic properties are not entirely determined by this kind of microstructure.

Ion bombardment during sputter deposition also alters the correlation. Moustakas (Moustakas 1984) deposited a-Si:H by rf diode reactive sputtering with little ion bombardment and found that the defect density is monotonically increased with R. However, another series of films grown with more ion bombardment had an opposite trend. In RMS a-Si:H, 70 eV ion bombardment also increases R (Yang and Abelson 1993). Thus, Mahan's correlation is clearly not universal.

Hydrogen thermal evolution has also been compared with electronic properties. In PACVD a-Si:H and a-$Si_{1-x}C_x$:H films, a greater low temperature H_2 release correlates with inferior electronic properties (Baker, Spear, and Gibson 1990 and Beyer and Wagner 1983). We have observed the opposite relationship in RMS a-$Si_{1-x}C_x$:H samples. Figure 1-20 shows H_2 evolution spectra from films grown at

P_{H2} = 0, 0.4, and 1.2 mTorr. a-$Si_{1-x}C_x$:H sample grown without H_2 shows a single peak at high temperature. As the H_2 partial pressure increases, this peak shifts towards lower temperature, and a low temperature peak appears and broadens. As noted earlier, the DOS, E_U, and $\mu\tau$ product are significantly *improved* when P_{H2} is increased from 0 to 1.2 mTorr. We speculate that the difference in observed trends arises because the H content and microstructure are strongly coupled in PACVD, but relatively independent in RMS.

In summary, there is no *unique* correlation between electronic properties and the H-related microstructure fraction in terms of the dihydride-to-monohydride ratio or the hydrogen thermal evolution. Our results suggest that low R value is a necessary, but not sufficient, condition for high electronic quality.

Microvoids. Small-angle X-ray scattering measurements have been performed for a series of RMS a-Si:H films grown at T_S = 230°C with P_{H2} = 0 to 1.6 mTorr and three RMS a-$Si_{1-x}C_x$:H samples grown at T_S = 275°C, P_{H2} = 0.8 mTorr and P_{CH4} = 0.05 to 0.15 mTorr. The SAXS intensity of all samples is found reduced upon tilting, i.e. the measured tilting ratios Q_0/Q_{45} of both RMS a-Si:H and a-$Si_{1-x}C_x$:H samples are greater than unity. This indicates the existence of preferentially oriented microstructure, i.e. elongated scattering centers with their long axes perpendicular to the film plane. Figure 1-21 shows the measured tilting ratios Q_0/Q_{45} versus hydrogen contents. The uncertainty of the Q_0/Q_{45} measurement is about ±0.2. From this figure, we can see that in the series of a-Si:H films the degree of oriented microstructure is increased dramatically with the increased hydrogen contents but it is decreased for a-$Si_{1-x}C_x$:H films with x = 0.09, 0.21, 0.29 although these two a-$Si_{1-x}C_x$:H films with x= 0.21 and 0.29 have the highest hydrogen contents. This suggests that carbon incorporation actually reduces the degree of oriented microstructure in RMS a-$Si_{1-x}C_x$:H films.

Figure 1-22 shows the total volume fraction (V_f) of the scattering centers of these two series of a-Si:H and a-$Si_{1-x}C_x$:H films versus the hydrogen contents. The values of V_f are calculated with a model which assumes that all voids are ellipsoids of various sizes and shapes, with their cylindrical symmetry axis perpendicular to the film plane (Chen 1994). The V_f of the series of a-Si:H films has been increased dramatically with the increased hydrogen contents [H]. The a-$Si_{1-x}C_x$:H film with the lowest carbon content, i.e. x = 0.09 falls the same trend as a-Si:H films. However, the a-$Si_{1-x}C_x$:H films with both higher [H] and x possess much lower V_f values compared to the trend from the series of a-Si:H films. The observation of reduced tilting effect and scattering center volume fraction indicates that carbon incorporation suppresses the microvoid formation in amorphous silicon films grown by RMS technique. To our knowledge, this is the first such result. The growth rate of a-$Si_{1-x}C_x$:H with the introduction of methane from P_{CH4} = 0 to 0.15 mTorr has been found to be significantly reduced from 313 Å/min to 227 Å/min. It has been found that the carbon growth flux is basically from the re-sputtered C from the target surface (Fitzner and Abelson 1994). Both the reduced growth rate and energetic C flux could be responsible for the microvoid suppression.

Figure 1-23 shows the relationship between the electronic properties and the volume fraction (V_f) of the scattering centers of the above series of RMS a-Si:H films. Both DOS and E_U are decreased with the increased V_f for the first three samples. The unhydrogenated a-Si film possesses the lowest V_f (0.2 %) but its properties are not shown since its photoconductivity is too low to measure its DOS and E_U by subgap photocurrent. However, it is well known that unhydrogenated a-Si possesses the highest DOS and E_U, which is in agreement with the above observed trend at low V_f values. A systematic correlation between a significant amount of SAXS-determined microstructure and the degraded opto-electronic properties has been reported by (Williamson, Chen, and Jones 1994). Our data at low amount of SAXS-determined microstructure provide a complementary evidence to depict a complete picture that less SAXS-determined microstructure is a necessary, but not sufficient, condition for high opto-electronic quality.

The effects of incorporated H on the size distribution of scattering centers is shown in Figure 1-24. The size distribution values are based on the fits to the data in the non-tilted position. Therefore these diameters represent the minor-axis dimension of ellipsoids of revolution. The average aspect ratios (v) of the major-to-minor axis dimensions, which are estimated from the tilting ratios, are increased with the H content. The scattering centers of large sizes as 18 and 36 nm are not likely due to voids but some large-scale structure such as surface roughness, H-rich regions, or H_2 - containing bubbles (Williamson 1994b). The unhydrogenated amorphous silicon exhibits the lowest both absolute and relative volume fractions of small size voids (~1 nm) and lowest average aspect ratio v. The incorporated H is found not only to increase both the absolute and the relative volume fraction of the small size voids but also the averaged aspect ratio v. The RMS a-Si:H film grown at P_{H2} = 1.6 mTorr has the highest absolute and relative fractions of the small size voids, and the most elongated ellipsoids.

Significant differences in SAXS microstructure of RMS and GD a-$Si_{1-x}C_x$:H have been reported by Chen (Williamson, Chen, and Jones 1994 and Chen, et al., 1992). It was found that oriented microstructure exists in the RMS a-Si:H and a-$Si_{1-x}C_x$:H while more random orientations exists in the GD materials with and without H_2 dilution. H_2 dilution is found to cause a large drop in Q_{SAXS} compared to GD a a-$Si_{1-x}C_x$:H without H_2 dilution. In general, RMS a-$Si_{1-x}C_x$:H films possess the most dense structure for a-$Si_{1-x}C_x$:H films with $x \leq 0.3$ (Williamson, Chen, and Jones 1994). Considering the influence of composition variation on microstructure, we propose that similar compositions should be the premise before the comparison of microstructure difference and the study of its influence on electronic properties. Table 1-2 gives the film density ρ, carbon content x, bandgap E_{203}, and Q for three a-$Si_{1-x}C_x$:H films grown by RMS and PACVD with similar carbon contents and bandgap. The PACVD film grown without H_2 dilution has the lowest film density and highest microvoid scattering. The PACVD film grown with H_2 dilution has significantly improved density and electronic properties (Williamson, Chen, and Jones 1994). The RMS a-$Si_{1-x}C_x$:H has the highest density, lowest Q, and electronic properties similar to the best PACVD film. Figure 1-25 shows I(h) vs h for the three

samples listed in Table 1-2. From these I(h) vs h curves we can conclude that both PACVD films have much larger fractions of very small voids (about 1 nm diameter) than the RMS sample and that the RMS film clearly has a much wider size distribution and a larger fraction of larger voids. The existence of the local maximum in both PACVD a-$Si_{1-x}C_x$:H films is indicative of an interference effect which is clear evidence of a rather narrow size distribution and a relatively high density of small voids (Williamson, Chen, and Jones 1994, Williamson 1994b, and Guinier and Fournet 1955). Thus, the growth technique has a strong effect on the microvoid populations.

Table 1-2 Comparison of the Q_{SAXS} and Floatation Film Density Measured from a-$Si_{1-x}C_x$:H Films Grown with Different Techniques. These two PACVD a-$Si_{1-x}C_x$:H Samples were Provided by Solarex Thin Film Division.

Sample ID	Growth Technique	x (at. %)	$E_{\alpha=2000}$ (eV)	ρ (gm/cm^3)	Q_{SAXS} ($10^{-6}nm^{-2}$)
2224C	RMS	0.21	1.97	2.08	12.0
S10729QF	PACVD, no H_2 Dilution	0.18	2.00	1.92	32.5
S11031HF	PACVD, with H_2 Dilution	0.23	2.00	2.06	14.0

In summary, we find a different correlation between the electronic properties and microstructure from RMS a-Si:H and a-$Si_{1-x}C_x$:H films at low amount of microstructure. Our study provides a complementary evidence and depicts a new whole picture that a low quantity of polyhydride bonding and small microvoid population is a necessary, but not sufficient, condition for high electronic quality.

Optimization of a-$Si_{1-x}C_x$:H films with $E_g \approx 1.9$ eV

We optimized the properties of a-$Si_{1-x}C_x$:H films with $E_g \sim 1.90$ eV because this is the bandgap required for the first absorber layer in a multi-junction solar cell. The transport of both signs of carrier is crucial to the efficiency of such a device (Li, Fieselmann, and Catalano 1991). The photoconductivity is not a sufficient diagnostic of quality, since an enhanced electron lifetime may be achieved (even in poor material) due to sensitizing defects, which strongly decrease the hole lifetime (Alvarez, et al., 1992 and Bube 1992). Therefore, we assess film quality based on a combination of

the majority carrier $\mu\tau$ product, ambipolar diffusion length (L_h), normalized photosensitivity ($\mu\tau/\sigma_D$), Urbach slope (E_U) and subgap absorption at photon energy 1.2 eV ($\alpha_{1.2}$, which is proportional to the DOS).

The properties of the optimized RMS films with 1.90 ± 0.01 eV Tauc bandgap (equivalent to E_{203} = 1.97 ± 0.01 eV, E_{04} = 2.11 ± 0.01 eV) are listed in Table 1-3. PACVD films with identical bandgap are shown for comparison (Li, Fieselmann, and Catalano 1991, Li and Fieselmann 1991, and Li 1993). The PACVD films grown without H_2 dilution exhibit the worst minority transport properties, although some of them possess very high $\mu\tau$. PACVD films with H_2 dilution are improved in all categories. The qualities of RMS films are superior to PACVD films grown at high T_S in most categories and comparable to the best quality PACVD films grown at low T_S. The subgap absorption ($\alpha_{1.2}$) for these PACVD samples measured by Photothermal Deflection Spectroscopy (PDS) is generally overestimated to some extent. However these films possess much higher Urbach energies than our RMS films. To the extent that electronic structure is crucial, our material may produce improved solar cells.

Table 1-3 Comparison of the Electronic Transport Properties of RMS a-$Si_{1-x}C_x$:H Films with PACVD a-$Si_{1-x}C_x$:H Films without and with H-Dilution. All these Films have E_g ~ 1.90 eV

	$\mu\tau$ (cm^2/V)	$\mu\tau/\sigma_\Delta$ ($cm^3\,\Omega\,V^{-1}$)	L_h (Å)	$\alpha_{1.2}$ (cm^{-1})	E_U (meV)
RMS	~ 2×10^{-8}	~ 10^4	~ 620	0.4 to 1	60 to 62
PACVD without H_2 Dilution	4×10^{-9} to 2×10^{-7}	10^3 to 10^4	~ 290	~ 25	79 to 81
PACVD with H_2 dilution, low T_2	~ 10^{-7}	7×10^4 to 2×10^5	520 to 840	5 to 7	72 to 79
PACVD with H_2 dilution, high T_2	~ 3×10^{-8}	10^3 to 10^4	400	9 to 15	62 to 70

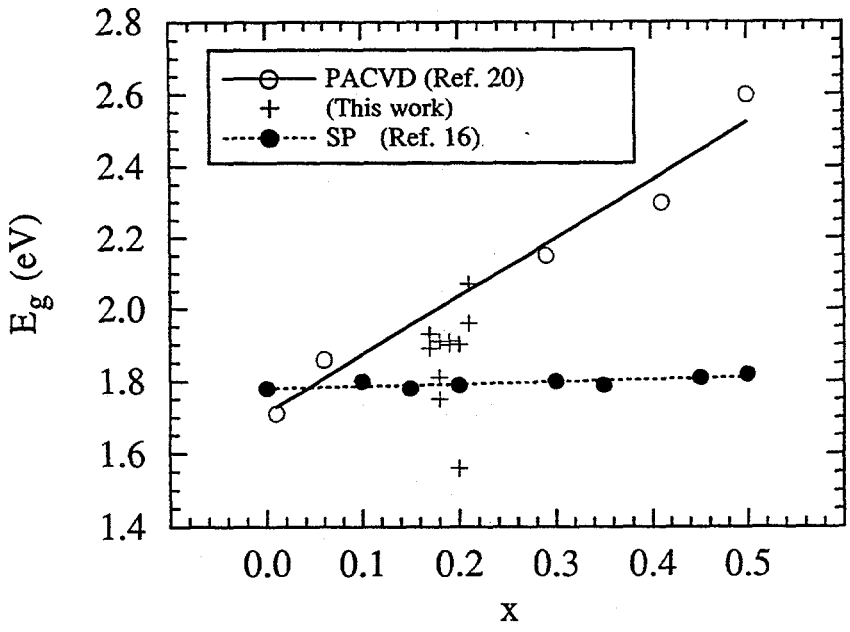

Figure 1-1 The dependence of optical bandgap on carbon composition *x* in a-$Si_{1-x}C_x$:H reported by different groups using various growth methods.

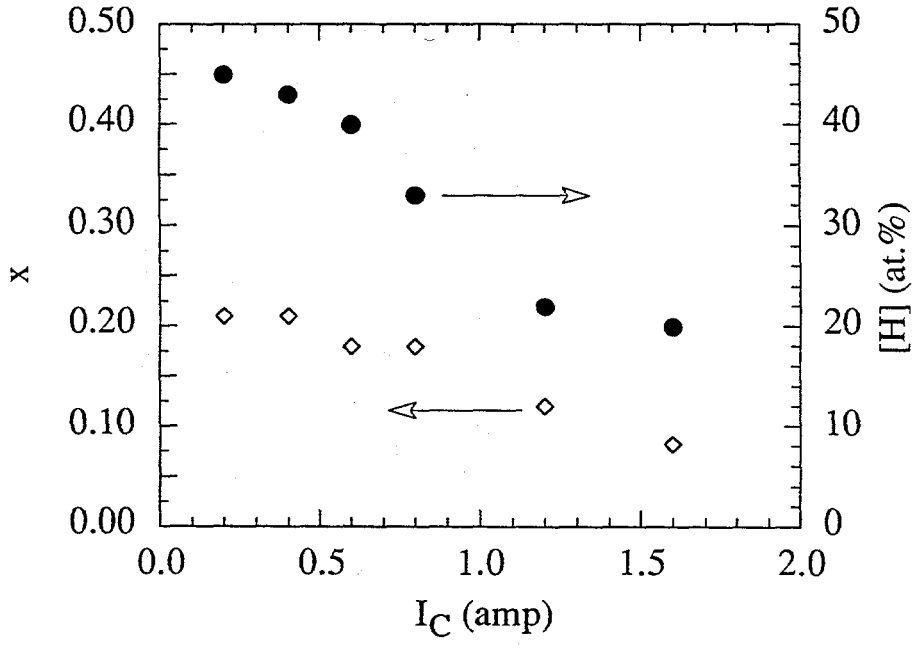

Figure 1-2 The variation of carbon composition *x* and hydrogen content [H] with the increasing cathode current I_c. The [H] is obtained from hydrogen thermal evolution without correction for film density.

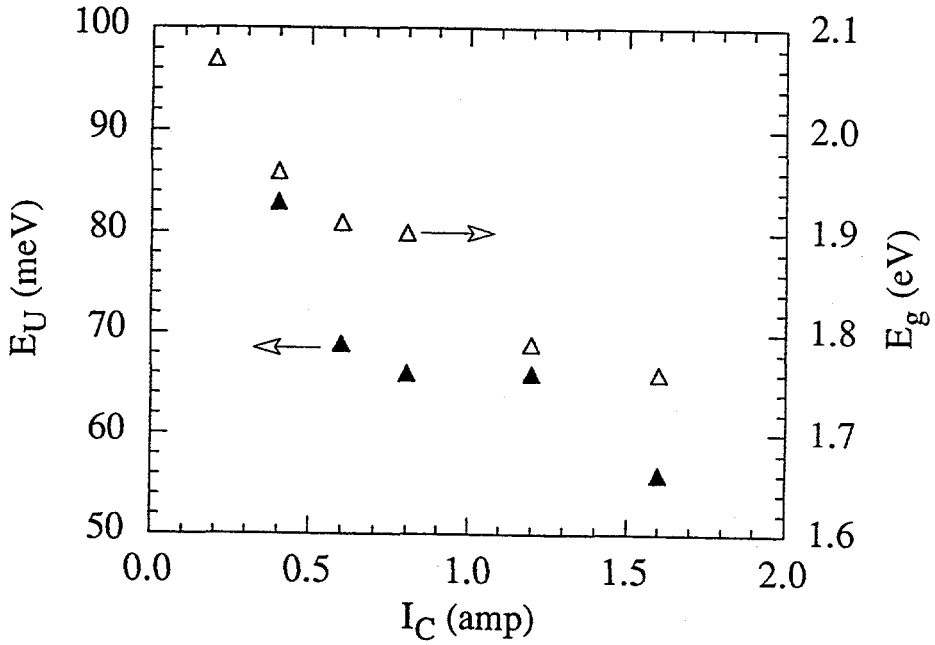

Figure 1-3 The variation of E_U and E_g in a-$Si_{1-x}C_x$:H films grown with increasing cathode current I_C. The DOS of the film grown at I_C = 0.2 amp is missing since its σ_{ph} is too low to measure DOS and E_U. This film should possess the highest DOS and E_U.

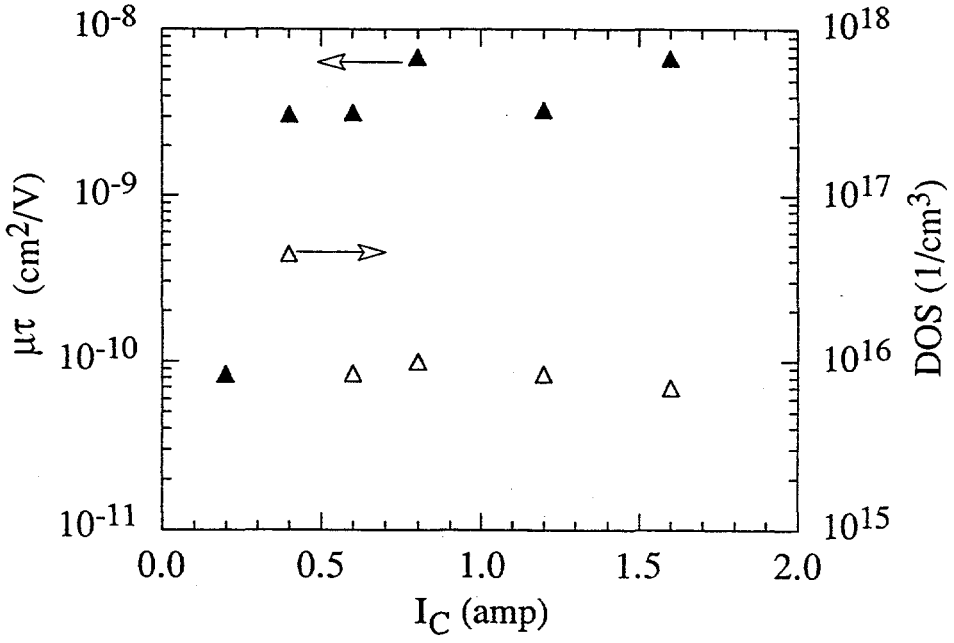

Figure 1-4 The variation of μt and DOS in a-$Si_{1-x}C_x$:H films grown with increasing cathode current I_C. The DOS of the film grown at I_C = 0.2 amp is missing since its σ_{ph} is too low to measure DOS and E_U. This film should possess the highest DOS and E_U.

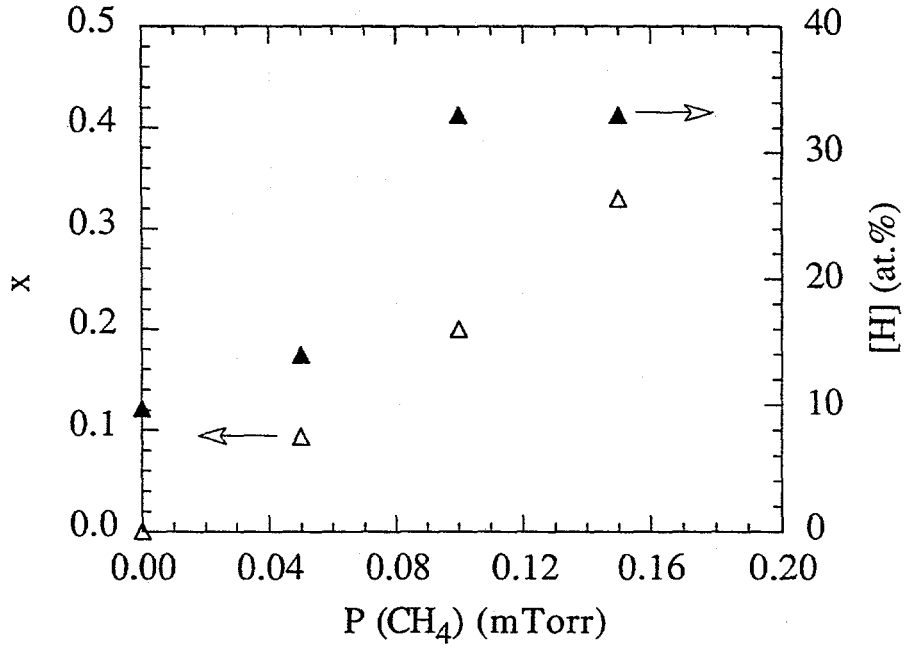

Figure 1-5 The variation of carbon composition *x* and hydrogen concentration [H] with increasing methane partial pressure. The [H] is obtained from hydrogen thermal evolution without correction for film density.

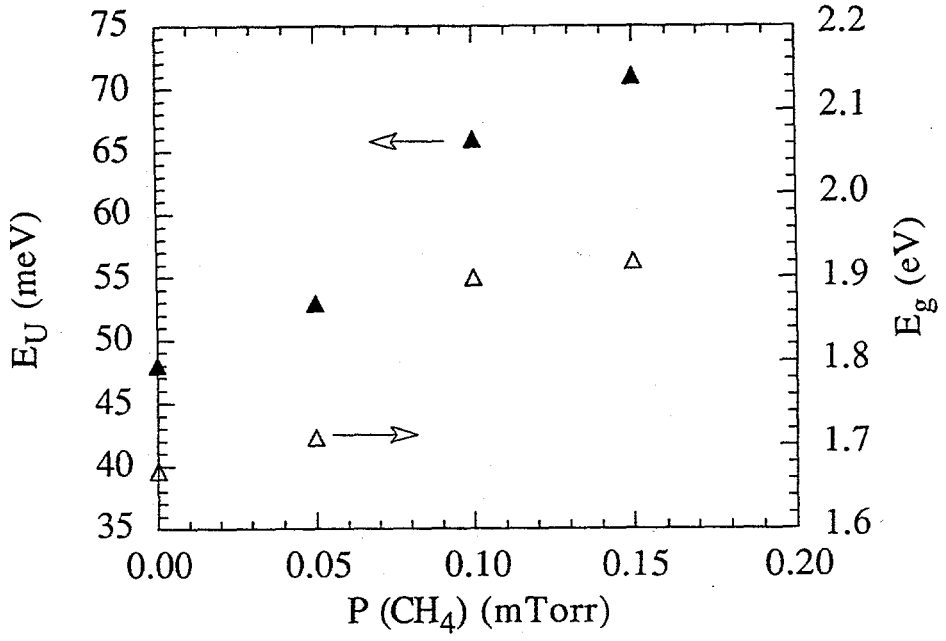

Figure 1-6 The variation of E_U and E_g in a-$Si_{1-x}C_x$:H films grown with increasing methane partial pressure.

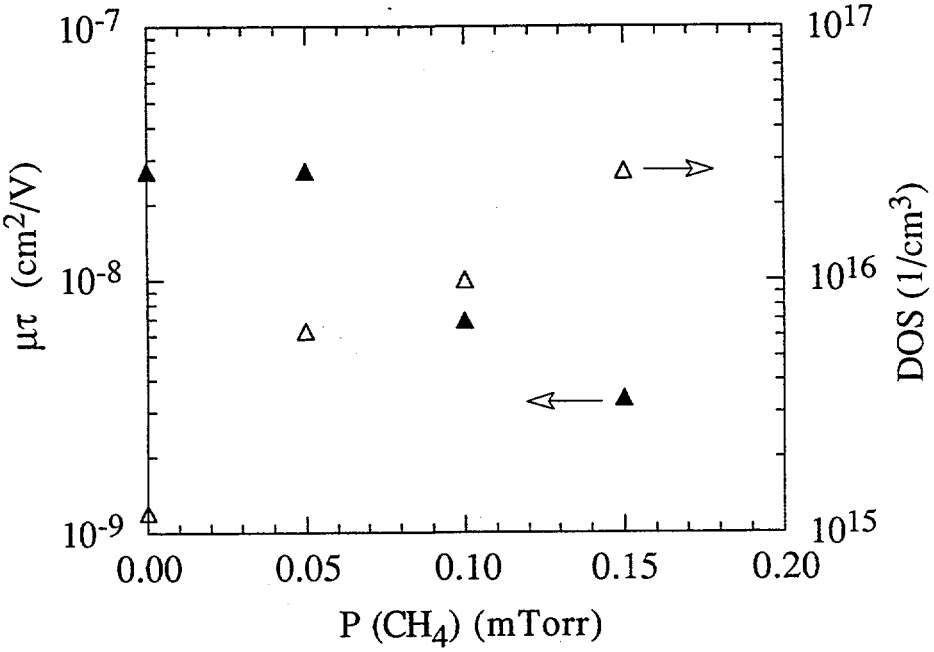

Figure 1-7 The variation of μt and DOS in a-$Si_{1-x}C_x$:H films grown with increasing methane partial pressure.

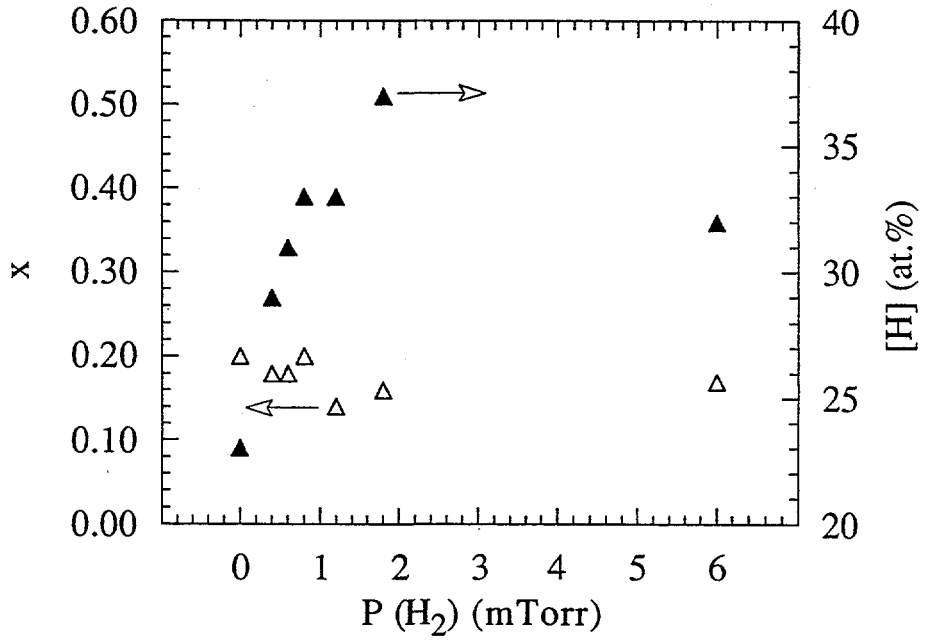

Figure 1-8 The variation of carbon composition *x* and hydrogen concentration [H] with increasing hydrogen partial pressure. The [H] is obtained from hydrogen thermal evolution without correction for film density.

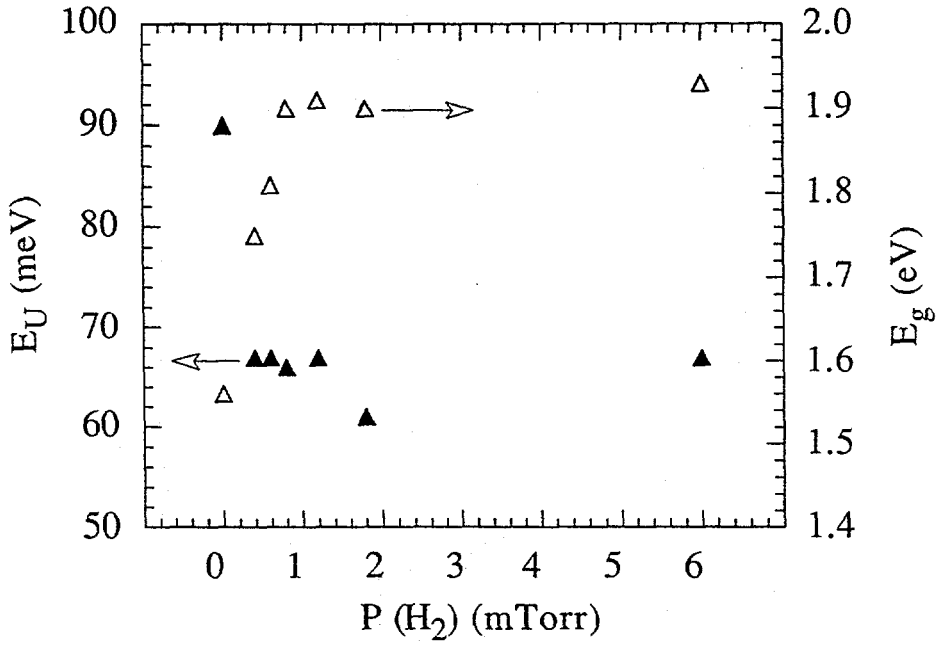

Figure 1-9 The variation of E_u and E_g in a-$Si_{1-x}C_x$:H films grown with increasing hydrogen partial pressure.

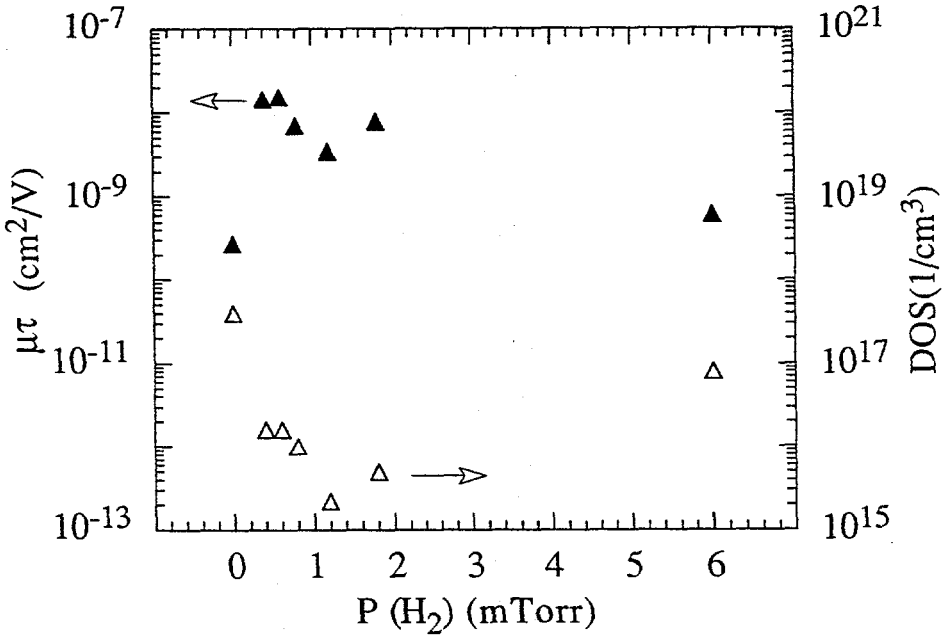

Figure 1-10 The variation of μt and DOS in a-$Si_{1-x}C_x$:H films grown with increasing hydrogen partial pressure.

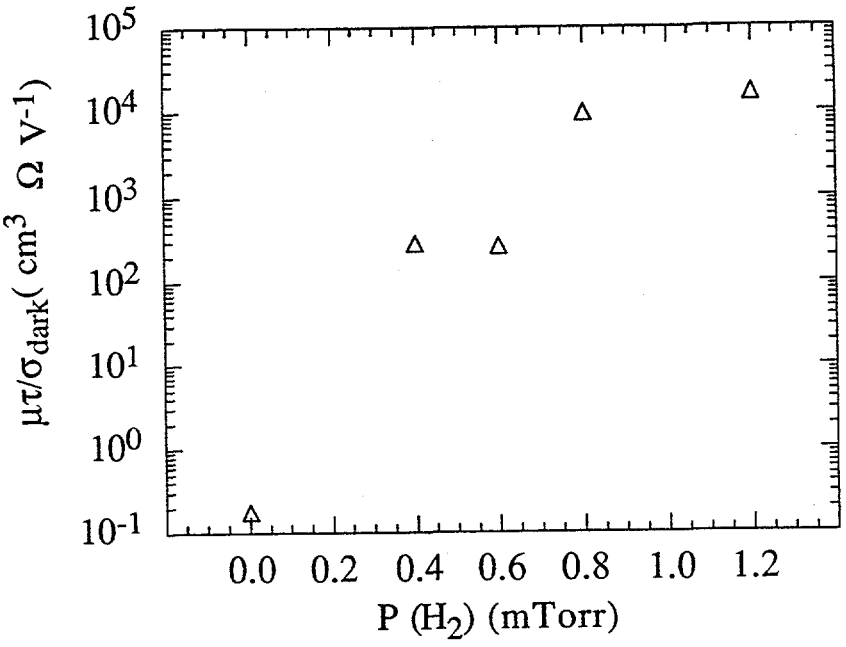

Figure 1-11 The variation of normalized photoconductivity ($\mu t/\sigma_{Dark}$) with increasing hydrogen partial pressure from 0 to 1.2 mTorr.

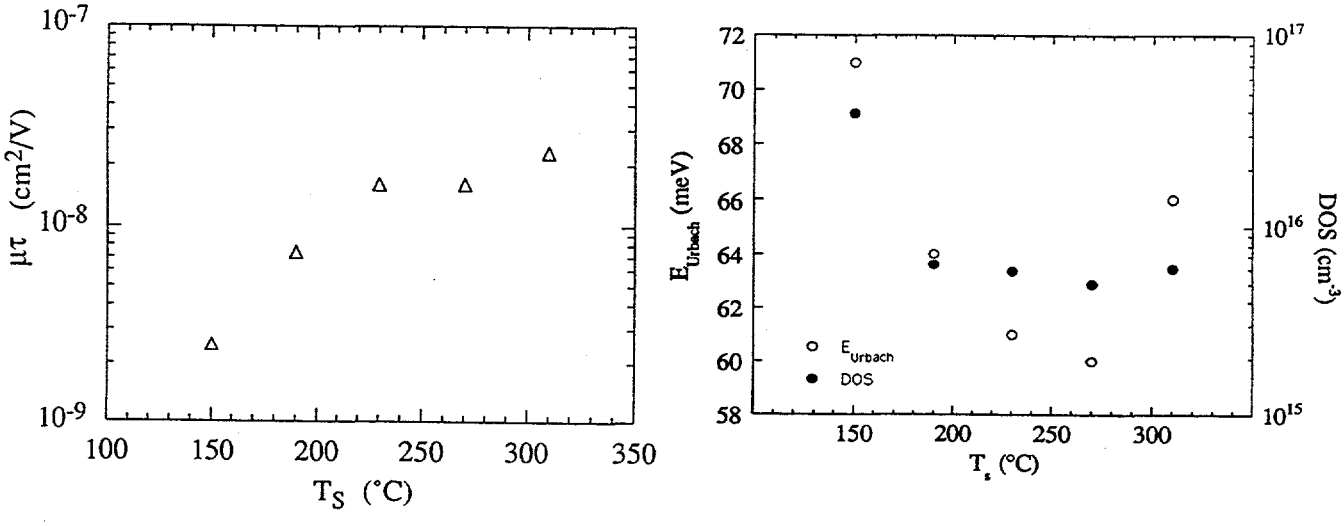

Figure 1-12 The variation of (a) μt (b) E_U and DOS with respect to growth temperature. These a-$Si_{1-x}C_x$:H films were grown with different hydrogen partial pressures but the same methane pressure so that both [H] and *x* are constant.

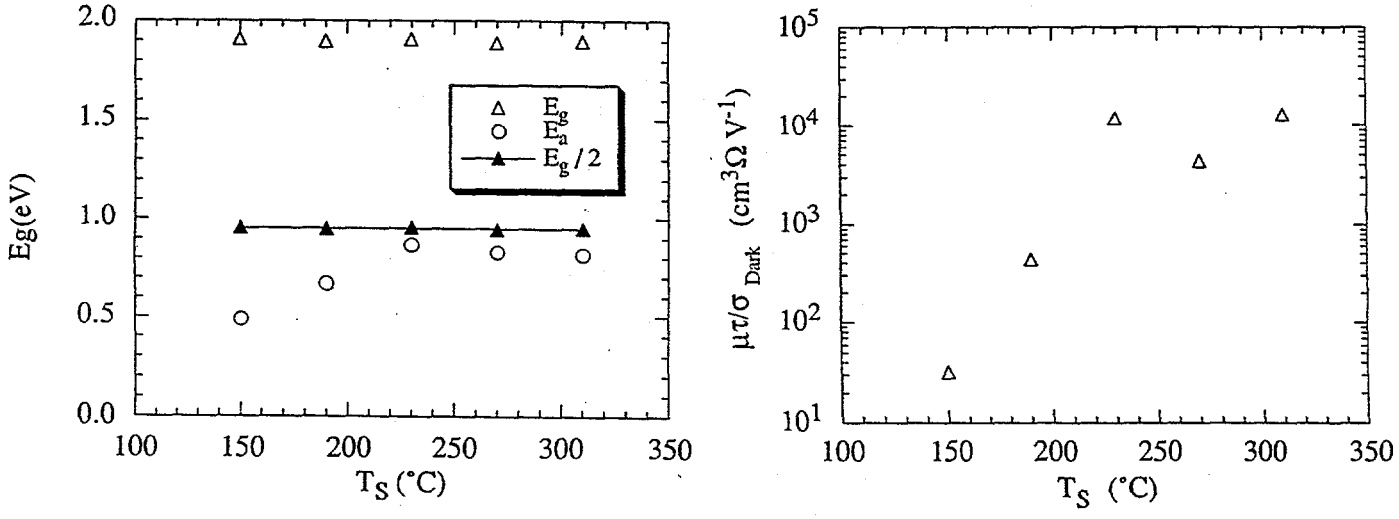

Figure 1-13 The variation of the thermal activation energy of dark conductivity (a) and the normalized photoconductivity ($\mu t/\sigma_{Dark}$) (b) with respect growth temperature for the a-$Si_{1-x}C_x$:H films in Figure 12.

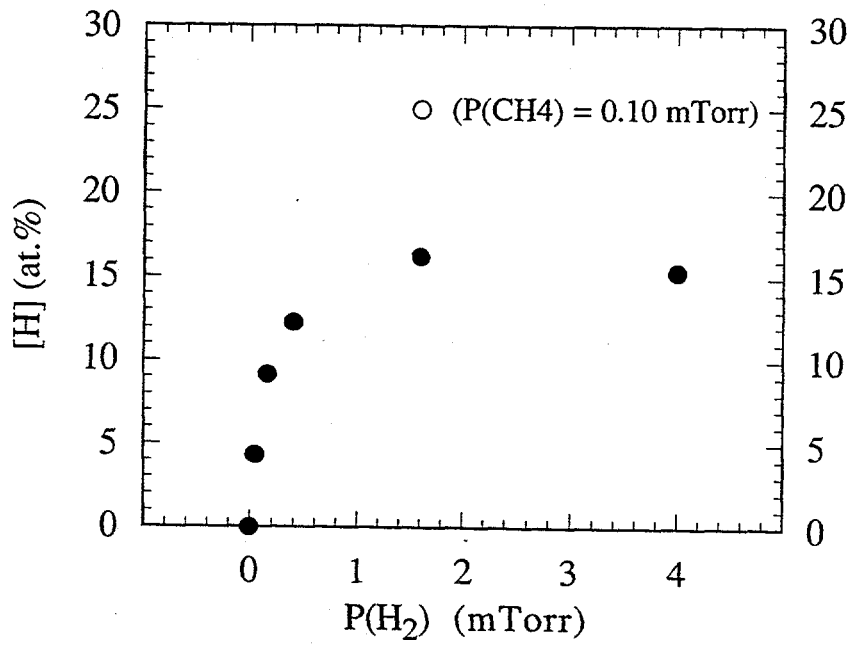

Figure 1-14 The dependence of [H] with the hydrogen partial pressure and methane partial pressure. The solid circles are a-Si:H films without introduction of methane. The open circle is the a-$Si_{1-x}C_x$:H film grown with P_{H2} = 1.2 mTorr and P_{CH4} = 0.10 mTorr at same growth temperature.

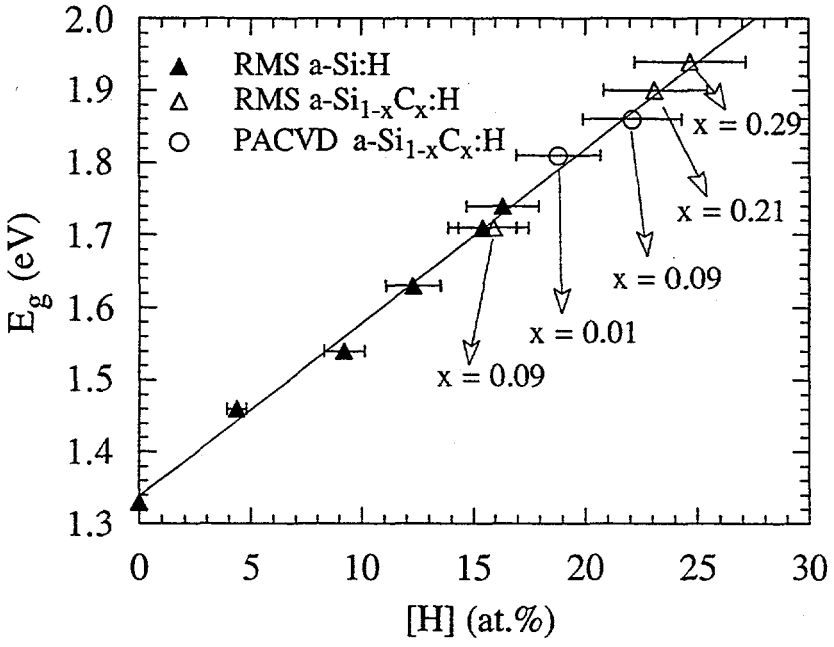

Figure 1-15 The relation between Tauc bandgap and [H] in RMS a- Si:H, RMS a-$Si_{1-x}C_x$:H and PACVD a-$Si_{1-x}C_x$:H films. These two PACVD a-$Si_{1-x}C_x$:H films were provided by Solarex Thin Film Division. All [H] in this graph are determined including the correction for film density.

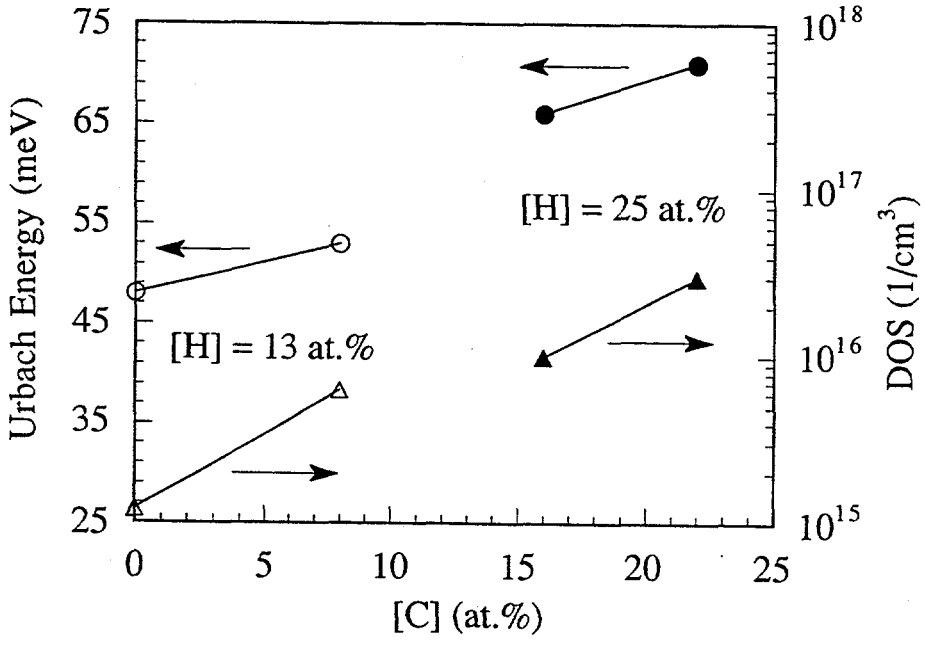

Figure 1-16 The variation of E_U and DOS with respect to [C] of two pairs of a-$Si_{1-x}C_x$:H films. [H] = 13 at.% for the first pair of films. The second pair has [H] = 25 at.%.

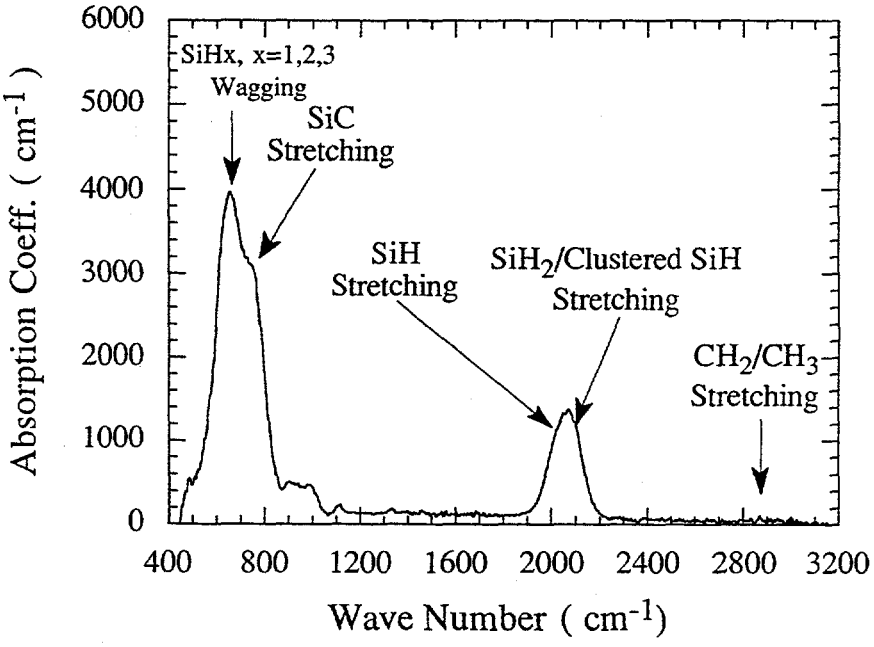

Figure 1-17 A typical infra-red absorption spectrum from a RMS a-$Si_{1-x}C_x$:H with E_g~2.0eV.

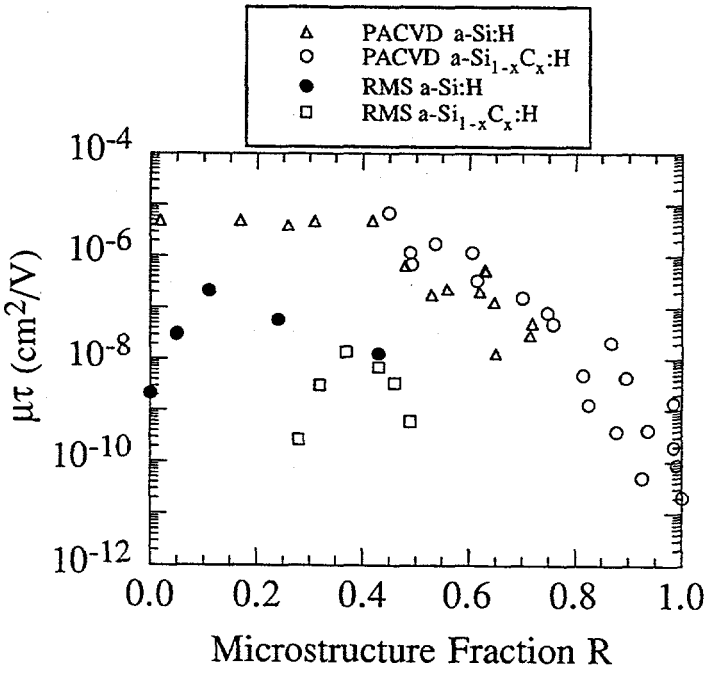

Figure 1-18 The variation of μτ products with respect to microstructure fraction R in both RMS a-Si:H and RMS a-$Si_{1-x}C_x$:H films grown at same temperature but with different hydrogen partial pressures. Mahan's data of PACVD a-$Si_{1-x}C_x$:H films are also included for comparison.

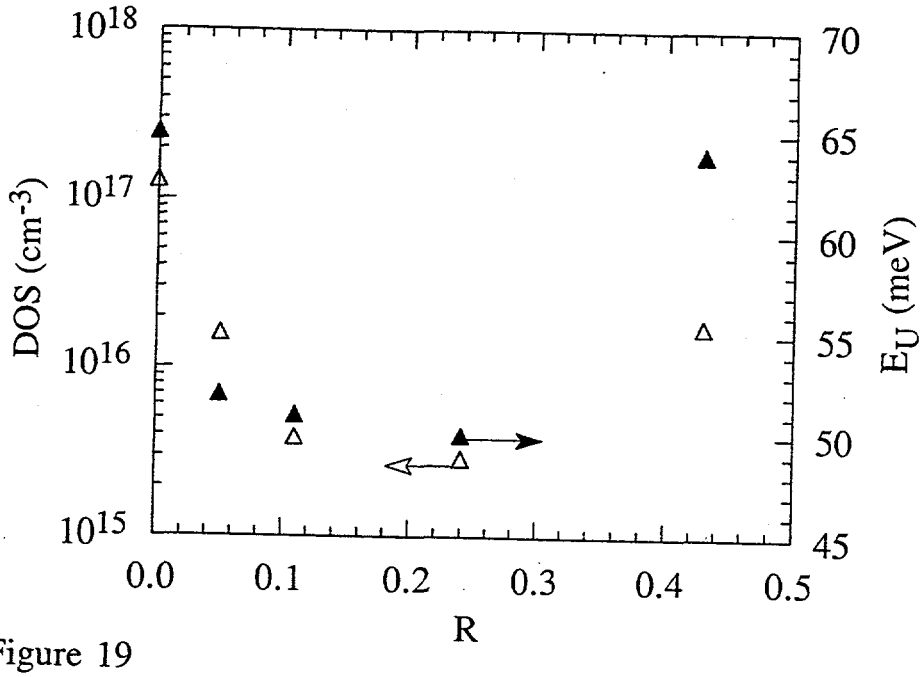

Figure 19

Figure 1-19 The variation of DOS, E_u versus R in a series of RMS a-Si:H films.

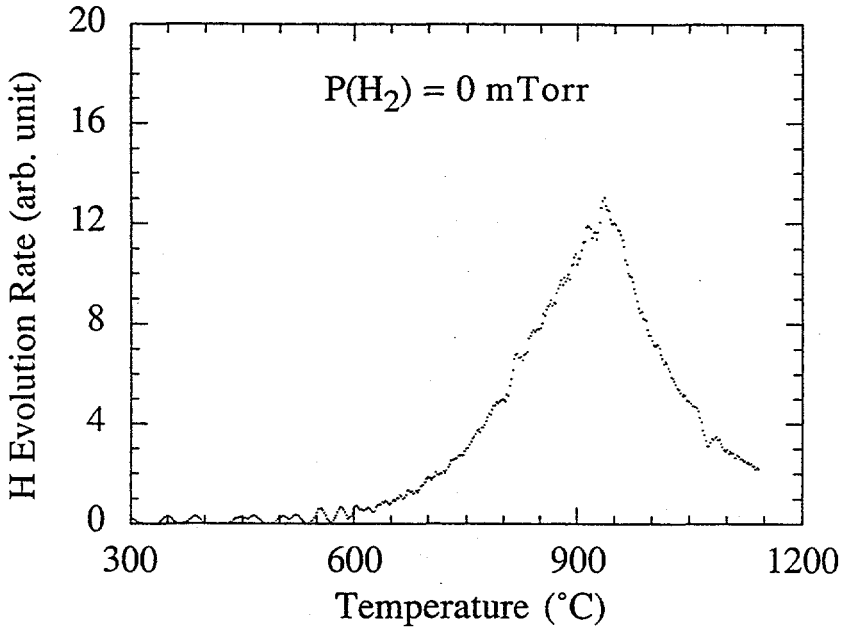

Figure 1-20(a) The hydrogen thermal evolution spectra of three RMS a-$Si_{1-x}C_x$:H films grown atP_{H_2} = 0 mTorr, with the rest of the growth parameters fixed.

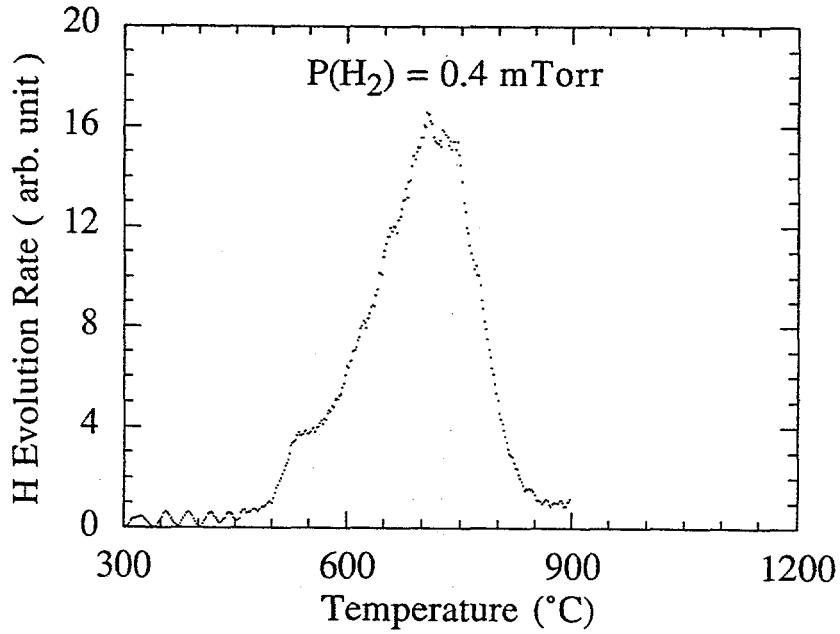

Figure 1-20(b) The hydrogen thermal evolution spectra of three RMS a-$Si_{1-x}C_x$:H films grown at P_{H2} = 0.4 mTorr, with the rest of the growth parameters fixed.

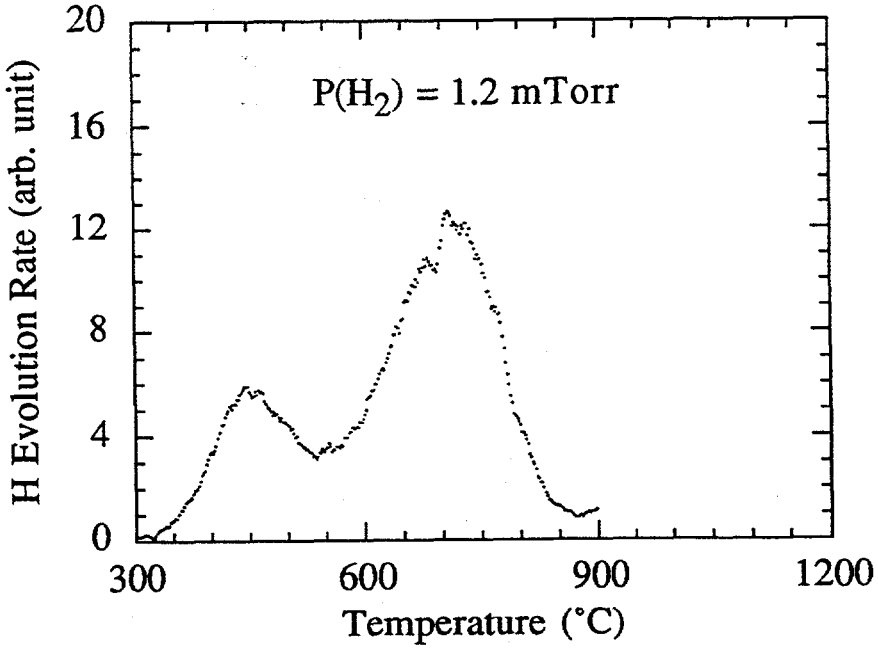

Figure 1-20(c) The hydrogen thermal evolution spectra of three RMS a-$Si_{1-x}C_x$:H films grown at P_{H2} = 1.2 mTorr, with the rest of the growth parameters fixed.

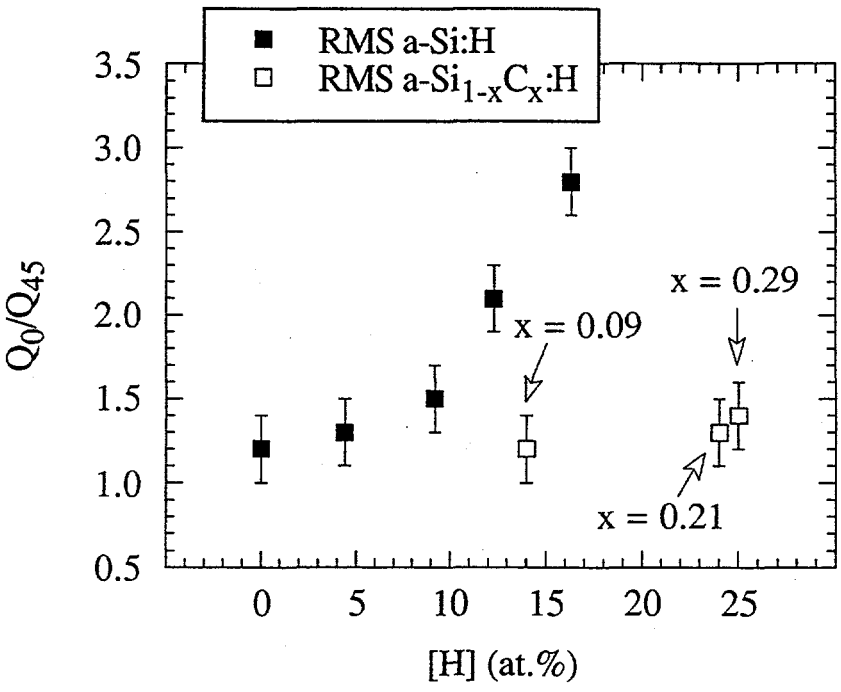

Figure 1-21 The variation of tilting ratios Q_0/Q_{45} with respect to [H] and *x* in RMS a-Si:H and RMS a-$Si_{1-x}C_x$:H films. The uncertainty in the Q_0/Q_{45} measurement is about ±0.2.

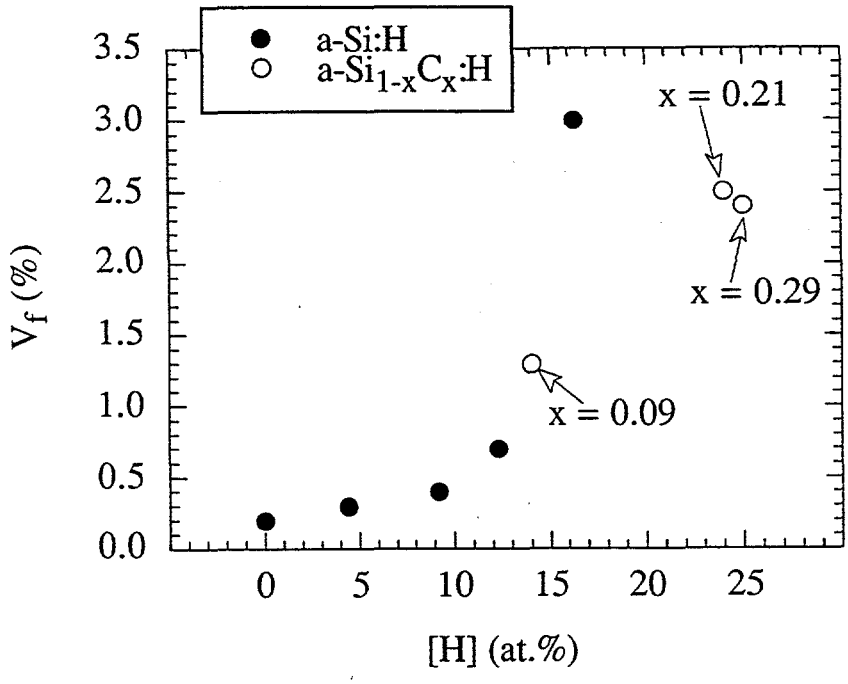

Figure 1-22 The variation of V_f with respect to [H] in RMS a-Si:H and a-$Si_{1-x}C_x$:H films.

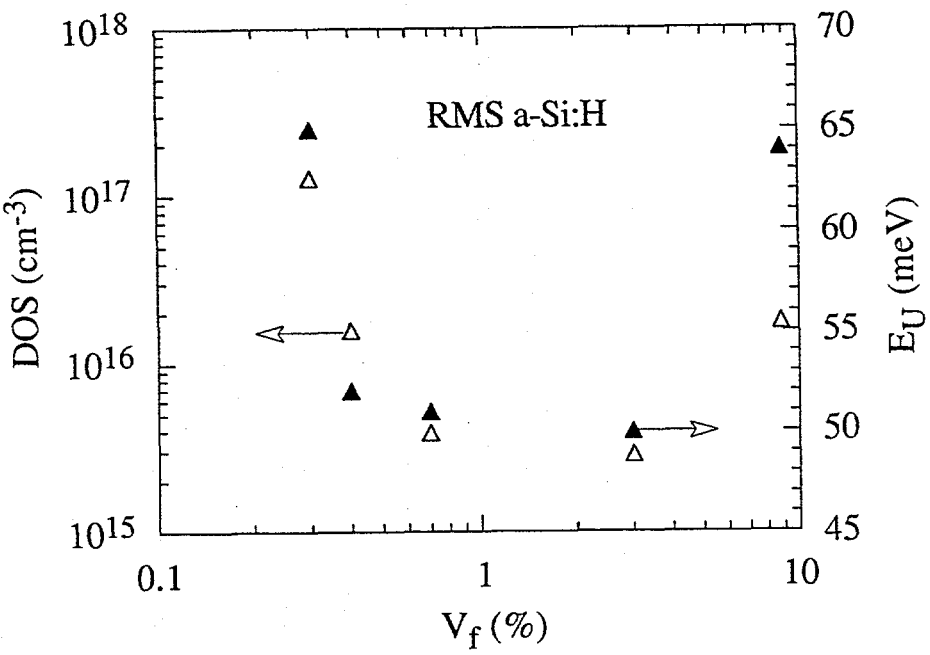

Figure 1-23 The variation of DOS and E_U versus V_f in a series of RMS a-Si:H films.

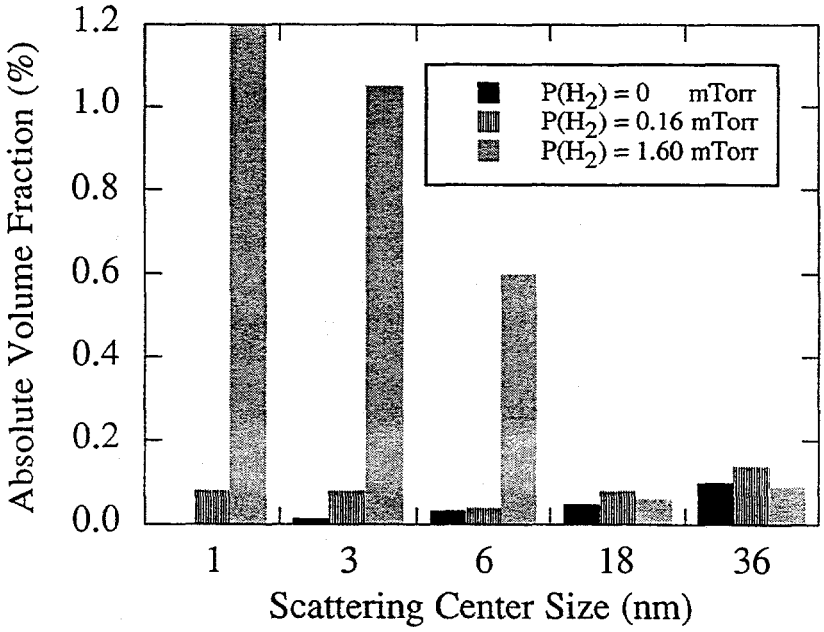

Figure 1-24 The absolute volume fraction of the scattering centers from three RMS a-Si:H films grown at P_{H2} = 0, 0.16 and 1.60 mTorr. Their [H], V_f, and v are [H] = 0, 9.2, 16.3 at.%, V_f = 0.2, 0.4, 3.0 %, v = 1.4, 2.0, 4.5, respectively.

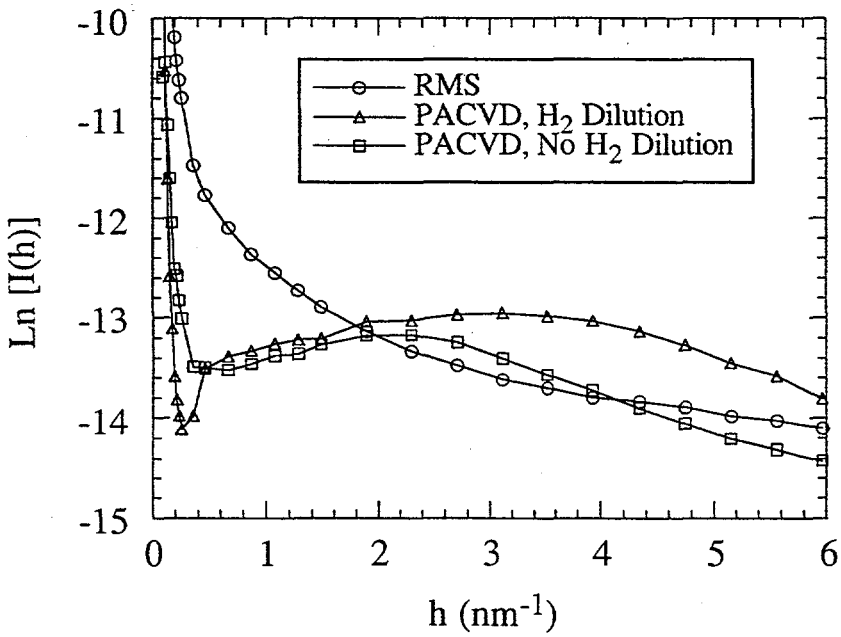

Figure 1-25 The I(h) vs h plot of three a-$Si_{1-x}C_x$:H films grown by different techniques. These two PACVD samples were provided by Solarex Thin Film Division.

p-Type Doping of a-Si,C:H

Introduction

High bandgap amorphous silicon carbon thin films (a-Si,C:H) have attracted a great deal of attention with regards to their applications in tandem solar cells, p^+ window layers in heterojunction solar cells and thin film displays (Nashashibi, et al., 1982, Furakawa 1989, and Carlson 1990). The electrical and optical properties of p^+ layers significantly affect the performance of photovoltaic devices. The optical bandgap (E_g) and thermal activation energy (E_a) are the most important factors: higher bandgap reduces the optical absorption in the p^+ layer and recombination loss due to the back diffusion of carriers and lower activation energy increases the built-in potential, thus open circuit voltage (V_∞). Various deposition techniques, notably plasma-enhanced chemical vapor deposition (PECVD) in a mixture of silane and methane, and reactive sputtering of silicon in hydrocarbons atmosphere have been employed to deposit p^+ a-Si,C:H films (Tawada 1982 and Uthana, Schroder, and Oechsner 1991). Extensive studies have shown that among all the possible p type dopants boron is the most effective one in the amorphous silicon alloys (Carlson 1990). Boron doping for p^+ a-Si,C:H films has been studied extensively recently in the literature. Dopants are normally introduced through feeding gases, such as B_2H_6, $B(CH_3)_3$, and BF_3 (Tawada 1982, Asano and Sakai 1989, and Nakano, et al., 1988). The typical PECVD p^+ a-Si,C:H film has $\sigma_d \sim 10^{-6}\Omega^{-1}cm^{-1}$ with $E_g \sim 1.9eV$ and $E_a \sim 0.4eV$.

Solid-source doping was reported by (Thompson 1984) who used a doped Si target in reactive diode sputtering. They showed that the dopant was sputtered from the target and actively incorporated into the film. Due to less optimized solid-source doping process and the impurities incorporated into the film, the doped a-Si:H films from solid source were not as good as PECVD doped films. (Moustakas 1986) also investigated the doping of a-Si:H films by rf diode sputtering from boron doped silicon targets. Their results show that the solid source doping is less efficient than the gas phase doping. Since then much less effort has been extended on the optimization of sputtered doped films from doped targets (Moustakas 1986). Recently excellent quality a-Si:H and a-Si,C:H films have been deposited by reactive magnetron sputtering (RMS) (Pinarbasi et al., 1989a and Yang and Abelson 1994). RMS appears to yield better material than diode sputtering, and thus raises the interest in the sputtering process. The a-Si,C:H films contain less microvoid and are more homogeneous compared with PECVD a-Si,C:H films. Here, we extend the reactive magnetron sputtering technique to p^+ layers. We present a first systematic study on the doping of a-Si,C:H films from Si,B targets. The electrical, optical and microstructural properties of the p-doped a-Si,C:H films were investigated.

Experimental

The p^+ a-Si,C:H films are grown by dc reactive magnetron sputtering of a powder-pressed boron-silicon target in an Ar + CH_4 + H_2 gas mixture. The details of the UHV deposition system are described elsewhere (Pinarbasi, et al., 1989a). The conditions which produce high quality intrinsic a-Si,C:H films (Yang and Abelson 1994) are chosen in this study. The A_r and CH_4 pressures are kept constant at 1.5 mT and 0.1 mT, respectively, and the substrate temperature is fixed at 230°C. The H_2 pressure is varied from 0.4 ~ 8mT. The targets are prepared by hot pressing a silicon and boron mixture at 1100°C under N_2 ambient. The target boron concentration is 1 at.%. We have tried various target boron concentrations and our results to date show that the 1 at.% target produces the highest quality doped a-Si,C:H films. The films are deposited with a thickness of ~1μm on Corning 7059 glass for optical and electrical measurements, and c-Si wafer for structural analysis. Both film thickness and optical bandgap are deduced from optical (R,T) measurements. The conductivity is measured in a co-planar configuration. Cr electrodes of 0.64 cm length are evaporated 0.13 cm apart previous to the deposition. Thermal activation energy is derived from the temperature dependence of the conductivity. The sample is slow cooled while the conductivity of the film is monitored. The annealing of the sample for 1/2 hour at 150°C in the dark is done previously to the measurement to remove surface adsorbates or light induced defects.

Infrared (IR) transmission measurements are carried out using a Fourier transform infrared spectrometer, and the data are converted to absorption coefficients using the method prescribed by (Brodsky, Cardona, and Cuomo 1977), and corrected by Langford et al., (Langford, et al. 1992). Hydrogen thermal evolution (TE) spectra are obtained by monitoring the pressure rise in a closed cell of known volume during sample heating at a constant rate (15°C/min). Secondary ion mass spectroscopy (SIMS) is used to analyze boron and impurity concentrations in the films. Carbon concentration is determined by both SIMS and X-ray photoelectron spectroscopy (XPS). The sample surface was pretreated by HF and ~20 minutes sputtering cleaning by 3keV Ar^+ before the actual XPS data collection.

Results

Compositional Analysis

The boron concentration in the a-Si,C:H films is measured by SIMS with a primary beam of O_2^+ ions. A boron implanted crystal silicon sample is used as a standard to calibrate the concentration profiles. Since the actual films are quaternary compounds, the absolute value of boron concentration is only accurate to first order. In order to diminish the surface induced error in determining the carbon concentration, we have deposited a multilayer doped film with various H_2 pressures for each layer,

used SIMS to probe the concentration profiles throughout the sample, and the profile has been calibrated by XPS measurements. The SIMS depth profiles reveal that the silicon, carbon and boron concentrations are very uniform throughout each film. The H concentration is obtained from TE. Figure 2-1 shows the B, C and H concentrations as a function of hydrogen pressure. As shown in the figure, the relative carbon concentration decreases from 22 to 18 at.% as the hydrogen pressure increases from 0 to 8mT. The H concentration increases from $1.9x10^{22}$ ~ $3.1x10^{22}$ cm^{-3} as the hydrogen pressure increases from 0.4 ~1.5mT and then the H concentration decreases to $2.1x10^{22}$ cm^{-3} as the P_{H2} reaches 8mT. We have deposited doped film with only Ar + CH_4, and the compositional analysis is also plotted in Figure 2-1. Both boron and carbon concentrations reach the maxima for this film, while H content decreases to the minimum. The schematic of H incorporation under various H_2 pressure is very similar to that of the undoped a-Si:H and a-Si,C:H films (Pinarbasi, et al., 1989a and Yang and Abelson 1994). However, the H content in the doped a-Si,C:H is ~ 30% larger than that of undoped films under similar deposition conditions, and the H content of the doped films saturate at a higher H_2 pressure than that of undoped ones. Similar observations have been reported in PECVD and RMS gas phase boron doping (Beyer, Wagner, and Mell 1981, Wagner, et al., 1983, and Jousse, et al., 1986). The mechanism of the observed enhancement of H incorporation in p^+ a-Si,C:H film is not clear understood so far. In the RMS process the dopant is sputtered from the target as boron atoms, and the fraction of boron hydrides formed in the plasma is relatively small. The large increase in H incorporation cannot be explained by the boron hydride incorporation. The existence of boron at the growth surface may play an important role.

The boron incorporation does not depend on the substrate temperature, but depends on H_2 pressure during the deposition. The boron concentration drops continuously from $3.6x10^{20}$ to $1.6x10^{20}$ cm^{-3} as P_{H2} increases from 0.4 to 8mT. The boron incorporation efficiency is relatively high: ~30-70% of the boron from the target is incorporated into the film. For all the doped films the oxygen concentration stays $2\sim3x10^{20}cm^{-3}$, the nitrogen concentration $\sim5x10^{18}$ cm^{-3} and Ar concentration $\sim10^{19}cm^{-3}$.

Optical and electrical properties

Figure 2-2a shows the optical as a function of H_2 pressure for the boron doped a-Si,C:H films. The Tauc bandgap increases from 1.72 to 1.85 eV as H_2 pressure increases from 0.4 to 1.5mT. When H_2 exceeds 1.5mT, the Tauc bandgap stays at ~1.82eV. The initial increase of bandgap can be explained by the increase of H content in the films, and then the H content saturates at a higher H_2 pressure. Figure 2-2b shows the conductivity and photo-conductivity $\mu\tau$ product as a function of the hydrogen pressure. The room temperature conductivity of the p^+ a-Si,C:H films decreases upon increasing H_2 pressure initially, from $3x10^{-7}$ to 9 $x10^{-8}\Omega^{-1}cm^{-1}$, which may be due to the decrease of conductivity prefactor σ_0 as shown in the later section. When the H_2 pressure exceeds 4mT, the conductivity starts to increase and reaches $8x10^{-6}\Omega^{-1}cm^{-1}$ at P_{H2} = 8mT. This may be attributed to the decrease of the

thermal activation energy, thus a better doping efficiency. The $\mu\tau$ product follows a similar trend as that of the room temperature conductivity.

The temperature dependence of conductivity of the boron doped a-Si,C:H films is shown in Figure 2-3. The undoped a-Si,C:H with 16 at.% carbon, has an E_a ~0.95eV. The higher conductivity and lower thermal activation energy of boron doped a-Si,C:H indicates that the Fermi level shifts towards the valence band. Figure 2-4 shows the thermal activation energy and the pre-exponential factor as a function of the hydrogen pressure. The temperature dependence of conductivity does not follow a linear function on a $\ln\sigma$ vs. 1/T plot, which is consistent with PECVD boron doped a-Si,C:H films (Gutierrez, Carabe, and Gandia 1992). The thermal activation energy derived from the slope of the Arrhenius plot near room temperature depends on the cooling rate of the sample (Ast and Brodsky, 1979). We obtain our thermal activation energy from the high temperature range (150°C) in the Arrhenius plot. We have extended the maximum temperature to 250°C on certain samples, found the same activation energies. The thermal activation energy reduces from 0.42 to 0.28eV as the hydrogen pressure increases from 0.4 to 8mT, the lowest value reported so far for p^+ a-Si,C:H in the literature (Asano and Sakai 1989, Nakano, et al. 1988, and Thompson 1984). The pre-exponential factor decreases dramatically as P_{H2} increases to 1.5mT and then remain relatively insensitive upon further increase of H_2 pressure.

The Meyer-Neldel rule applies to these conductivity data. We have plotted the exponential pre-factor σ_0 as a function of E_a, as shown in the inset of Figure 2-4; a least mean square fit yields a simple relation $\sigma_0 = 7\times10^{-4}\exp(16E_a)\ \Omega^{-1}cm^{-1}$. The dependence of σ_0 on E_a is similar to that obtained in boron doped PECVD a-Si,C:H films. The Meyer-Neldel rule has been interpreted as a shift of either the mobility edge or Fermi level with temperature. Stronger effects are expected in materials containing a lower gap density of states with well defined structures in energy in the investigated E_F range. The strong dependence of σ_0 with E_a of our p^+ a-Si,C:H films suggests that they have a relatively small defect density.

Our typical best p^+ a-Si,C:H films have the conductivity $2\text{-}8\times10^{-6}\Omega^{-1}cm^{-1}$, $\mu\tau$~$1\text{-}3\times10^{-8}cm^2/V$, E_{Tauc}~1.8-1.84eV and E_a~0.28-0.33eV. The electrical and optical properties of the p^+ a-Si,C:H films are improved compared with PECVD p^+ a-Si,C:H films, the E_a is reduced to 0.3eV while for PECVD p^+ a-Si,C:H film E_a is ~0.4eV. The lower thermal activation energy is expected to improve the open circuit voltage in a p-i-n solar cell.

Microstructural Analysis

The H bonding configuration plays an extremely important role in the structural, optical and electrical properties of the boron doped a-Si,C:H films. Both IR and TE are very informative techniques with respect to the understanding of chemical bonding configurations and thermal

stability of the doped films. We have used both techniques to systematically investigate our p^+ a-Si,C:H films.

Figure 2-5 shows the IR spectra of the boron doped a-Si,C:H films with various H_2 pressures. A significant absorption appears in the wavelength from 580 to 900 cm^{-1}, which have been attributed to Si-H, Si-C and Si-B vibration modes as discussed in details below. The shoulder at 900 ~ 1000cm^{-1} is due to various carbon hydrides modes (Rubel, et al., 1987 and Bellamy 1975). A doublet at 2000-2100 cm^{-1} is attributed to Si-H stretching modes (Langford, et al., 1992). The IR spectra of the doped films show no absorption at 2500 cm^{-1} and 2900 cm^{-1}, which are assigned to B-H and C-H vibration modes, respectively (Carlson, et al., Rubel, et al., 1987). The absorption peak in the range of 580 to 900 cm^{-1} can be deconvoluted into three peaks: 640 cm^{-1}, 700 cm^{-1} and 780 cm^{-1}. Figure 2-6 shows the integrated intensities of 640, 700 and 780cm^{-1} peaks as a function of the hydrogen pressure. It is generally accepted that 640 cm^{-1} is attributed to Si-H wagging mode (Maley, et al., 1989 and Brodsky, Cardona, and Cuomo 1977) and correlated with total H content in a-Si:H films. The analysis of 640 cm^{-1} shows that the H content in the films increases initially, and tends to saturate at high H pressure. As shown in the inset of Figure 2-6, the linewidth of 640cm^{-1} peak reduces as the H pressure increases, and reaches minimum at P_{H2}=8mT. However, the absolute H content determined from Si-H wagging mode is not reliable, since the overlap among 640, 700 and 780 cm^{-1} peaks may introduce error in the deconvolution process.

The absorption near 2000 cm^{-1} consists of a doublet: 2000 and 2100 cm^{-1}. It has been general accepted that 2000 cm^{-1} peak comes from isolated Si-H and 2100 cm^{-1} from Si- H_2 or clustered Si-H vibration (Brodsky, Cartlona, and Cuomo, 1977 and Langford, et al., 1992). The absorption of boron doped a-Si,C:H film is dominated by 2100 cm^{-1} in the investigated composition range, which is much different from that of the undoped a-Si,C:H films. This indicates that the SiH bonding configuration and the microstructure vary upon boron incorporation. Using an oscillator strength for Si-H stretching modes (Maley, et al., 1989 and Langford, et al., 1992), we estimate the H content from Si-H stretching modes. The result is in good agreement with the H content obtained from TE. This reveals that most of the H atoms incorporated in the film are bonded to Si. The featureless IR spectra of boron doped a-Si,C:H near 2900 cm^{-1} wave range supports above argument. The absorption near 2900 cm^{-1} has been attributed to C-H stretching modes. The absence of C-H stretching modes indicates the C-H bond density in the film is beyond the detection limit.

The 700 cm^{-1} peak has been attributed to Si-B bonding in sputtered materials (Shen and Cardona 1981). The deconvolution of the IR spectra shows that the integrated intensity reduces by a factor of 2 as the H_2 pressure increases from 0.4 to 8mT. Using an oscillator strength of Si-B stretching mode ~$1.7x10^{17}cm^{-2}$ (Shen and Cardona 1981), we estimate the Si-B bond density as ~$8x10^{19}cm^{-3}$. With the increase of H pressure from 0.4 to 8mT, the relative amount of Si-B bonds in the film increases from 28 to 42 % of the total boron concentration in the film. The 780 cm^{-1} peak has the most profound

change upon H_2 pressure variation. As the hydrogen pressure increases from 0.4 to 8mT, the integrated intensity of peak 780 cm^{-1} reduces by a factor of 5. It has been reported that the Si-C stretching mode or Si-CH_3 rocking and wagging modes in sputtered a-Si,C:H films are located near 780 cm^{-1} (Gerault, et al., 1983 and Chatarine and Turban 1980). Since the carbon content decreases upon the increase of H_2 pressure, the remarkable decrease of 780 cm^{-1} could be attributed to the decrease of carbon concentration. However, there are some other factors such as B-B bonding in sputtered a-Si:H (Richter, et al., 1976). Since the B-B IR absorption is weak and the boron concentration is small, the large variation of 780 cm^{-1} peak cannot be explained by the change of B-B bonds only. The carbon concentration is several orders of magnitude larger than the boron concentration in the film, the dramatic change of 780 cm^{-1} might be largely due to the Si-C bonding configuration change.

As shown in Figure 2-7(a), thermal H_2 evolution occurs in three peaks in our boron doped a-Si,C:H films which we refer to as low temperature (LT) 350 to 500°C, medium temperature (MT) 500 to 600°C, and high temperature (HT) 630 to 700°C. PECVD a-Si,C:H films display only the LT and HT peaks, the LT peak is related to molecular hydrogen formed at the internal surface of microvoid and followed by a rapid out-diffusion through a network of voids, and the HT peak corresponds to the atomic H atoms diffused through the bulk and desorbed at the film surface (Bullot and Schmidt 1987). We suggest that in sputtered materials the LT and MT peak corresponds to SiH_2 and clustered Si-H release, respectively, and the HT peak corresponds to isolated Si-H release. Figure 2-7(b) shows the peak positions as a function of P_{H2}. At P_{H2} = 0.4mT, the H_2 evolution spectrum is dominated by a HT peak centered at ~700°C, and MT and LT peaks centered at 580°C and 470°C respectively. As the P_{H2} increases to 1.5mT, the HT peak reduces and the peak position remains unchanged. The LT peak starts to increase and shifts to ~430°C with an even broader width. The MT peak reduces and downshifts. As P_{H2} reaches 4mT or above, the HT peak reduces further and moves to about 600°C, the MT peak moves to 500°C and LT peak centers at 350°C. The spectrum of high P_{H2} film is similar to that of a-Si:H film. In order to isolate the effect of doping, we have also plotted the TE spectrum of undoped a-Si,C:H film. The carbon concentration of this film is about 16 at.%. It shows similar peaks with LT centered around 430°C, MT peak at 570°C and HT peak located at ~750°C. The HT peak occurs at a slightly higher temperature compared with the doped a-Si,C:H films. Since the HT peak relates to bulk hydrogen diffusion, the shift might be due to an enhanced H diffusion coefficient in doped films. The mechanism responsible for the peak shift of TE spectra is not clearly understood.

Discussions

The improvements of boron doped a-Si,C:H films by RMS from doped targets can be understood under a surface reaction model. In the reactive magnetron sputtering process, the higher H_2 pressures during the deposition could manufacture a large atomic H flux and impinge to the growth surface, which in turn enhances the surface diffusivity. The deposition precursors could find more energetic

favorable site to attach and more homogeneous structure can be formed. Our ellipsometry study reveals that at high H_2 pressure the surface roughness dimishes much faster than that at low H_2 pressure. This is a evidence of enhanced surface diffusivity at high hydrogen pressure during the deposition. Researchers from our group have deposited microcrystalline Si and microcrystalline SiC by using reactive magnetron sputtering at higher H_2 pressures. The formation of microcrystalline phase needs larger surface mobility and more reconstruction during the growth. This provides an additional evidence of enhanced surface diffusivity under higher H_2 pressure. The variation of electrical and optical properties of our boron doped a-Si,C:H films can be understood in this model.

The thermal activation energy reduces to 0.28eV at P_{H2}~8mT, and the σ_d increases by two orders of magnitude when P_{H2} exceeds 4mT. These results can be easily understood using the above model. At higher P_{H2}, the surface diffusivity increases. The amorphous network tends to be homogeneous and has less weak bonds and bond angle distortions. Therefore the active boron dopants in the films increases and the Fermi level shifts further towards valence band, which increases the room temperature conductivity. Our IR studies provide further evidences of the influence of higher H_2 pressure on the microstructure. For boron doped a-Si,C:H deposited at higher H_2 pressure, the linewidth of IR absorption peaks at 640cm^{-1}, 2000cm^{-1} and 2100cm^{-1} decreases compared with that of films deposited at low H_2 pressure. Since the linewidth of IR absorption is related to the bond angle distortion, the smaller linewidth indicates less bond angle distortion in the film. Another evidence of microstructural variation under high H_2 pressures is the optical bandgap. The E_{Tauc} remains unchanged in the high H_2 pressure range, but from our compositional analysis the H content in the film decreases by ~30% as P_{H2} increases from 4 to 8mT. The apparent constant bandgap must comes from the variation of microstructures in the films.

The optical bandgap of the p^+ layers depends on H content, microstructure and impurity concentrations in the films pressures. (Yang and Abelson 1994) have shown that the hydrogen content in the sputtered a-Si,C:H films determines the optical bandgap for low carbon concentration. The optical bandgaps of the doped films are also linearly with respect to H concentration in our investigated carbon concentration range (~20at.%). The initial increase of bandgap of doped films is due to the H content increase. When P_{H2} exceeds 1.5mT, the bandgap saturates at 1.82eV even though the H content decreases as the P_{H2} increases further, which could be due to the improved microstructures under high H_2 pressures. However, the incorporation of boron could reduce the bandgap: we have deposited undoped a-Si,C:H film with the same carbon and hydrogen concentrations, the E_{Tauc} is ~1.9eV. For the boron doped a-Si,C:H film (~0.7at.% boron) with the same carbon and hydrogen compositions, the E_{Tauc} is ~ 1.82eV. For heavily doped a-Si,C:H films (~10 at.% boron), the optical bandgap shrinks further to ~1.7eV. The similar bandgap shrinkage has also been observed in PECVD boron doped films (Uthana, Schroder, and Oechsner 1991, Asano and Sakai 1989, Nakano, et al., 1988, and Li, et al., 1994). The actual cause of the bandgap shrinkage is unclear, the increases of B-B bonds may reduce the bandgap as argued by (Nakano, et al., 1988).

However, the microstructure change induced by the boron incorporation may also play an important role to the optical bandgap. We believe that the variation of the optical bandgap in the p^+ a-Si,C:H films comes from the mixed effects of hydrogen, boron incorporation and microstructure.

The increase of doping efficiency at high H_2 pressure can be attributed to several factors. First, as the H pressure reaches 4mT, the surface diffusivity of precursors increases. The deposition species may find a low energy site to stay, and thus form a better amorphous network. Our IR result shows that the relative Si-B bond density with respect to the boron concentration in the film increases as the H pressure increases. The amount of active dopants (fourfold symmetry) may increases even though the total boron concentration decreases under high H_2 pressures, which subsequently increases the doping efficient. Second, the amount of B-B bonds could also be reduced by the increase of H pressure. For powder pressed boron and Si target, the boron clusters can be sputtered off the target and incorporated into the film. The IR analysis of heavily doped films (~20 at.% boron) shows that the B-B vibration mode at 780 cm^{-1} appears, and it decreases at the H_2 pressure increases. Since the boron content in our doped a-Si,C:H film is relatively small (< 0.2 at.%), the influence of B-B bonds on doping efficient may be small. Finally there may exist some microcrystal phases in the film at this H pressure range, which will explain the apparent increase in the doping efficient. Selected films have been checked by x-ray diffraction technique. The result shows that our p^+ a-Si,C:H films are amorphous under the detection limit of x-ray apparatus. We believe that at high H pressure (4-8mT) the huge amount of atomic H atoms dissociated by the plasma affects both the microstructure and the boron incorporation during the deposition, consequently increases the doping efficient.

Previously Moustakas et al., investigated the doping of a-Si:H by rf diode sputtering from doped targets (Moustakas 1986). Their results show that the doping from doped target is much less efficient than the gas phase doping. The σ_d for boron doped a-Si:H is two orders of magnitude smaller than that of gas phase doping. The apparent difference between rf diode sputtering and reactive magnetron sputtering may account for the current results. In reactive magnetron sputtering, the operating pressure is several mTorr, while the diode sputtering uses a much higher working gas pressure (~100mTorr). The particle transport could be significantly different between these two techniques. We attribute our success in RMS doped a-Si,C:H to the optimized deposition process.

Our results indicate that the boron doping can be achieved in reactive magnetron sputtering through a powder pressed doped target. The doping efficiency increases as the P_{H2} exceeds 4mT under our deposition conditions. Best boron doped a-Si,C:H films are obtained in RMS at P_{H2}~4-8mT with T_s=230°C. The optimized boron doped a-Si,C:H films are better compared with PECVD boron doped a-Si,C:H films, the activation energy for the sputtered doped films is ~20% lower than that of PECVD doped films. We interpret the results by an enhanced surface diffusivity at higher P_{H2}. The growth species might found an energetically more favorable site to stay, and the amorphous network tends to be more homogeneous. Therefore the doping efficiency is increased.

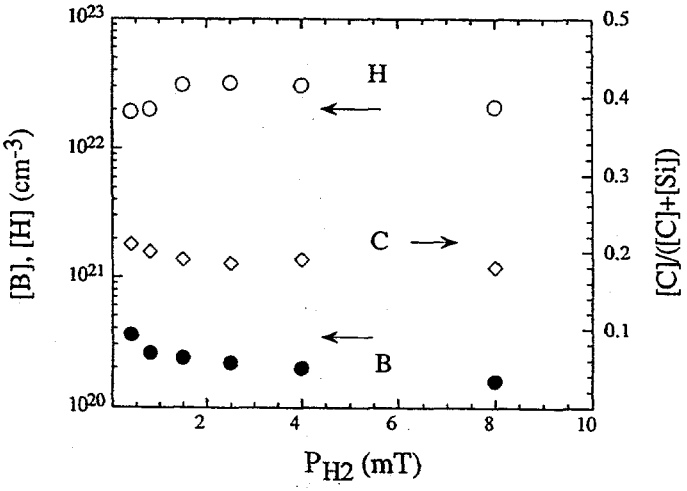

Figure 2-1 The composition analysis of p+ a-Si,C:H films for various hydrogen pressures prepared by reactive magnetron sputtering.

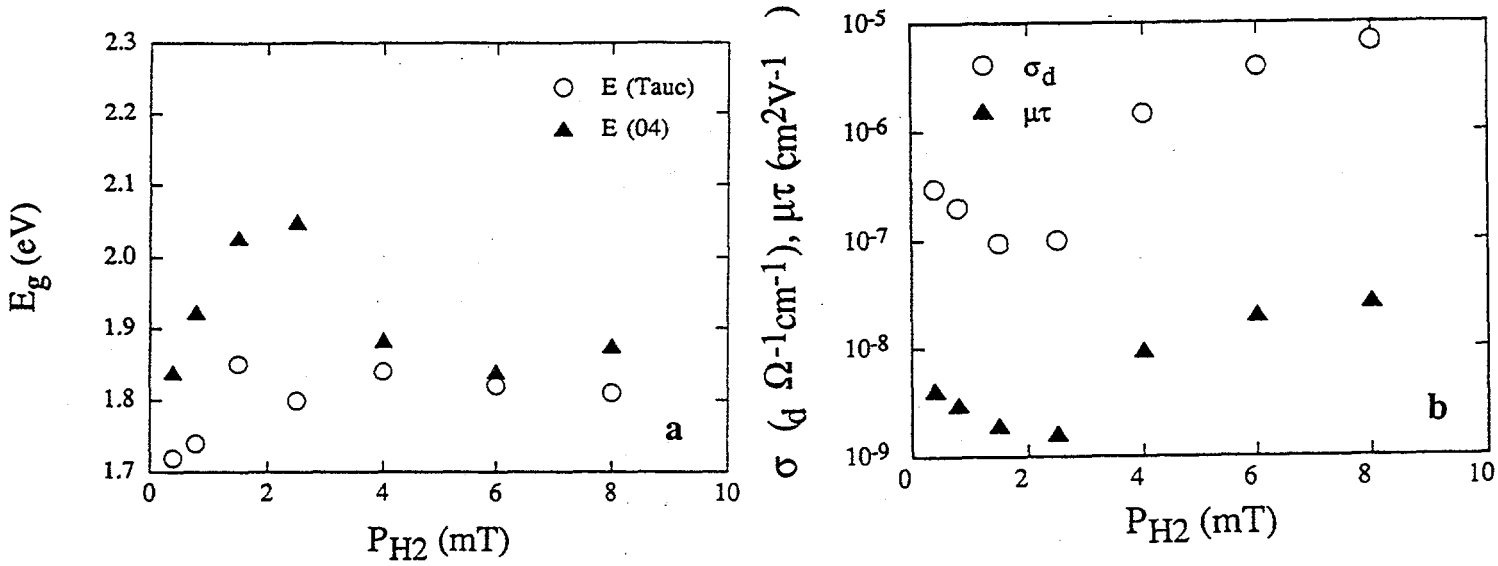

Figure 2-2 (a) The optical bandgap (E_{Tauc}, E_{04}) as a function of hydrogen pressure. (b) The room temperature conductivity and $\mu\tau_e$ as a function of hydrogen pressure.

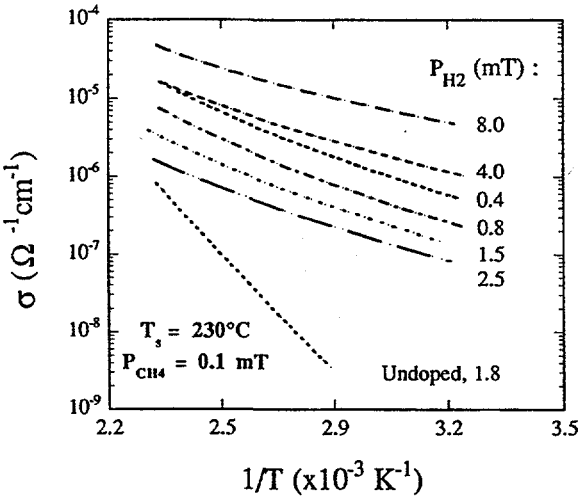

Figure 2-3 The temperature dependence of the conductivity of p⁺ a-Si,C:H film with various hydrogen pressures. The conductivity spectrum of undoped a-Si,C:H film is also plotted against the temperature.

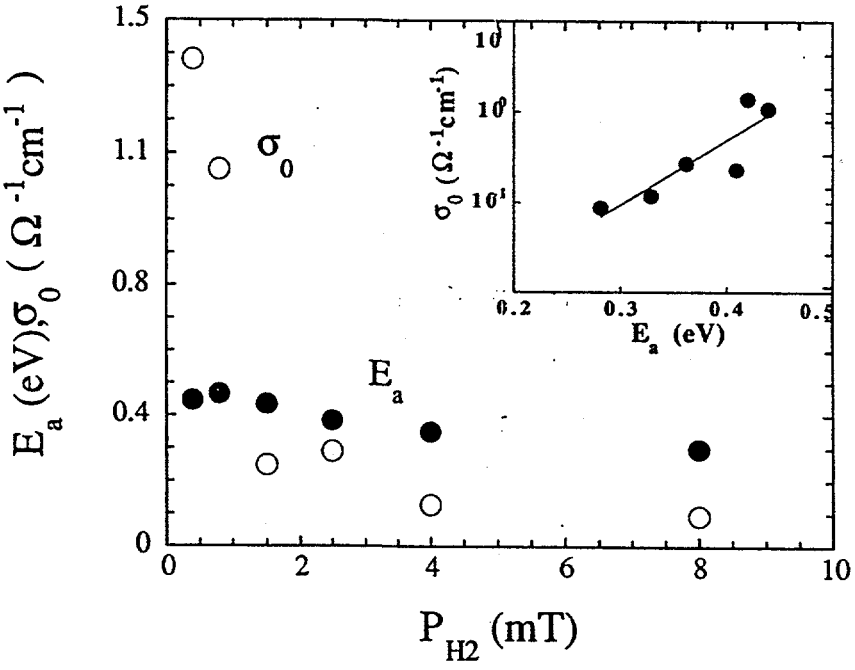

Figure 2-4 The thermal activity energy E_a and the conductivity prefactor σ_0 are plotted against the hydrogen pressure. The inset shows the relation of the prefactor σ_0 as a function of E_a.

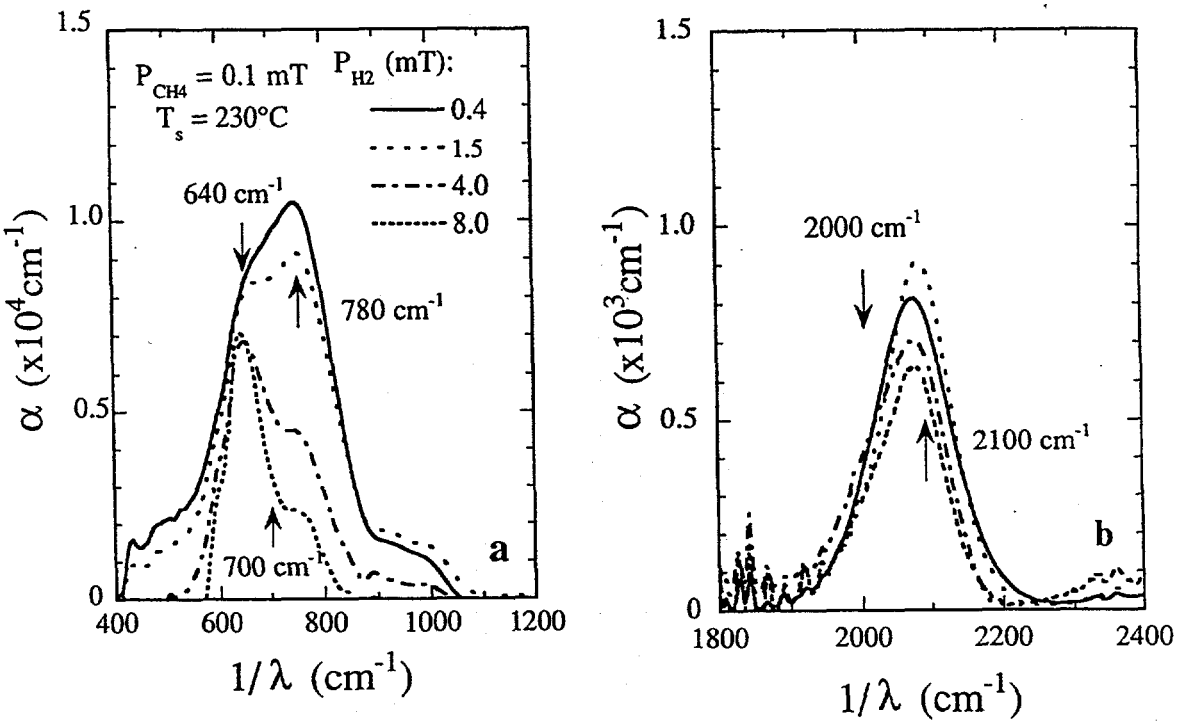

Figure 2-5 (a,b) The infra-red spectra of p⁺ a-Si,C:H films with a series hydrogen pressures. The arrows indicate the dominant peaks in the wave length range.

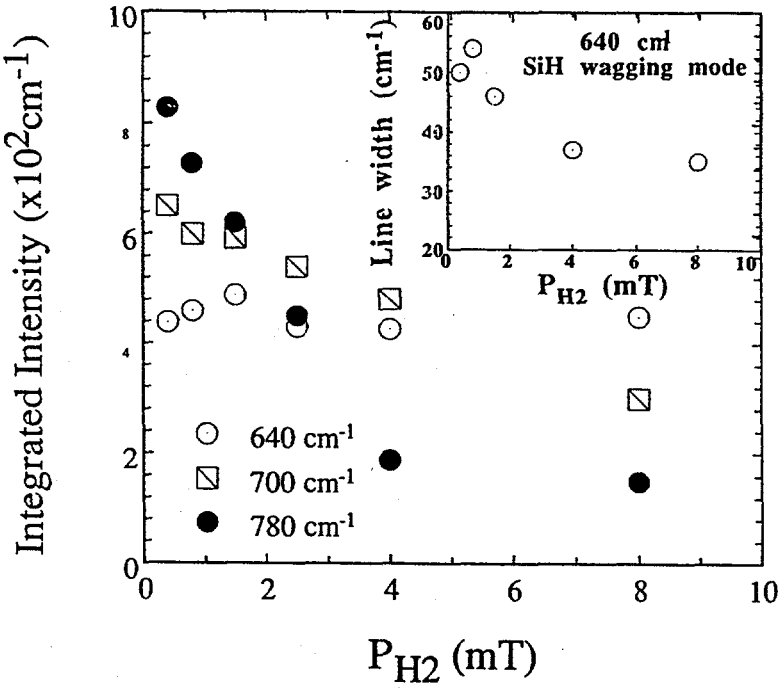

Figure 2-6 The integrated intensities of 640, 700 and 780 cm⁻¹ peaks as a function of the hydrogen pressures. In the inset the line width of 640 cm⁻¹ peak are plotted against the P_{H2}.

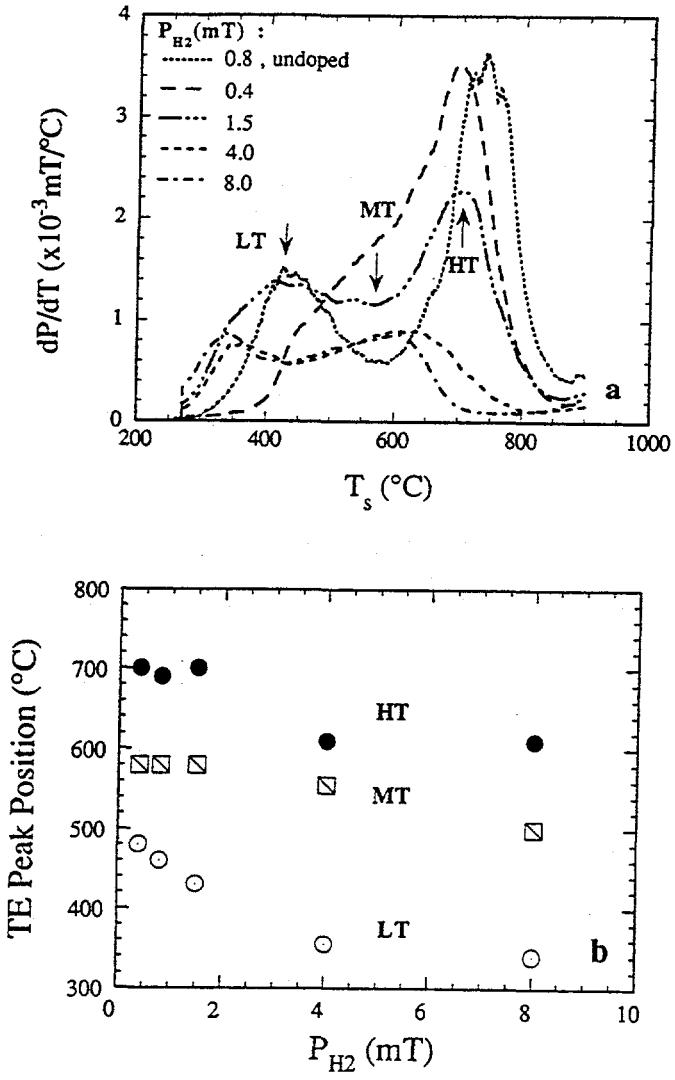

Figure 2-7 (a) The hydrogen thermal evolution spectra of p⁺ a-Si,C:H films as a function of the hydrogen pressure. The thermal evolution spectra of undoped film is also shown. (b) The thermal evolution peak positions are plotted as a function of H_2 pressure.

Chemical Reduction of TCO Substrates

Introduction

The interface between p-type a-Si:H or a-Si,C:H films and transparent conductive oxide (TCO) coated substrates plays an important role in a-Si:H device technology. The two materials of current interest are tin oxide (SnO_2) and zinc oxide (ZnO). Both are degenerate semiconductors with high conductivity and high transparency in the visible light range; SnO_2 is currently used as the transparent electrode in p-i-n amorphous silicon solar cells.

It is technologically desirable to deposit p^+ μc-Si,C:H/TCO as the top contact in the wide bandgap p-i-n cell. This involves (i) developing a method to grow p^+ μc-Si,C:H, and (ii) adapting that method for TCO substrates such that the interface has high optical transmission and low contact resistance. As a first step, we have grown μc-Si:H/ZnO by RMS, and investigated the microstructural features using in situ ellipsometry. We expect that the characteristics of this interface will strongly resemble those of μc-Si,C:H due to the large quantity of hydrogen used in all μc- film growth. The key issues are (i) does the ZnO suffer any chemical reduction, and (ii) does the μc-Si:H nucleate directly on the ZnO, or only after the formation of an a-Si:H interfacial layer?

Here, we deposit a-Si:H by reactive magnetron sputtering (RMS) of a Si target in an (Ar + H_2) atmosphere (Abelson, et al., 1991). This process produces high quality a-Si:H films (Pinarbasi, et al., 1989a), and allows independent control of the H flux via the partial pressure of H_2 injected in the discharge. To determine the effects of plasma-generated H on TCO substrates, we deposited a series of films by RMS as a function of hydrogen partial pressure, from zero (a-Si) to 0.8 (a-Si:H) to 5.3 mTorr (μc-Si:H). Specular SnO_2 and sputtered ZnO substrates were supplied by Solarex.

Several studies of a-Si:H growth on SnO_2 by PECVD have found elemental tin at the a-Si:H / SnO_2 interface (Thomas and Catalano 1983, Koinuma, Nakano, and Gonda 1990, Kawabata, et al., 1988, Eicke and Bilger 1988, and Kumar and Drevillon 1989). By in situ XPS, Koinuma, et. al. found that a-Si:H was partially oxidized as it grew to a thickness of about 15Å, while the SnO_2 bottom layer was reduced to metallic Sn and SnOx ($0<x<2$) (Koinuma, Nakano, and Gonda 1990). Kumar and Drevillon used real time ellipsometry to infer that the substrate temperature is the most important deposition parameter influencing the reduction of tin oxide (Kumar and Drevillon 1989). The reduction of SnO_2 is generally attributed to hydrogen in the SiH_4 plasma, based in part on H plasma exposure experiments (Thomas 1983, and Major, et al., 1988). However, these experiments do not reveal the role of Si in SnO_2 reduction.

In the present study, we deposit thin amorphous silicon layers on SnO_2 or ZnO coated substrates in a RMS chamber under different conditions, especially in the absence of hydrogen. All the depositions

are monitored by real time in situ ellipsometry (Feng, et al., 1992a), and the chemical states at the a-Si:H / SnO_2 interface are examined by XPS in a separate system.

Experimental

Nominally specular SnO_2 films, 0.2 μm thick, and over 85% transmission in visible light range, deposited on corning glass substrates were provided by Solarex Corporation for the present experiments. A 5 cm diameter silicon target is sputtered by Ar or (Ar + H_2) plasma which is magnetically confined near the target surface. Samples are about 12 cm away from target and heated radiatively by a tantalum wire in the backside. The partial pressure of Ar is always kept at 1.6 mTorr, a constant cathode current 80 mA is used, and the partial pressure of H_2 is varied from 0 up to 0.8 mTorr. Very thin layers of amorphous silicon are usually deposited in our DC magnetron sputtering chamber on SnO_2 substrates for two minutes.

A rotating analyzer ellipsometer (RAE) coupled to the deposition chamber was used to monitor film growth in real time (Feng, et al., 1992a). The results are presented as trajectories of the pseudo-dielectric function with time interval 6 sec at fixed photon energy of 4.5 eV. At this photon energy both a-Si:H and tin oxide are strongly absorbing and ellipsometry is very sensitive to surface layer evolution.

XPS (PHI model 5400) is performed in a separate system to directly determine the chemical state at surface of the Si layer deposited on the SnO_2. Spectra were excited with a Mg Kα X-ray source operated at 400 W input and obtained at 17.9 eV pass energy, 0.05 eV increment, 100 ms dwell and 40 scans; the photoelectron take off angle is fixed at 45 degrees.

Results and Discussion

$Sn_{3d5/2}$ core level spectra taken from two samples are shown in Figure 3-1. The amorphous silicon films were deposited at the same substrate temperature (210°C). The difference is in the hydrogen partial pressure: sample (a) is deposited with 0.8mTorr H_2, which leads to 20% atomic concentration of hydrogen in the bulk film (Feng, et al., 1992a). Sample (b) is grown with no hydrogen. Figure 3-1 shows that $Sn_{3d5/2}$ spectra can be deconvoluted into two Gaussian-Lorentz line peaks: the major peak at 487 eV is due to photoelectrons emitted from the oxidized form, SnO_X, and the chemically shifted peak at 485 eV binding energy is from metallic Sn°. The area ratio under these two components is 64 : 36 for a-Si:H / SnO_2 and 91 : 9 for a-Si / SnO_2 . Thus there is more metallic tin at the a-Si:H / SnO_2 interface. The total $Sn_{3d5/2}$ core level signal from a-Si:H / SnO_2 is much larger than that of a-Si / SnO_2 in Figure 3-1. This results from a smaller Si thickness because the deposition rate is lower when there is hydrogen in the plasma; under the same conditions on glass substrates, we calculate that the deposition rate for a-Si is 55 Å/min, while for a-Si:H is just 38 Å/min .

Figure 3-2 shows the real time ellipsometry trajectories recorded for the two films shown in Figure 3-1; the starting points A and B are slightly different due to different surface roughness of the SnO_2 substrates. For the initial stages of a-Si:H deposition on SnO_2 by PECVD, Kumar and Drevillon observed kinks in the ellipsometric trajectories (Kumar and Drevillon 1989). They attributed this to reduction of SnO_2 by H in the SiH_4 plasma. For a simple interpretation, the horizontal displacement indicates tin formation, while vertical displacement indicates that Si deposition takes place. In Figure 3-2, we observe similar kinks for the deposition of a-Si:H and a-Si on SnO_2 by RMS; and this kink is more pronounced for a-Si:H deposition. These ellipsomerty results agree with XPS results in Figure 3-1 that Si flux alone can reduce tin oxide, however, when H is present in the plasma, a much stronger reduction reaction produces more reduced tin.

Figure 3-3 shows another two ellipsometry trajectories. One is SnO_2 exposure to H plasma at 210°C, the ellipsometry trajectory is very flat, after one hour exposure, the transmission of the SnO_2 substrate drops to less than 25% in the visible light range, this clearly indicates the existence of a strong absorbed metallic tin layer. The other one is during an a-Si film deposited on SnO_2 at room temperature, no kink is observed in this case, therefore there is much less or no reduction reaction at all. This indicates that the reduction reaction of SnO_2 substrates by Si in magnetron sputtering is dependent on the deposition temperature. The detailed mechanism behind the reaction is not clear. If the reaction is directly driven by the low energy bombardment associated with the Si flux, there should not have such temperature effect.

Additional XPS investigations on unhydrogenated amorphous films have been carried out for deposition temperatures varied from 22°C to 322°C. For each deposition, the temperature was randomly picked among this range to minimize the possible effects due to chamber wall history. During each 2 min deposition, the cathode current was kept at 40 mA, and the floating voltage at the substrate holder remained at -42 V, which indicated that the plasma conditions were essentially identical for all samples. Figure 3-4 shows three XPS $Sn_{3d5/2}$ spectra taken from these samples. As the deposition temperature increases, the Sn° shoulder grows; the total $Sn_{3d5/2}$ core level signal also increases with temperature which implies a thinner Si overlayer on the a-Si / SnO_2 interface. Standard Gaussian-Lorentz curve fitting was carried out to deconvolute each spectrum into two components as in Figure 3-1. We obtain the spectral intensity ratio $\eta = I_{Sn}° / (I_{Sn}°+I_{SnOx})$, where I_{SnOx} refers to the oxidized SnO_x signal intensity, while $I_{Sn}°$ is the Sn° component intensity. Actually the bare substrate SnO_2 is not strictly stoichiometric, giving high conductivity through O vacancy doping, and we found the spectral intensity ratio η_0 to be 0.018.

In order to compare the observations here with previous report by Thomas and evaluate individual role of Si and H flux in SnO_2 reduction (Thomas 1983), we need to estimate the metallic Sn layer thickness. An uniform planar sandwich structure is assumed here without taking account of surface

roughness, photoelectrons from the $Sn_{3d5/2}$ core level are emitted at the interface and proceed through the silicon overlayer and a possible carbon contamination overlayer. Assuming that a uniform slab of elemental Sn of thickness d is formed between a-Si and SnO_2 as shown in Figure 3-5, the $Sn_{3d5/2}$ XPS intensities are expressed as

$$I_{Sn}^{\circ} = \alpha\, I_{Sn}^{\circ}(Sn)\, \{1 - \exp[-d/(\lambda \sin\theta)]\} + \alpha\, \eta_0\, I_{SnOx}(SnO_2) \exp[-d/(\lambda \sin\theta)] \quad (1)$$

$$I_{SnOx} = \alpha\, (1-\eta_0)\, I_{SnOx}(SnO_2) \exp[-d/(\lambda \sin\theta)] \quad (2)$$

where λ is the electron escape depth in Sn layer, θ is the photoelectron take off angle, α is the common attenuation factor due to the Si overlayer, $I_{Sn}^{\circ}(Sn)$ is the intensity from pure Sn, while $I_{SnOx}(SnO_2)$ is the intensity of $Sn_{3d5/2}$ core level signal (including both Sn° and components) from SnO_2 substrate. To a first order approximation, $I_{Sn}^{\circ}(Sn) = 3\, I_{SnOx}(SnO_2)$, i.e., the intensity of $Sn_{3d5/2}$ core level signal is proportional to the molar fraction of Sn in the host material. Therefore,

$$d = -\lambda\, \mathrm{Sin}\theta\, \ln\{\, 3\,(1-\eta) \,/\, [3\,(1-\eta) + (\eta-\eta_0)]\,\} \quad (3)$$

It is noticeable that the common attenuation factor α is canceled out in Equation (3) because we assume there is no diffusion of Sn into a-Si layer. Adapting the same value 39 Å for λ as Thomas used in reference (Thomas 1983), we obtain the equivalent Sn interface layer thickness d, shown in Figure 3-5 for various deposition temperatures. It is very obvious that when the temperature goes up, d increases. These values of d obtained here are always much less than those for bare SnO_2 reduced by the H plasma treatment: Thomas finds 8 Å (about 4 monolayers) after 2 min H exposure (Thomas 1983).

The reduction of SnO_2 at the interface between a-Si:H and SnO_2 has very important implications on solar cell technology. The excessive Sn layer at the interface will severely reduce the mount of light penetrating to reach the active layer in the solar cell, and directly degrade the device performance; on the other hand, the metallic tin can act as recombination centers which lead to decrease the efficiency of collecting electrons and holes generated in the absorbing layer. There is a possible way to minimize the reduction of SnO_2 by RMS. Katiyar, *et al.*, studied hydrogen incorporation mechanisms by *in situ* FTIR, and found that the H flux in RMS can penetrate about 50 Å deep in the subsurface region and post-hydrogenate a-Si layer (Katiyar, et al., 1992). This suggests that we can grow a thin a-Si on SnO_2 and then turn H_2 on during the growth. However, the feasibility of this method will also depend on the electric properties of post-hydrogenated silicon layer, and future studies are needed.

For deposition on ZnO substrates, no reduction was found under any conditions, including very high hydrogen pressures. Ellipsometry data were taken for the growth of μc-Si:H / ZnO; a nucleation-coalescence model provided the best fit (Yang, et al.). For the initial growth, the μc-Si:H film appears

porous with a 20 % void content, and the film coalesces at 100 Å. The surface roughness, which is the "residue" of the nucleation and coalescence, decreases exponentially to ~ 50 Å when the film reaches 250 Å thick. The rough film morphology would be detrimental in p-i-n solar cells, where the p^+ layer is a few hundred angstroms thick. For the growth of a-Si and a-Si:H on ZnO, the trajectories are also fit by the nucleation-coalescence model, but with a smaller coalescence thicknesses (~ 60 Å). For all three cases, the coalescence thickness is far larger than on SnO_2 or c-Si substrates, where ~ 20 Å is found. We thus attribute the initial growth behavior to the ZnO substrate.

In conclusion, it is observed from both ellipsometry and XPS measurements that both H and Si fluxes in RMS can reduce SnO_2 to elemental Sn; compared to reactive H atoms, the role of Si in reduction is a secondary effect. For a-Si deposition, a simple estimate of the reduced Sn layer thickness is just a half monolayer at 322°C, and much less at room temperature. No reduction is found for growth on ZnO under any conditions, but the initial nucleation-coalescence behavior is relatively rough.

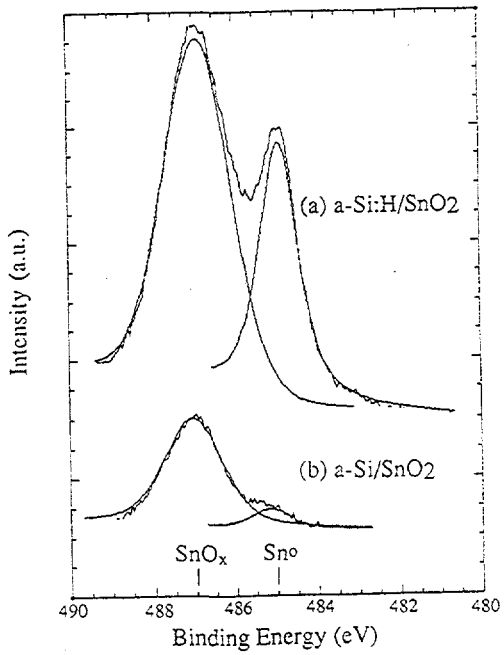

Figure 3-1. XPS spectra of $Sn_{3d5/2}$ at (a) a-Si:H/SnO_2 interface and (b) a-Si/SnO_2 interface.

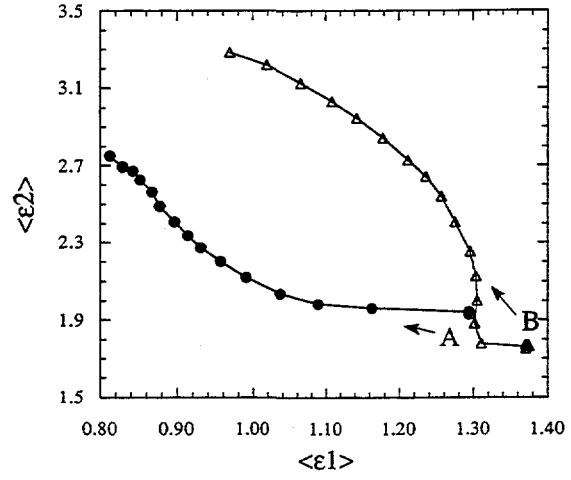

Figure 3-2. Ellipsometry trajectories recorded for the two samples shown in Figure 1. • points refer to 2min deposition of a-Si:H on SnO_2, P_{H2} = 0.8 mTorr. Δ points refer to 2min deposition of a-Si on SnO_2, P_{H2} = 0 mTorr. The other conditions are: P_{Ar} = 1.6 mTorr, $I_{cathode}$ = 80 mA, T_S = 210°C.

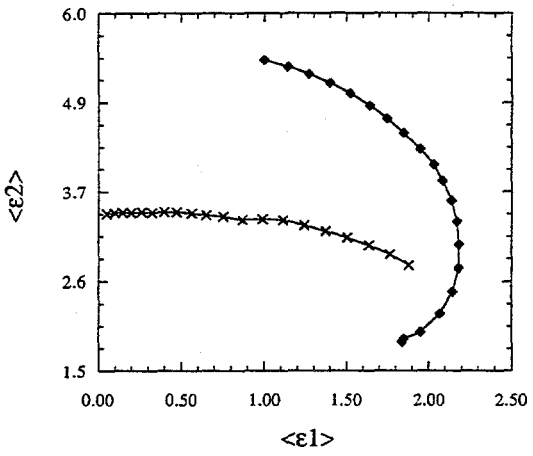

Figure 3-3. Real time ellipsometry trajectories of a-Si film deposited on SnO_2 at 22°C (♦ points) and SnO_2 exposed to H plasma at 210°C (× points).

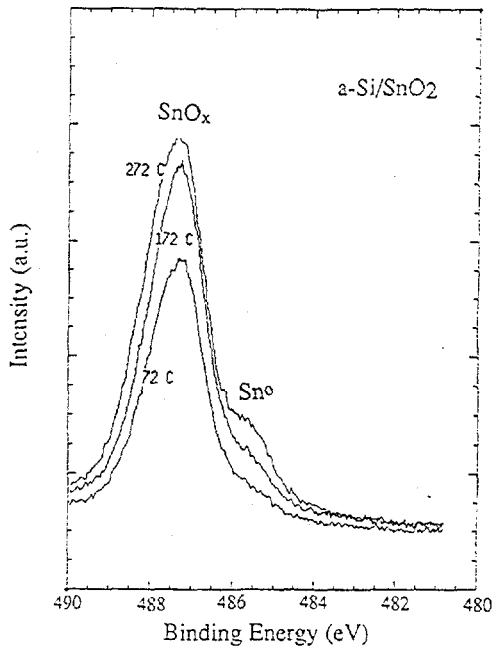

Figure 3-4. XPS spectra of $Sn_{3d5/2}$ for thin layers of a-Si deposited on SnO_2 substrates at different temperatures.

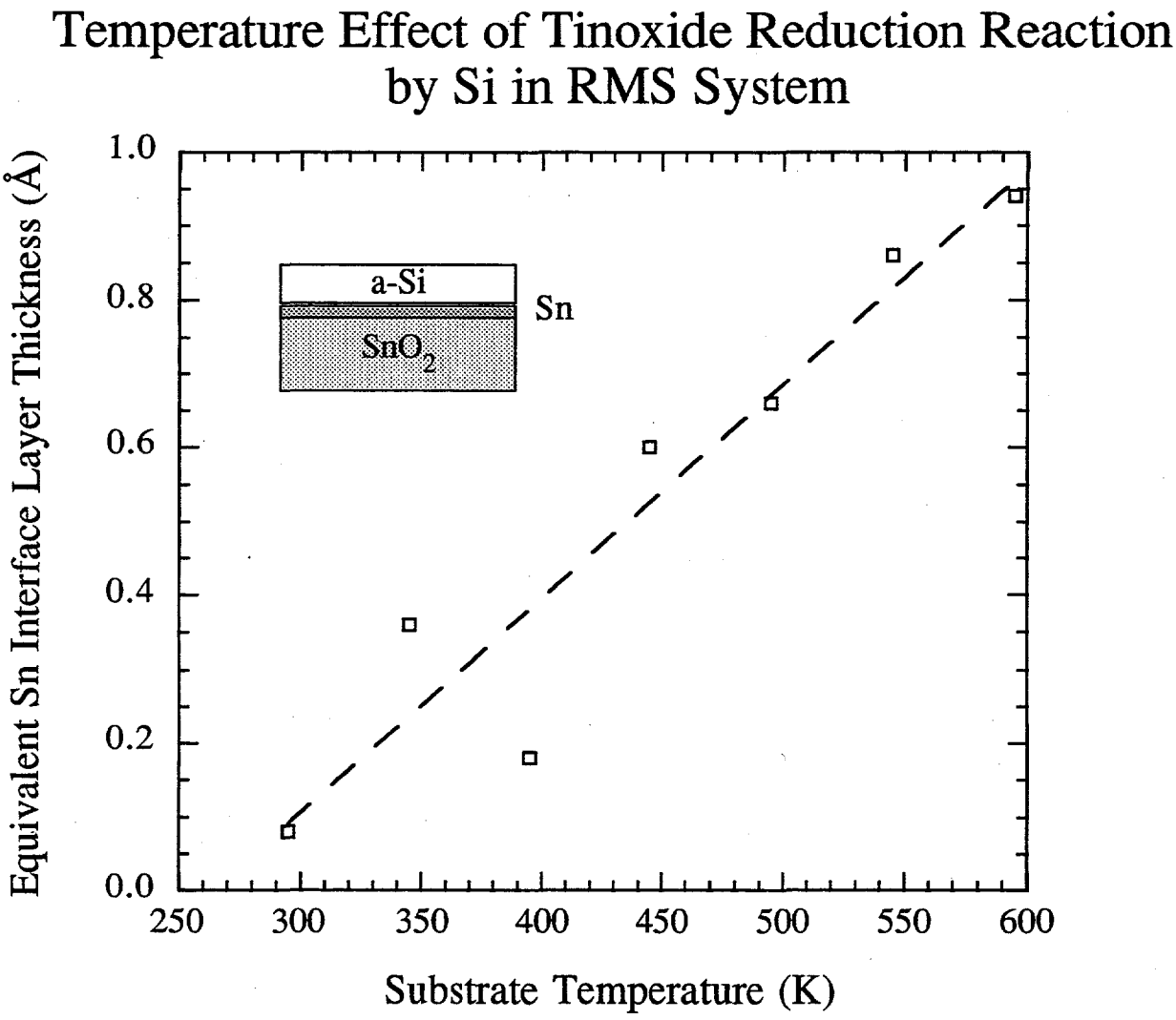

Figure 3-5. Equivalent reduced Sn interface layer thickness d vs deposition temperature T_s.

Sub-surface Transformation of a-Si:H to μc-Si:H

Both plasma enhanced chemical vapor deposition (PECVD) and reactive magnetron sputtering (RMS) produce fine grained polycrystalline, dubbed microcrystalline Si (μc-Si:H) under conditions of high H_2 pressure ("dilution") in the growth plasma and moderate substrate temperatures (~200°C) (Matsuda 1983, Saito, et al., 1984, Logothetidis and Kiriakidis 1988, Wang, et al., 1989, Banerjee, et al., 1989, and Feng, et al., 1992b). μc-Si:H can be doped more efficiently than amorphous silicon (a-Si:H), and the existence of a low temperature growth process makes μc-Si:H attractive for a wide range of opto-electronic applications, especially solar cells (Guha, et al., 1986 and Hamasaki, et al., 1984). The general view is that H atoms, abundant in the H_2-rich plasma, contribute directly to the low temperature formation of μc-Si:H. However, the specific behaviors of atomic H remain controversial due to a lack of detailed in situ data. There are three schools of thought. First, Veprek et al., have shown that H atoms etch Si to form a volatile species, and propose that a "partial chemical equilibrium" between deposition and etching exists at the growing film surface (Veprek, et al., 1981 and Veprek, et al., 1988); if a-Si:H is preferentially etched, as proposed by Tsai et al., then only μc-Si:H survives (Tsai, et al., 1989). Second, Matsuda suggests that the flux of H atoms increases the dynamic H coverage of the growing surface, which in turn enhances the surface diffusion of ad-radicals such as SiH_3, which in turn leads to μc-Si:H rather than a-Si:H formation (Matsuda 1983). Third, Shibata et al., suggest that H atoms penetrate several layers below the growing surface and promote a sub-surface transformation of a-Si:H into μc-Si:H, which they term a "network-propagation reaction" or "H chemical annealing (Shibata, et al., 1987)."

In this section, we report the spectroscopic ellipsometry measurements during the growth of μc-Si:H on a-Si:H by reactive magnetron sputtering of a Si target in (Ar + H_2). We previously identified the region of parameter space which produces μc-Si:H in our system, i.e. substrate temperature T_S = 150 - 300°C and hydrogen partial pressure $P_{H2} \geq 4$ mTorr (Feng, et al., 1992b). A similar region exists for PECVD growth, although the phase boundaries are not exactly the same (Matsuda 1983). For the depositions in this section, the following conditions are used: Ar partial pressure P_{Ar} = 1.6 mTorr and T_s = 210°C; for a-Si:H deposition, P_{H2} = 0.8 mTorr; for μc-Si:H deposition P_{H2} = 5.3 mTorr.

Ellipsometry is a powerful technique to characterize both thin film and interface microstructures, and to provide feedback for process control (Aspnes, Theeten, and Hottier 1979, Collins 1989, and Feng, et al., 1992) The interpretation of ellipsometry data is dependent upon the dielectric contrast between the different layers or the different constituent phases. We previously derived such data for our RMS deposited Si films. Figure 4-1 shows the reference dielectric function spectra for two a-Si:H films of different hydrogen contents (C_H) and a μc-Si:H film; in the following analyses, an accuracy of 10Å in thickness and 5 volume % in composition can be obtained using these reference spectra. The original experimental data have been converted to "bulk" values by subtracting the contribution from the surface roughness layer, as described by Feng et al., (Feng, et al., 1992) As C_H increases in a-Si:H, the

peak decreases and shifts slightly to the blue as H alloying changes both the valence and conduction band densities of states. The dielectric spectrum of the μc-Si:H film is strongly modified from that of bulk c-Si due to finite size effects in the small grains. From X-ray diffraction measurements, we know that the μc-Si:H film used to deduce this reference data was free of any amorphous phase due to the lack of the X-ray amorphous peak (Veprek, et al., 1988). And the average grain size, estimated using the Scherrer formula, is about 50 Å.

In this work, we have taken ellipsometric spectra after every minute of deposition by closing the shutter between the plasma and the film. Figure 4-2 shows three representative $<\varepsilon_2>$ spectra: one is the initial a-Si:H film, and the other two are after 4 minutes and 7 minutes growth at higher P_{H2}, respectively. During the first 4 minutes of growth, the $<\varepsilon_2>$ peak continuously lowers and shifts position toward higher photon energies; by comparison with Figure 4-1, this indicates the formation of high C_H a-Si:H on the sample surface. We have fit the measured spectra assuming a "one overlayer" model, using the dielectric function of high C_H (~ 24 at.%) a-Si:H at this substrate temperature as the optical input for this overlayer. This is the simplest model which gives us good fits for the initial growth. More complex models, eg., adding a layer to account for the surface roughness, or including some void fraction in the high C_H layer, improve the spectra fit very little.

For deposition time beyond four minutes, the measured spectra cannot be fit well by this "one overlayer" model. This demonstrates that new phases or microstructures are formed. From Figure 4-2, we can see that the spectrum taken after 7 minutes growth has a shoulder appearing around the photon energy of 4.1 eV. This indicates that there is a contribution from the microcrystalline phase in the newly deposited layer. We therefore introduce a "two-overlayer" model, which works well as shown by the best fits in Figure 4-2. We refer to the upper layer as the μc-Si:H layer, which is composed of a variable composition of μc-Si:H, a-Si:H, and voids; the lower layer is high C_H a-Si:H as before.

Figure 4-3 shows the thickness of the layers as a function of time; over the first four minutes the high C_H a-Si:H layer from the one-overlayer model increases linearly at a deposition rate of 16.2 Å/min. However, the early time data extrapolate to a positive intercept of 45Å. This demonstrates that the high C_H a-Si:H layer actually consists two parts – the newly deposited layer, and the conversion of the a-Si:H substrate surface to a high C_H layer. This post-hydrogenation is not surprising because the RMS growth flux contains a large component of fast (≤ 250 eV) H species, which arise from reflection of H_2^+ ions at the Si target (Abelson, et al., 1991). The implantation of H into the growing film presumably happens throughout the whole deposition, but reaches a steady state with H release events on a scale of seconds. In situ IR observations of H incorporation (Katiyar, et al., in press) and binary collision simulations of fast H interactions with the a-Si:H surface (Abelson, Katiyar and Möller 1994) clearly support this interpretation.

After the initial 4 minutes deposition, the two-overlayer model indicates changes in the thicknesses of the high C_H a-Si:H layer (black dots), and the μc-Si:H layer (triangles). The formation of μc-Si:H is delayed until the high C_H amorphous interface layer builds up during the first 5 minutes of deposition. The dashed line is the total thickness increase for the two overlayers; it is fairly linear both before and after μc-Si:H layer formation, i.e., there is no observed difference in the deposition rates for these two phases. Feng et al., observed by single wavelength ellipsometry that the growth rate of the initial a-Si:H layer was higher than that of bulk μc-Si:H (Feng, et al., 1993). The difference may arise because the earlier study made no attempt to distinguish the contributions from H implantation and μc-Si:H deposition in fitting the real time trajectory. Collins et al., reported that in PECVD, the crystallite nucleation process is also delayed by the formation of 44-75Å low density a-Si:H (Collins and Yang 1989). Because of the limited data contained in the single wavelength ellipsometry trajectory, compositional information can not be derived.

Figure 4-4 shows the details of the μc-Si:H microstructural evolution during the nucleation stage (4–10 minutes), as deduced from best fits to the ellipsometry data. The volume fraction of μc-Si:H jumps up, as expected for nucleation, during the initial 20Å of the μc-Si:H layer growth; the fraction then slowly increases as coalescence proceeds. The void fraction is around 15 volume % during nucleation and drops to ~5 % during the coalescence process. Meanwhile, the thickness of the high C(H) layer decreases until the μc-Si:H layer exceeds 100Å.

The interesting and crucial point for this section is that the high C_H a-Si:H interface layer thickness actually *decreases* by ~40 Å with subsequent μc-Si:H deposition as shown in Figure 4-3. This indicates that a-Si:H can be transformed into μc-Si:H in a sub-surface region after μc-Si:H has nucleated at the growing-film surface. There is no evidence for the role of etching in this sub-surface phase transformation: if a-Si:H were etched away between the μc-Si:H nucleation sites, then we would expect larger values of void content in the μc-Si:H layer and a lower net growth rate; neither of these is observed. We previously observed with in situ IR absorption that a high H content in the near-surface is associated with the nucleation of crystallites (Feng, et al., 1993). Here, the near-surface rapidly achieves a high, steady-state C_H value, followed by μc-Si:H nucleation, then a transformation of near-surface a-Si:H into μc-Si:H and steady-state growth of μc-Si:H. In RMS, the μc-Si:H nucleation and growth process may be assisted by several forms of energy deposition in the film surface, including the translational energy of the sputtered Si, plasma ions, and fast H.

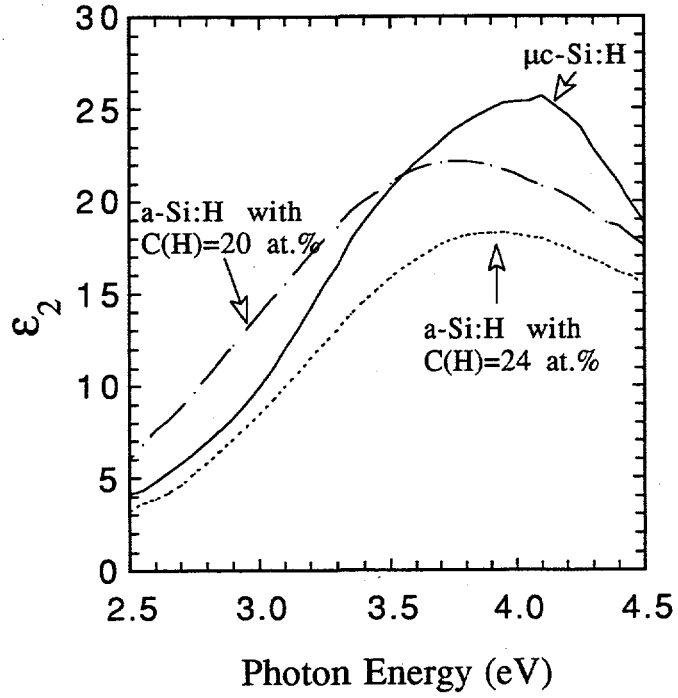

Figure 4-1 Reference dielectric function ε_2 spectra as input for the ellipsometry models, including two a-Si:H films with different H content and the μc-Si:H phase.

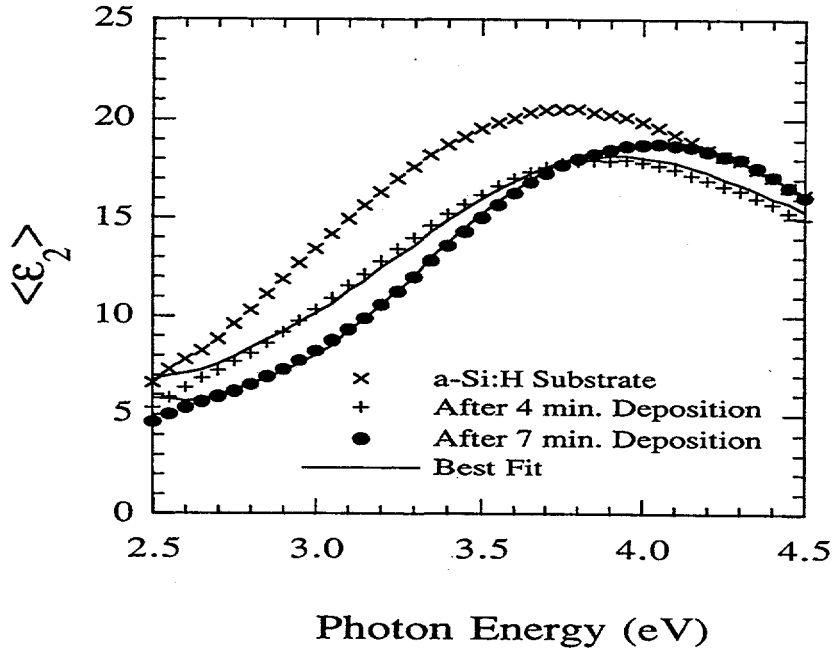

Figure 4-2 The real time $\langle\varepsilon_2\rangle$ spectra with the best fit (solid lines): x stands for the a-Si:H substrate before deposition, + after 4 minutes growth, • after 7 minutes growth.

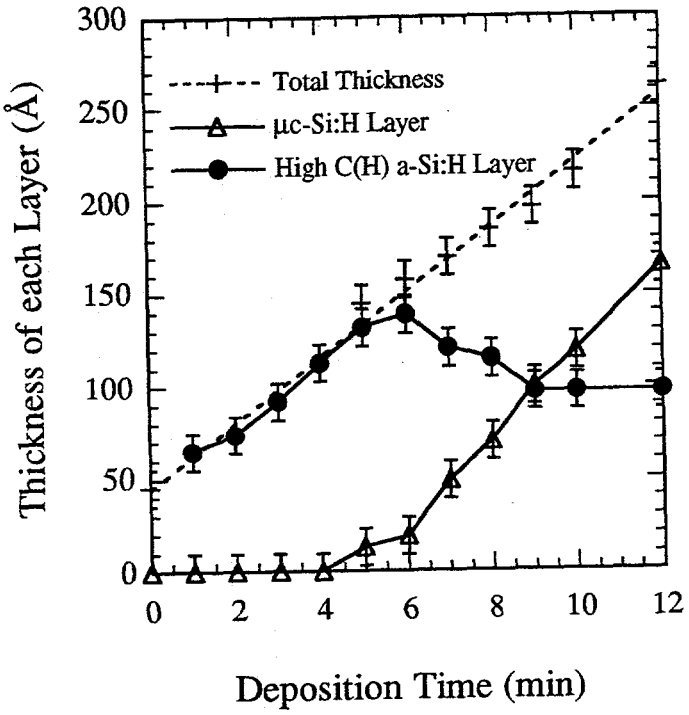

Figure 4-3 The thickness of each layer in the model vs. the deposition time (with error bar). Dashed line is the linear fit to the total thickness of both, solid lines are guides to the eye.

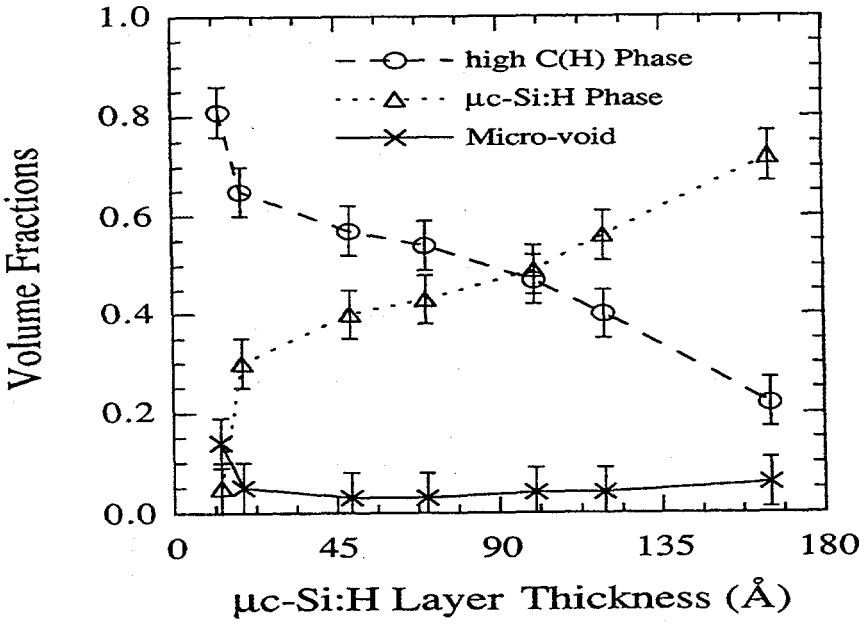

Figure 4-4 The detailed microstructure evolution of the μc-Si:H layer during nucleation & transformation stage (with error bar). Lines are guides to the eye.

Improved Film Adhesion by UV-ozone Substrate Cleaning

Introduction

Hydrogenated amorphous silicon (a-Si:H) and amorphous silicon carbon alloys (a-Si,C:H) are important materials for large area electronic applications including solar cells, thin film transistors, image scanners, electrophotography etc. Various techniques such as glow discharge and reactive magnetron sputtering have been employed to deposit a-Si:H and a-Si,C:H thin films. Different substrates have to be used to study the electronic transport properties and microstructures: films deposited on 7059 Corning glass substrate are used for conductivity, density of states (DOS), and optical absorption coefficient measurements, c-Si substrates are employed for IR absorption spectroscopy and thermal evolution of hydrogen (TE) to study the nature of the hydrogen bonding configurations and to measure the total hydrogen content of the films. Films on c-Si substrates can also be used to determine the growth morphology by scanning electron microscopy (SEM) and impurity levels by secondary ion mass spectroscopy (SIMS).

Substrate cleaning plays an important role in semiconductor fabrication and processing. In particular, the thermal oxidation of silicon and silicon epitaxial growth require very stringent surface cleanliness, and various wafer cleaning techniques have been developed (Wolf and Tauber 1986). By contrast, the surface cleanliness of silicon wafers for a-Si:H and a-Si,C:H film deposition would appear to be much less critical. However, the adhesion of amorphous silicon and alloy films can vary with deposition conditions, such as substrate bias, hydrogen partial pressure, discharge current, etc. In this study, we grow films by reactive magnetron sputtering and focus on the influence of substrate cleaning and ion bombardment on the film adhesion.

Infra-red (IR) absorption is used to study the hydrogen bonding configurations. The Si-H stretching modes can be deconvoluted into two Gaussian peaks centered around 2000cm^{-1} and 2100 cm^{-1} wavenumbers. The 2000cm^{-1} vibrational mode is attributed to isolated SiH bonds and the 2100cm^{-1} mode is attributed to silicon dihydride SiH_2 or clustered Si-H bonds on the internal surfaces of microvoids (Lucovsky, Nemanich, and Knights 1979 and Brodsky, Cardona, and Cuomo 1977). The 2000cm^{-1}/2100 cm^{-1} peak area ratio is recognized as an important signature of the microstructure.

Hydrogen thermal evolution (TE) is one of the most direct methods for measuring the amount of hydrogen in a-Si:H (Fritzsche et al., 1979 and Maley, et al., 1989) The H release process yields information on the SiH_n bond rupture and (to a limited degree) on the diffusivity of H. In a-Si:H, the H effusion around and above 500°C has been identified as the H bonded in the isolated SiH configuration, while the H released at lower temperature has been related the dihydride and clustered SiH (Beyer 1985) The relationship between IR and TE spectra has been found to depend on the growth technique (Beyer, et al., 1983).

Experimental

We deposit thin films of amorphous silicon alloys by reactive dc magnetron sputtering in an UHV chamber which is very similar to the one previously described (Pinarbasi, et al., 1987) a-Si:H is grown by sputtering a Si target in Ar and H_2, and methane (CH_4) is introduced additionally to grow a-Si,C:H. Films were deposited over a wide range of conditions on 1"x1" c-Si (100) wafers.

We compared the following cleaning procedures.

(1) A simple solvent degreasing which employed acetone, IPA (isopropyl alcohol) and subsequent deionized (DI) water rinse.

(2) The standard "RCA" cleanup procedure which is composed of the following steps (Kern 1970):

   (i) Remove gross organics with tetrachloroethylene and residual organic films with an H_2O_2-NH_4OH (basic) solution.

   (ii) Remove metallics with an H_2O_2-HCl (acidic) solution.

   (iii) Rinse thoroughly in deionized water.

(3) Hydrofluoric acid (HF) chemical etching in which silicon wafer is dipped in diluted HF solution (HF:H_2O=1:4 by volume) about 30 to 60 seconds to strip off the native silicon oxide on the surface.

(4) Cycles of dilute HF etching and UV/ozone exposure with a final HF dip. The UV/ozone is produced by a low-pressure mercury lamp which emits UV light in an ambient of air at room temperature (Grunthaner, et al., 1986). A single exposure is about 20 to 30 minutes. The mechanism of the cleaning (Tabe 1984) is the oxidation of hydrocarbon contaminants to form volatile CO_2 and CO. On the other hand, silicon is also oxidized to form SiO_2 which will be stripped off by a subsequent HF dip.

To explore the influence of ion bombardment, films were grown at two different substrate potentials, i.e. electrically grounded and floated. In our system, the anode is biased at +70 volts with respect to ground. We measured the plasma potential as +75 volts and the self-bias of the floated substrate as +60 to +55 volts with a Langmuire probe (Doyle, Nuruddin, and Abelson 1994); so the growing film on the grounded substrate and floated substrate will experience 75 eV and 15 to 20 eV ion bombardment, respectively, for singly charged ions. The ions in the plasma for a-Si:H film deposition are mainly Ar^+ and H_2^+.

The a-Si:H films deposited on c-Si substrates were used for both IR and TE measurements. An ANALECT RFX-65 FTIR spectrometer was used to measure the infra-red transmittance which was

converted to absorption coefficients using the method described by N. Maley (Maley and Szafranek 1990). Hydrogen evolution spectra were obtained by heating up samples of known volume in a quartz tube at a constant rate (15°C/min) and measuring the pressure rise in a closed cell. The rate of H_2 evolution is proportional to the first derivative of the H_2 pressure. The technical details were described previously (Maley, et al., 1989) High resolution SEM micrographs of the film surface morphology were taken with a Hitachi S 800. DEKTAK 3030 stylus surface profilometer with the ability of measuring step height down to a few nm was used to scan the film surface and measure the size of pits where film peeled off. We evaluate the quality of the film adhesion only by whether film peeled off or not, and by the areas of the pits where film peeling occurred.

Results and Discussions

Effects on a-Si:H and a-Si,C:H Film Adhesion

Film adhesion was found to depend on the cleaning procedures and the growth conditions. For simple solvent degreasing cleaning, the deposited a-Si:H and a-Si,C:H films adhered well to their substrates only under growth conditions of low H_2 partial pressure and low deposition rate (low cathode current). Films began to peel off leaving "pits" of various sizes for high hydrogen partial pressure and high deposition rate. The range of pit sizes varied with growth conditions. For example, for the growth conditions of 0.80mTorr H_2 partial pressure, 0.80 ampare cathode current, 275°C deposition temperature and 1.7 mTorr Ar partial pressure, the a-Si:H film deposited on solvent degreased substrate peeled off after it was cooled down to room temperature. The diameter of the pits up to 200μm and the same depth as film thickness were determined by the DEKTAK profilometer. The film adhesion for these growth conditions was improved by both the standard RCA cleaning and dilute HF dip. And the dilute HF dip was found much simpler and more effective than RCA cleaning for both a-Si:H and a-Si,C:H films grown with a wide range of growth parameters. No pits of any size have been found for the a-Si:H films grown on HF etched substrates even with the high resolution (x100K) scanning electron microscopy. However, it was found that a-Si,C:H film growth needs more stringent cleaning than the simple dilute HF dip. The a-Si,C:H film grown on the HF dipped c-Si substrate at the above conditions plus 0.10mTorr CH_4 was found to have a small fraction of peeled off area with pit diameters up to 80μm. Two cycles of 30 minutes UV/ozone exposure and HF dip were employed in this case and found to improve the film adhesion greatly. No part of this film peeled off: no pits were found by either the profilometer or high resolution SEM. These examples are summarized in Table 5-I. These films are 1 to 2 μm thick.

Film adhesion is also effected by the substrate potential. Table 5-II compares two a-Si:H films A and B grown on substrates cleaned by the same solvent degreasing procedure and under the same conditions except that A was grounded and B was floated electrically. The film B grown on the electrically floated substrate did not peel off but some very small bubbles were observed in high

resolution SEM. The radii of the bubbles range from 0.2 to 5 μm. Figure 5-1 shows the surface morphology and the fracture cross section. From this comparison, we conclude that floating substrate significantly improves film adhesion. We interpret this as the effect of reduced intrinsic stress on the film adhesion. It is known that the quality of film adhesion depends not only on the film-to-substrate bond, which is determined by the conditions of the substrate surface and altered by substrate cleaning, but also on the total stress of the film-substrate composite (Thornton and Hoffman 1989). The total stress is composed of thermal stress and the intrinsic stress. The thermal stress is due to the difference of the thermal expansion coefficients of the deposited film and the substrate. The intrinsic stress is produced by nonequilibrium growth processes, hence sometimes it is called growth stress (Nix 1989). The intrinsic stresses of the a-Si:H films have been extensively studied (Hansen 1989). Sputtered amorphous silicon films, both unhydrogenated and hydrogenated, exhibit compressive intrinsic stresses over a wide range of preparation conditions (Ross and Messier 1984 and Windischmann, et al., 1986). With increasing hydrogen partial pressure, the compressive stress of the sputtered a-Si:H films first increases and then decreases. The glow-discharge deposited amorphous silicon thin films exhibit a very similar picture for the intrinsic stress (Matsuda, et al., 1984 and Kakinuma, et al., 1986). Ion bombardment effects on the intrinsic stress of rf-sputtered a-Si:H films have been studied by Ross and Messier (Ross and Messier 1981). They found that compressive intrinsic stress increases with an increase in ion bombardment energy from 15 to 60 eV. In our dc reactive magnetron sputtering system, the growing film is subject to 15 to 20 eV ion bombardment on the floated substrate but about 75 eV on the grounded one. We believe that the compressive intrinsic stress of the film grown on floated substrate must be lower than that on grounded substrate, though we did not directly measure the stress of the films. The reduced compressive intrinsic stress made the film-to-substrate bond capable of withstanding the force produced by the integrated compressive internal stress, even though the film-to-substrate bond is poor due to the poor cleaning procedure. However, the formation of the tiny bubbles on the surface of the a-Si:H film reveals the relatively weak film-to-substrate bond due to the solvent degreasing procedure. Obviously, strain relief occurred during the bubble formation.

Effects on a-Si:H microstructure

We examined the changes in IR and hydrogen thermal evolution spectra on a-Si:H. In the following, we compare the effects of substrate cleaning and substrate potential among the a-Si:H films B, C, and D. They had different combination of substrate cleaning and potential which are shown in Table 5-III. The rest of growth conditions are the same as film B, which has been described in Table 5-II. Figure 5-2 shows the SEM micrographs of the surface morphologies for samples C and D; there is a considerable size difference of the characteristic surface roughness. The hydrogen thermal evolution spectra of the samples B, C and D and their overlays for comparison are shown in Figure 5-3. The hydrogen contents in these films have been determined as 15 atomic% from the total hydrogen pressure released through 800°C. The IR $2000cm^{-1}/2100cm^{-1}$ peak area ratios were obtained by

deconvoluting the stretching modes into two Gaussian peaks after subtracting the linear background, which are shown in Figure 5-4. The results of SEM, IR and hydrogen evolution measurements are summarized in Table 5-III.

The difference of the surface morphology of the a-Si:H films grown at different substrate potentials is a consequence of ion bombardment of the growing films. During film deposition, the topographical features which protrude from the rest of the surface plane, such as over-hangs, are forward sputtered down onto the underlying surface. This is an inevitable consequence of energetic particle bombardment above the threshold for sputtering (typically a few tens of electron volts) (Rossnagel and Cuomo 1989). The growing film on electrically grounded substrate is subject to higher energetic ions (~75 eV Ar^+) therefore would exhibit smoother surface morphology than that on electrically floated substrate.

The IR absorption spectra from samples B and D grown at the same substrate potential show that the $2000cm^{-1}/2100cm^{-1}$ peak area ratio is not effected by the cleaning methods, as expected. However, the hydrogen evolution rates shown in Figure 5-3 are unexpectedly very different at low temperature. A very high but narrow peak at ~ 410°C appeared in the sample B grown on the solvent cleaned substrate. On sample D, grown on the substrate cleaned by HF dip, this peak is much lower and broader, and more H was released at ~700°C. This seems unusual since they were grown under the same conditions and same substrate potentials and there is no difference of the microstructure from the IR measurement. The only difference between these two films is that there are bubbles formed on the film B grown on the poorly cleaned substrate. We believe that these bubbles were formed after film deposition due to the compressive intrinsic stress relaxation on the areas where film-to-substrate bond was relatively poor. It is the stress relaxation that originates the film peeling when the film-to-substrate bond is too poor or the stress is too high. This is the only difference which could be responsible to the sharp and high peak at low temperature and lower H evolution rate at high temperature. Our results show that strain relief to some extent does not alter hydrogen bonding configurations seen in IR but will change the hydrogen thermal evolution processes especially at low temperature.

Comparing the a-Si:H films C and D grown on the substrates cleaned by the same procedure but with different substrate potentials, we found that both the IR absorption spectra and the hydrogen evolution rates at low temperature were significantly altered. This must be attributed to the ion bombardment effect including the implantation of H_2^+ ions. However, less hydrogen were released at low temperature from the film C which has more SiH_2 or clustered SiH bondings shown in $2100cm^{-1}$ mode of IR absorption spectrum, which is unusual. Again, the stress difference could be responsible for this trend. As mentioned earlier, the a-Si:H films grown on electrically grounded substrate are subject to more energetic ion bombardment and shall have higher compressive intrinsic stress, which has been reported in literature and also confirmed above in the case that films grown on electrically

grounded substrate are more easily peeled off. Hence the film D grown on floated substrate should have lower compressive intrinsic stress. This is one more evidence to support that more hydrogen evolves at low temperature for the a-Si:H films with lower compressive intrinsic stress.

Conclusions

Both improved substrate cleaning and decreased ion bombardment improve the adhesion of amorphous silicon alloy films deposited by reactive dc magnetron sputtering. Dilute HF dip of c-Si substrates is a simple and effective cleaning procedure for a-Si:H films grown in a wide range of growth parameters. The a-Si,C:H film growth needs more effective cleaning. Combination of cycles of HF dip and UV/ozone exposure with a final HF dip turns out to be more effective than a simple HF dip. The substrate surface cleaning improves the film adhesion through strengthening the film-to-substrate bond. Better film adhesion is also obtained for films deposited on electrically floated substrates. This is interpreted as the effect of the reduced intrinsic stress due to the lower energetic ion bombardment.

The film surface morphology and microstructure are also influenced by the ion bombardment. The smoother surface of the films grown on electrically grounded substrates is interpreted due to the forward resputtering by more energetic argon ions. However, this more energetic ion bombardment results in more loosely bonded hydrogen in the configurations of silicon dihydride and clustered monohydride.

The hydrogen evolution process, especially at low temperature, is found to be related to the film stress. Films where stress relaxation occurred, or with lower compressive intrinsic stress, evolve more hydrogen at low temperature. Indeed, thermal evolution appears to detect aspects of microstructure that can not be sensed by infra-red absorption.

Table 5-1. Comparison of the effect of substrate cleaning on a-Si:H and a-Si,C:H film adhesion. The a-Si:H films were grown under the following conditions: P_{H2}=0.80 mTorr, P_{Ar}=1.7 mTorr, cathode Current=0.80 Amp, Ts=275°C. The a-Si,C:H films were deposited with additional 0.10mTorr C_{H4}. All of the substrates were electrically grounded.

Film Type	Substrate Cleaning	Adhesion Status Size of Pits
a-Si:H	Solvent Degreasing	Peeling Off up to 200 μm
a-Si:H	Single HF Dip	No Peeling Off
a-Si,C:H	Single HF Dip	Peeling Off up to 80 μm
a-Si,C:H	2 Cycles of HF Dip & UV/Ozone + Final HF Dip	No Peeling Off

Table 5-2. The a-Si:H films A and B were grown on electrically grounded and floated c-Si substrates respectively. The simple solvent degreasing method was used for both substrates. The rest of growth conditions are P_{H2}=0.80 mTorr, P_{Ar}=1.70 mTorr, cathode current = 0.30 Amp, T_S=275°C.

Sample ID	Substrate Potential	Film Adhesion Status
A	Grounded	Peeling Off Pit Size: up to 150μm
B	Floated	No Peeling Off Bubble Radius: ≈ 0.2 to 5 μm

Table 5-3 Summaries of the measurement results for the comparison between films grown with different cleaning and different substrate potentials.

Sample ID	Substrate Status	SEM Surface Morphology	IR2000/2100cm^{-1}	Hydrogen Released at Low Temperature
B	Solvent Degreasing/ Floated	With Bubbles Radius: ≈ 1 μm	3.9	Sharp and High Peak at ≈ 410°C
C	HF Dip/ Grounded	Island Size: 200Å to 600Å	2.6	Very Low Peak at ≈
D	HF Dip/ Floated	Island Size: 500Å to 2000Å	4.0	Broad and Low Peak at ≈ 422°C

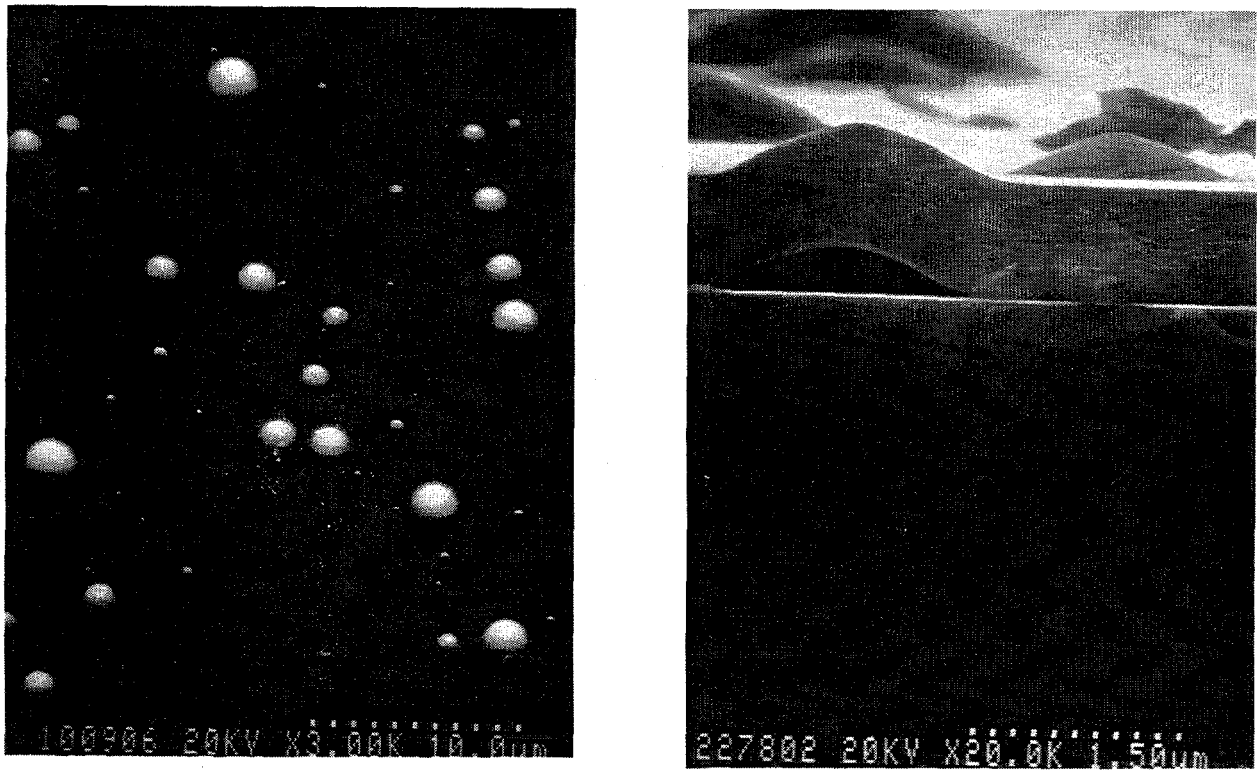

Figure 5-1. SEM micrographs for the sample B grown on electrically floated c-Si substrate. (a) Surface morphology (b) Fracture cross section of a bubble.

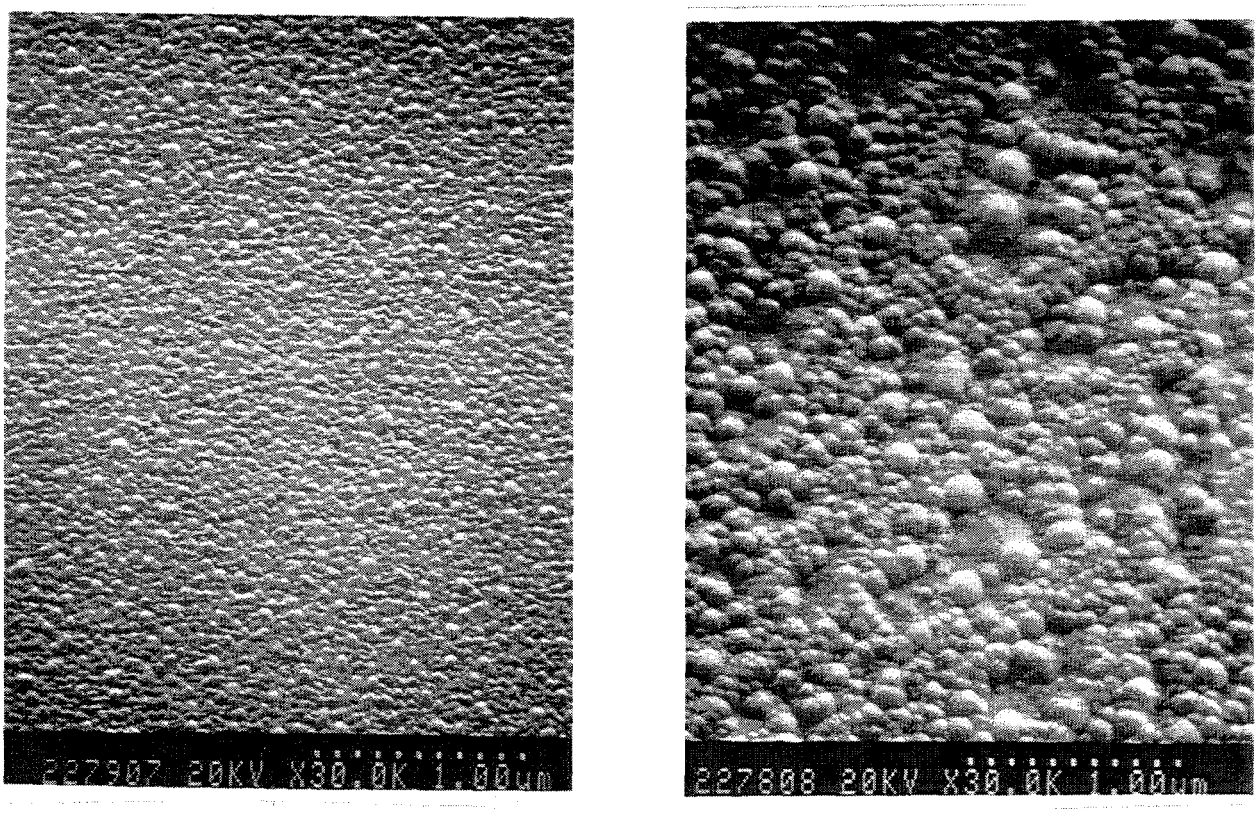

Figure 5-2 The SEM micrographs (a) and (b) of film surfaces for sample C and D respectively.

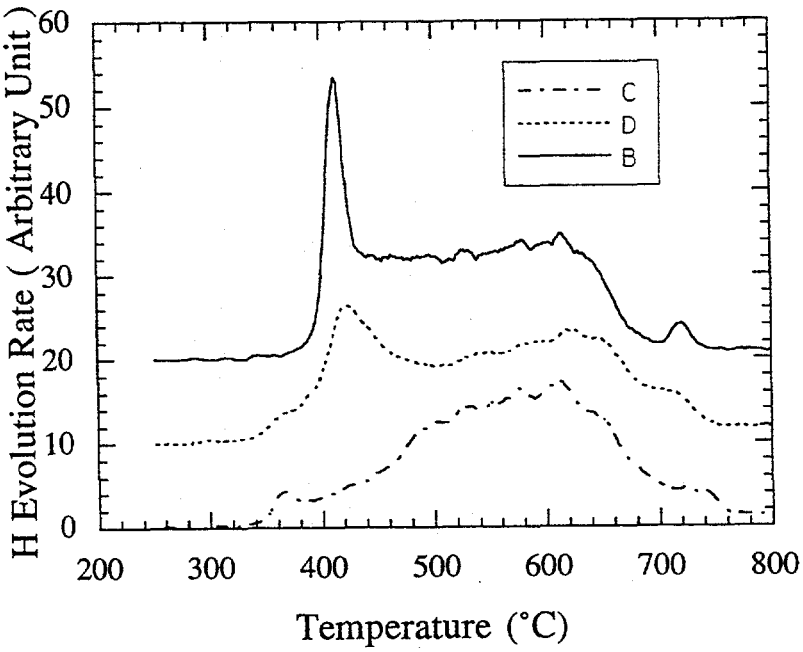

Figure 5-3 Hydrogen thermal evolution spectra for sample B, C and D.

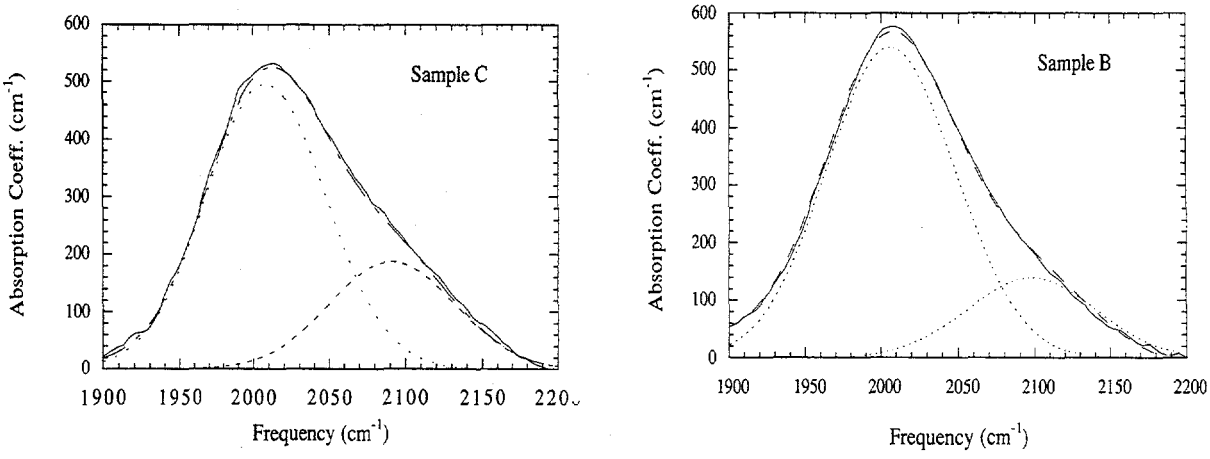

Figure 5-4 Absorption spectra of samples C, and B in the stretching-mode regions.

Conclusions

Growth and properties of wide bandgap a-Si,C:H

We have optimized the quality of a-$Si_{1-x}C_x$:H films grown by dc reactive magnetron sputtering (RMS). Films with a bandgap of 1.9 eV have electronic properties comparable to, or slightly better than, those grown by plasma assisted chemical vapor deposition (PACVD). The micro-structure is very dense and essentially free from CH_x bonding. The discharge current, methane partial pressure, hydrogen partial pressure and substrate temperature have been manipulated in order to separate effects due to the film composition from those due to particular growth variables. The key results are as follows.

Growth temperature

Previous studies of substrate temperature effects in the literature had included implicit compositional changes. a-$Si_{1-x}C_x$:H films of constant composition were deposited at temperatures of 150-325°C; those grown between 230 and 310°C had the best properties.

Optical bandgap

The optical bandgap was found to have a unique linear relationship with hydrogen content for both a-Si:H and a-$Si_{1-x}C_x$:H films. The correlation with carbon content is poor, with considerable experimental scatter. Empirically, the role of carbon incorporation is to increase the hydrogen content above the solubility limit in a-Si:H for a given growth temperature.

Silicon-hydrogen bonding

We found that the electronic properties were not uniquely determined by the ratio of silicon-hydrogen bonding as mono- vs dihydrides. A low amount of dihydride bonding serves as a necessary, but not a sufficient, condition for good electronic quality.

Microvoids

Incorporated H was observed by SAXS to increase the volume fraction of microvoids, and to broaden their size distribution. C incorporation suppressed void formation and reduced the degree of oriented microstructure. RMS deposited a-Si,C:H is more dense than PACVD material.

p-type doping of a-Si,C:H

Excellent p^+ a-Si,C:H films have been deposited from a Si target doped with 1 atomic % B. The properties appear superior to PECVD material. For an optical bandgap of 1.8-1.84 eV, the films have

a thermal activation energy of 0.28 eV, electron mobility-lifetime product of $1\text{-}3\text{x}10^{-8}$ cm^2/V, and room temperature conductivity of $2\text{-}8\text{x}10^{-6}$ $/\Omega\text{-cm}$. As the H_2 pressure increases, the boron concentration in the film decreases by a factor of 3; the highest conductivity occurs for P_{H2} = 4-8 mT.

Chemical reduction of TCO substrates

Spectroscopic ellipsometry and XPS measurements were used to determine the degree to which the H and Si fluxes in RMS reduce SnO_2 to elemental Sn during a-Si:H deposition. Si atoms alone caused a slight reduction: for unhydrogenated a-Si deposition, the atomic Sn layer thickness was ~ 0.5 monolayer at 325°C, and much less at lower temperatures. H atoms led to several monolayers of SnO_2 reduction, increasing with substrate temperature. We deposited μc-Si:H on ZnO substrates and found no chemical reduction under any experimental conditions. However, the coalescence thickness (100 Å) and initial roughness were far larger than for growth on SnO_2 or c-Si substrates. This indicates that the details of the ZnO surface play a critical role.

Sub-surface transformation of a-Si:H to μc-Si:H

Spectroscopic ellipsometry was used to analyze the nucleation and growth of μc-Si:H on a-Si:H, which is important for the "tunnel" junctions between cells in a multi-junction device. We found the first clear evidence for a sub-surface reaction in which ~ 50 Å of a-Si:H is transformed into μc-Si:H, as follows. Upon raising the hydrogen pressure during film deposition, the a-Si:H near-surface rapidly achieves a high hydrogen content, then μc-Si:H nucleates, then the a-Si:H near-surface transforms into μc-Si:H, and finally steady-state μc-Si:H growth occurs. It is thus possible to consume the amorphous transition layer and attain a sharp interface. We found no evidence for the role of etching in this process. The μc-Si:H nucleation and growth process is assisted by the fast H flux during RMS.

Improved film adhesion by UV-ozone substrate cleaning

We used cycles of UV/ozone exposure and dilute HF etching to improve the adhesion of a-Si,C:H films on Si substrates. The UV/ozone cleaning procedure is expected to be effective for other types of substrates, eg., conductive oxides. We also obtained better film adhesion and smoother surface topographies for film deposition on electrically floating substrates, which receive ion bombardment at ~ 20 eV instead of ~ 75 eV for grounded substrates. The improvement in adhesion is attributed to a reduction in the intrinsic stress state. Changes in the hydrogen thermal evolution spectra correlated with the adhesion behavior.

p-i-n device fabrication

As of this writing (after the end of the contract period), p-i-n photovoltaic devices are being fabricated. n^+ films are deposited from a P-doped target, similar to the results on p^+ films reported herein. The devices are grown either with all RMS deposited layers, or with RMS p^+ and n^+ layers and a remote PACVD absorber layer. Future publications will report the performance of these devices, which serve as a critical test to the apparently improved properties of the RMS materials.

References

Abelson, J. R., Katiyar, M. and Möller, W. (1994). To be submitted.

Abelson, J. R., Maley, N., Doyle, J. R., Feng, G. F., Fitzner, M., Katiyar, M., Mandrell, L., Myers, A. M., Nuruddin, A., Ruzic, D. N., and Yang, S. (1991). in *Amorphous Silicon Technology*, edited by A. Madan, Y. Hamakawa, M. J. Thompson, P. C. Taylor, and P. G. LeComber, *Mater. Res. Soc. Proc.* Vol. 219, (Anaheim, CA), p. 619.

Alvarez, F., Sebastiani, M., Ozzilli, F., Fiorini, P., and Evangelisti, F. (1992). *J. Appl. Phys.* Vol. 71, p. 267.

Anderson, H. H. and Bay, H. L. (1981). Sputtering Yield Measurements, Chapter 4 in *Sputtering by Particle Bombardment I, Physical Sputtering of Single-Element Solids*, Ed by R. Behrisch, (Topics in Applied Physics Vol. 47) (Springer-Verlag, New York).

Asano, A. and Sakai, H. (1989). *Appl. Phys. Lett.*, Vol. 54, p. 904.

Aspnes, D. E., Theeten, J. B., and Hottier, F. (1979). *Phys. Rev. B* Vol. 20, p. 3292.

Baker, S. H., Spear, W. E., and Gibson, R. A. G. (1990). *Phil. Mag., B* Vol. 62, p. 213.

Banerjee, P. K. (1989). *Properties of Amorphous Silicon*, EMIS Datareview, 2nd ed. (INSPEC, London), p.293.

Banerjee, R., Bandyopadhyay, A. K., Sharma, S. N., Batabyal, A. K., and Barua, A. K. (1989). in *Materials Issues In Microcrystalline Semiconductors*, edited by P. M. Fauchet, K. Tanaka, and C. C. Tsai, Mater. Res. Soc. Proc. Vol. 164, p. 69.

Baum, J., Gleason, K. K., Pines, A., Garroway, A. N., and Reimer, J. A. (1986). *Phys. Rev. Lett.* Vol. 56, p. 1377.

Beyer, W. (1983). et al., *Thin Solid Film,* Vol. 90, pp. 145-152.

Beyer, W. (1985). Hydrogen Incorporation in Amorphous Silicon and Processes of Its Release, in *Tetrahedrally Bonded Amorphous Semiconductors*, Ed by D. Adler and H. Fritzsche, (Plenum, New York), p.129

Beyer, W., and Wagner, H. (1983). *Journal of Non-Crystalline Solids,* Vols. 59 & 60, p. 161.

Bhattacharya, E. and Mahan, A. H. (1988). *Appl. Phys. Lett.* Vol. 52, p. 1587.

Brodsky, M. H., Cardona, M., and Cuomo, J. J. (1977). *Phys. Rev. B* Vol. 16, p. 3556.

Bube, R. H. (1992). *Photoelectronic Properties of Semiconductors*, (Cambridge University Press).

Bullot, J., and Schmidt, M. P. (1987). *Phys. Stat. Sol. B* Vol. 143, p. 345.

Carlson, D. E. (1990). Critical Review in Solid State and Materials Science, Vol. 16, p. 117.

Chatarine, Y. and Turban, G. (1980). *Thin Solid Films,* Vol. 70, p. 101.

Chaudhuri, P., Ray, S., Batabyal, A. K., and Barua, A. K. (1984). *Thin Solid Films*, **121**, 233.

Chen, Y. (1994). Ph.D. Thesis, *Microstructure Study of Amorphous Silicon-Based Semiconductors by Small Angle X-Ray Scattering*, Colorado School of Mines, Golden, Colorado.

Chen, Y., Jones, S. J., Williamson, D. L., Yang, S., Maley, N. and Abelson, J. R. (1992). *Mat. Res. Soc. Symp. Proc.* Vol. 258, p. 311.

Collins, R. W. (1989). in *Advances in Amorphous Semiconductors*, edited by H. Fritzsche (World Scientific, Singapore), p. 1003.

Collins, R. W.and Yang, B. Y. (1989). *J. Vac. Sci. Technol.* Vol. B 7, p. 1155x.

Doyle, J. R., Nuruddin, A., and Abelson, J. R. (1994). "Effect of Anode Bias on Plasma Confinement in DC Magnetron Discharges," *J. Vac. Sci. Tech. A* Vol. 12(3), pp. 886-8.

Eicke and Bilger, G. (1988). *Surface and Interface Analysis* Vol. 12, p. 344.

Enomoto, K., Nishiwake, H., Watanabe, K., Nakashima, Y., Tsuda, S., Ohnishi M., and Kuwano, Y. (1982). *Jpn. J. Appl. Phys.* Suppl. No.21-2, p.265.

Feng, G. F., Katiyar, M., Maley, N. and Abelson, J. R. (1991). in *Amorphous Silicon Technology*, edited by A. Madan, Y. Hamakawa, M. J. Thompson, P. C. Taylor, and P. G. LeComber, Mater. Res. Soc. Proc. Vol. 219, (Anaheim, CA) p. 709.

Feng, G. F., Katiyar, M., Abelson, J. R. and Maley, N. (1992). *Phys. Rev. B* 45, p. 9013.

Feng, G. F., Katiyar, M., Abelson, J. R., and Maley, N. (1992a). *Phys. Rev.* Vol. B45, p. 9103.

Feng, G. F., Katiyar, M., Yang, Y. H., Abelson, J. R. and Maley, N. (1992b). in *Amorphous Silicon Technology* edited by M. J. Thompson, Y. Hamakawa, P. G. LeComber, A. Madan, and E. Schiff, *Mater. Res. Soc. Proc.* Vol. 258, (San Francisco, CA) p. 179.

Feng, G. F., Katiyar, M., Yang, Y. H., Abelson, J. R., and Maley, N. (1993). presented at *Mater. Res. Soc. Fall Meeting*, Boston, MA.

Fitzner, M. and Abelson, J. R. (1994). *Mat. Res. Soc. Symp. Proc.* Vol. 339, San Francisco.

Fritzsche, H., et al., (1979). *J. Appl. Phys.* Vol. 30, p. 3366.

Furakawa, S. (1989). Springer Proceedings in Physics, edited by L.G. Harris and C.Y. Yang (Springer, Berlin), Vol. 34, p. 58.

Gerault, J. P., Morancho, R., Constant, G., Mazrolles, P., Erhardt, J. J., and Aluot, M.(1983). *Thin Solid Films,* Vol. 101, p. 83.

Grunthaner, F. J., et al., (1986). *Mater. Sci. Rep.* Vol. 1, p. 69.

Guha, S., Yang, J., Nath, P., and Hack, M. (1986). *Appl. Phys. Lett.* Vol. 49, p. 218

Guinier, A. and Fournet, G. (1955). *Small-Angle Scattering of X-rays* (Wiley, New York) p.30.

Guivarc'h, A., Richard, J., Le Contellec, M., Ligeon, E., and Fontenille, J. (1980). *J. Appl. Phys.* Vol. 51, p. 2167.

Gutierrez, M. T., Carabe, J., and Gandia, J. J. (1992). *J. Appl. Phys.*, vol. 71, no. 12, p. 6140.

Hamasaki, T., Kurata, H., Hirose, M., and Osaka, Y. (1984). *Appl. Phys. Lett.* Vol. 37, p. 1084.

Hansen, F. (1989). Intrinsic Stress in a-Si and a-Si:H films, pp 475, *Properties of Amorphous silicon*, 2nd Edition, INSPEC, London and New York.

Kakinuma, H., et al., (1986). *J. Appl. Phys.* Vol 59 no.9, p. 3110.

Katiyar, M., Feng, G. F., Yang, Y. H., Maley, N. and Abelson, J. R. (in press) *Appl. Phys. Lett.*

Katiyar, M., Feng, G. F., Yang, Y., Abelson, J. R. and Maley, N. (1992). presentation (J9-WeA5) at AVS 39th National Symposium, Chicago.

Kawabata, K., Shiratsuki, Y., Miyazaki, S., and Hirose, M. (1988). *Jpn. J. Appl. Phys.* Vol. 27, p. L1190.

Kern, W. (1970). *RCA Review* Vol. 31, p. 187-206.

Koinuma, Nakano, M., and Gonda, S. (1990). *Mat. Res. Soc. Symp. Proc.* Vol. 192, p. 201.

Kruangam, D. (1991). in *Amorphous & Microcrystalline Semiconductor Devices: Optoelectronic Devices*, edited by Jerzy Kanicki (Artech House, Boston. London), p.195.

Kumar, S. and Drevillon, B. (1989). *J. Appl. Phys.* Vol. 65, p. 3023.

Ley, L. (1984).*The Physics of Hydrogenated Amorphous Silicon II, Electronic and Vibrational Properties*, ed by J.D. Joannopoulos and G. Lucovsky, (Springer-Verlag, Berlin).

Li, Y.-M. and Fieselmann (1991). B. F., *Appl. Phys. Lett.* Vol. 59; p. 1720.

Li, Y.-M., Fieselmann, B. F., and Catalano, A. (1991). *Proc. 22nd IEEE Photovoltaic Specialists Conference (PVSC)*, IEEE, New York; p.1231.

Li, Y.-M., Catalano, A., and Fieselmann, B. F. (1992). *Mat. Res. Soc. Symp. Proc.* Vol. 258, (San Francisco, Spring) p.923.

Li, Y.-M. (1993). Mat. Res. Soc. Symp. Proc. Vol.297, (San Francisco, Spring) p.803.

Logothetidis, S. and Kiriakidis, G. (1988). *J. Appl. Phys.* Vol. 64, p. 2389.

Lu, H. Y. and Petrich, M. A. (1992). *J. Appl. Phys.* Vol. 71, p. 1693.

Lucovsky , G., Nemanich, R. J., and Knights, J. C. (1979). *Phys. Rev. B* Vol. 19, p. 2064.

Luft, W. and Tsuo, Y. S. (1993). *Hydrogenated Amorphous Silicon Alloy Deposition Processes*, (Marcel Dekker, Inc., New York) p.49.

Madan, A. and Shaw, M. P. (1988). *The Physics and Applications of Amorphous Semiconductors*, (Academic Press Inc., San Diego, CA) p.155.

Mahan, A. H., Raboisson, P. and Tsu, R. (1987). *Appl. Phys. Lett.* Vol. 50, p. 335.

Mahan, A. H., Raboisson, P., Williamson, D. L., and Tsu, R. (1987). *Solar Cells*.Vol. 21, p. 117.

Mahan, A. H., Williamson, D. L., Nelson, B. P. and Crandall, R. S. (1989a). *Phys. Rev. B* Vol. 40, p. 12024.

Mahan, A. H., Williamson, D. L., Nelson, B. P. and Crandall, R. S. (1989b). *Solar Cells*, Vol. 27, p. 465.

Major, S., Bhatnagar, M. C., Kumar, S., and Chopra, K. L. (1988). *J. Vac. Sci. Technol.* Vol. A6, p. 2415.

Maley, N., et al., (1989). *J. Vac.Sci.Technol. A* Vol. 7, no.3, p. 1267.

Maley, N., Myers, A., Pinarbasi, M., Leet, D., Abelson, J. R. and Thornton, J. A. (1989). J. Vac. Sci. Technol. A Vol. 7, no.3 , p. 1267.

Maley, N. and Szafranek, I. (1990). *Amorphous Silicon Technology*, Symposium Proceedings of Materials Research Society, vol. 192, pp.663 .

Maley, N. and Szafranek, I. (1990). *Mat. Res. Soc. Symp. Proc.* Vol.192, p. 663.

Matsuda, A. (1983). *J. Non-Cryst. Solids* Vol. 59&60, p. 767.

Matsuda, A., et al., (1984). *Jpn. J.Appl.Phys.* 2 (Japan) Vol.23, no.8, p.L567.

Matsuda, A., Yamaoka, T., Wolff, S., Koyama, M., Imanishi, Y., Kataoka, H., Matsuura, H., and Tanaka, K. (1986). *J. Appl. Phys.* Vol. 60, p. 4025.

Morimoto, A., Miura, T., Kumeda, M., and Shimizu, T. (1982). *J. Appl. Phys.*, Vol. 53, p. 7299.

Moustakas, T. D. (1984). in *Semiconductors and Semimetals*, Vol. 21, part A, edited by J. Pankove, (Academic Press), p.55.

Moustakas, T. D. (1986). *Solar Energy Materials* Vol. 13, p. 373.

Nakano, S., et al., (1988). In Proc. 8th E.C. Photovoltaic Solar Energy Conf., edited by I. Solomon, B. Equer and P. Helm, Kluwer Academic Publishers, Dordrecht, The Netherlands, p.641.

Nashashibi, T. S., Austin, I. G., Searle, T. M., Gibson, R. A., Spear, W. E., LeComber, P. G. (1982).*Philos.Mag. B* Vol. 45, p. 557.

Nix, W. D. (1989). Mechanical Properties of Thin Films, *Metallurgica Transactions A* Vol 20A, p. 2217-2245.

Petrich, M. A., Gleason, K. K., and Reimer, J. A. (1987). *Phys. Rev. B.* Vol. **36**, p. 9722.

Pinarbasi, M., Chou, L. H., Maley, N., Myers, A., Lee, D., and Thornton, J. A. (1987). *Superlattices Microstructures,* Vol. 3 , p. 331.

Pinarbasi, M., Maley, N., Myers, A. and Abelson, J. R. (1989a). *Thin Solid Films* Vol. 171, p. 217.

Pinarbasi, M. (1989b). Ph.D. thesis, *Growth, Properties and Electronics Stability of DC Magnetron Reactive Sputtered Hydrogenated Amorphous Silicon Thin Films*, University of Illinois at Urbana-Champaign.

Pinarbasi, M., M. Kushner, and Abelson, J. R. (1990). *J Appl. Phys.* Vol. 68, p. 2255.

Ray, S. (1989). *Properties of Amorphous Silicon*, EMIS Datareview, 2nd ed. (INSPEC, London), p.241.

Reimer, J. A., Vaughan, R. W., and Knights, J. C. (1981). *Phys. Rev. B* Vol. 24, p. 3360.

Richter, W., Weber, W., and Ploog, K. (1976). *J. Less-Common. Metals*, Vol. 47, p. 85.

Ross, R. C. and Messier, R. (1981). Bombardment Effects in a-Si:H Sputtered Films, *Tetrahedally Bonded Amorphous Semiconductor,* AIP Conference Proceedings, No.73, pp. 53-57.

Ross, R. C. and Messier, R. (1984). *J.Appl.Phys.* Vol. 56, p. 347.

Rossnagel, S. M. and Cuomo, J. J. (1989). Film Modification by Low Energy Ion Bombardment During Deposition, *Thin Solid Films*, Vol. 171, p. 143.

Rubel, H., Schroder, B., Fuhs, W., Kraruskopf, J., Rupp T., and Bethge, K. (1987). *Phys. Stat. Sol. B* Vol. 139, p. 131.

Saito, N., Sannomiya, H., Yamaguchi, T., and Tanaka, N. (1984). *Appl. Phys.* Vol. A 35, p. 241.

Saito, N., Yamada, T., Yamaguchi, T., Nakaaki, I. and Tanaka, N. (1985). *Philosophical Magazine B* **52**, 987.

Saito, N., Tanaka, N. and Nakaaki, I. (1985). *Appl. Phys, A* Vol. **38**, 37.

Schlichting, J., Czack, G., Kuhn, P., Schroder, F. (1984). *Gmelin Handbook of Inorganic Chemistry*, Silicon, Supplement Vol B2, 8th Edition, Chief Editor: G. Kirschstein, (Springer-Verlag, Berlin).

Schmidt, M. P., Bullot, J., Gauthier, M., Cordier, P., Solomon, I., and Tran-Quoc, H. (1985). *Philosophical Magazine B,* Vol. **51**, p. 581.

Shanks, H., Fang, C. J., Ley, L., Cardona, M., Demond, F. J., and Kalbitzer, S. (1980). *Phys. Stat. Sol. (B)* Vol. 100, p. 43.

Shen, S. C. and Cardona, M. (1981). *Phys. Rev. B* Vol. 23, p. 5322.

Shibata, N., Fukada, K., Ohtoshi, H., Hanna, J., Oda, S., and Shimizu, I. (1987). in *Amorphous Silicon Semiconductors--Pure and Hydrogenated*, edited by A. Madan, M. J. Thompson, D. Adler, and Y. Hamakawa, Mater. Res. Soc. Proc. Vol. 95, p. 225.

Shimada, T., Katayama, Y., and Komatsubara, K. F. (1979) *J. Appl. Phys.* Vol. **50**, p. 5530.

Tabe, M. (1984). "UV Ozone Cleaning of Silicon Substrate in Silicon Molecular Beam Epitaxy," *Appl.Phys.Lett.* Vol. 45, p. 1073.

Tawada, Y. (1982). Amorphous Semiconductor Technology and Devices. North Holland, Tokyo, Vol. 6, p. 148.

Thomas, III, J. H. (1983). *Appl. Phys. Lett.* Vol. 42, p. 794.

Thomas, III, J. H. and Catalano, A. (1983). *Appl. Phys. Lett.* Vol. 43, p. 101.

Thompson, M. J. (1984). Sputtered Materials, in Topics in Applied Physics, Vol. 55, The Physics of Hydrogenated Amorphous Silicon I, edited by J.D. Joannopoulos and G. Lucovshy, Springer-Verlap, Berlin , p. 119.

Thornton, J. (1986). in *Amorphous Metals and Semiconductors*, Edited by P. Haasen and R.I. Jaffee, ActaScripta Metallurgica Proceedings Series, Vol. 3 (Pergamon Press, New York) p.299.

Thornton, J. A. and Hoffman, D. W. (1989). *Thin Solid Films*, Vol. 171, p. 5.

Tsai, C.-C., Anderson, G. B., Thompson, R., and Wacker, B. (1989). *J. Non-Cryst. Solids* Vol. 114, p. 151.

Veprek, S. Iqbal, Z., Oswald, H. R., and Wedd, A. P. (1981). *J. Phys. C* Vol. 14, p. 295.

Veprek, S., Heintze, M., Sarott, F. A., Jurcik-Rajman, M., and Willmott, P. (1988). in *Amorphous Silicon Technology*, edited by A. Madan, M. J. Thompson, P. C. Taylor, P. G. LeComber, and Y. Hamakawa, Mater. Res. Soc. Proc. Vol. 118, p. 3.

Wang, C., Parsons, G. N., Buehler, E. C., Nemanich, R. J., and Lucovsky, G. (1989). in *Materials Issues In Microcrystalline Semiconductors*, edited by P. M. Fauchet, K. Tanaka, and C. C. Tsai, Mater. Res. Soc. Proc. Vol. 164, p. 21.

Watanabe, I., Hata, Y., Morimoto, A., Shimizu, T. (1982). *Jpn. J. Appl. Phys.* 2, **21**, No.10, p.L613-15.

Wieder, H., Cardona, M., and Guarnieri, C. R. (1979). *Phys. Stat. Sol. B* Vol. 92, p. 99.

Williamson, D. L., Mahan, A. H., Nelson, B. P., and Crandall, R. S. (1989). *Appl. Phys. Lett.* Vol. 55, p. 783.

Williamson, D. L., Chen, Y., and Jones, S. J. (1994). *AIP Conference Proceedings 306, 12th NREL Photovoltaic Program Review*, Eds: R. Noufi and H.S, Ullal (AIP, New York) p.442-451.

Williamson, D. L., (1994b), Private communication with Dr. D. L. Williamson.

Windischmann, H., et al., (1986). *J Non-Cryst. Solids* Vol 85, no.3, p. 261.

Wolf, S. and Tauber, R. N. (1986).*Silicon Processing for the VLSI Era*, Vol.1: Process Technology, Lattice Press.

Yang, Y., Katiyar, M., Abelson, J. R. and Maley, N. (1993). *Mat. Res. Soc. Proc.* p. 297.

Yang, S.-Y. and Abelson, J. R. (1993). *J. Vac. Sci. Techol. A* Vol. 11, p. 1327.

Yang, S.-Y. and Abelson, J. R. (1994). submitted to *J. Appl. Phys.*

Yoon, J. H., Xu, X., Kotharay, M., and Wagner, S. (1991). *Mat. Res. Soc. Symp. Proc.* Vol. 219, pp.93.

Zanzucchi, P. J. (1984). Chapter 4, The Vibrational Spectra of a-Si:H, *Semiconductors and Semimetals*, Vol.21, Part B, Volume Editor: J. I. Pankove, (Academic Press, Inc, New York) p.113.

REPORT DOCUMENTATION PAGE

Form Approved
OMB NO. 0704-0188

1. AGENCY USE ONLY (Leave blank)	2. REPORT DATE	3. REPORT TYPE AND DATES COVERED
	July 1995	Final Subcontract Report

4. TITLE AND SUBTITLE

Research on Silicon-Carbon Alloys and Interfaces

5. FUNDING NUMBERS

C: XG-1-10063-6

TA: PV531101

6. AUTHOR(S)

J. R. Abelson

7. PERFORMING ORGANIZATION NAME(S) AND ADDRESS(ES)

University of Illinois
Urbana, Illinois

8. PERFORMING ORGANIZATION REPORT NUMBER

9. SPONSORING/MONITORING AGENCY NAME(S) AND ADDRESS(ES)

National Renewable Energy Laboratory
1617 Cole Blvd.
Golden, CO 80401-3393

10. SPONSORING/MONITORING AGENCY REPORT NUMBER

TP-411-8111

DE95009243

11. SUPPLEMENTARY NOTES

NREL Technical Monitor: W. Luft

12a. DISTRIBUTION/AVAILABILITY STATEMENT

12b. DISTRIBUTION CODE

UC-1250

13. ABSTRACT *(Maximum 200 words)*

This report describes work performed to develop improved p-type wide-band-gap hydrogenated amorphous silicon-carbon alloy (a-$Si_{1-x}C_x$:H) thin films and interfaces for the "top junction" in hydrogenated amorphous silicon (a-Si:H)-based p-i-n solar cells. We used direct current reactive magnetron sputtering to deposit undoped a-$Si_{1-x}C_x$:H films with a Tauc band gap E_g of 1.90 eV, a sub-band-gap absorption of 0.4 (at 1.2 eV), an Urbach energy of 55 meV, an ambipolar diffusion length of 100 nm, an air-mass-one photoconductivity of $10^{-6}/\Omega$-cm, and a dark conductivity of $10^{-11}/\Omega$-cm. p^+ a-$Si_{1-x}C_x$:H films with a Tauc band gap of 1.85 eV have a dark conductivity of $8 \times 10^{-6}/\Omega$-cm and thermal activation energy of 0.28 eV. We used in-situ spectroscopic ellipsometry and post-growth X-ray photoelectron spectroscopy to determine the relative roles of H and Si in the chemical reduction of SnO_2 in the early stages of film growth. We used in-situ spectroscopic ellipsometry to show that a-Si:H can be transformed into μc-Si;H in a subsurface region under appropriate growth conditions. We also determined substrate cleaning and ion bombardment conditions which improve the adhesion of a-$Si_{1-x}C_x$:H films.

14. SUBJECT TERMS

silicon-carbon ; alloys ; interfaces ; photovoltaics ; solar cells

15. NUMBER OF PAGES
82

16. PRICE CODE

17. SECURITY CLASSIFICATION OF REPORT	18. SECURITY CLASSIFICATION OF THIS PAGE	19. SECURITY CLASSIFICATION OF ABSTRACT	20. LIMITATION OF ABSTRACT
Unclassified	Unclassified	Unclassified	UL